Interactions with bioenergetics by the mitochondria-targeted anti-apoptotic imidazole fatty acid derivative 'TPP-IOA'.

Lucas Anthony Maddalena, B.Sc. (Honours)

A thesis submitted in partial fulfillment of the requirements for the degree of

Master of Science

Biological Sciences (Cell & Molecular Biology)

Department of Biological Sciences

Brock University

St. Catharines, Ontario, Canada

I - Abstract:

The mitochondrial pathway of apoptosis contributes to cell death and tissue degeneration in a variety of human diseases. Targeting the molecular events of this pathway represents a promising therapeutic strategy under pathological scenarios, particularly in tissues with limited regenerative capability (e.g. brain, heart). Recently, the small molecule 'TPP-IOA' was designed to target mitochondria and therein inhibit the peroxidase activity of cytochrome *c* that promotes activation of the apoptotic death pathway (Atkinson et al., Nat. Commun. 2011; 2:497). Therefore, TPP-IOA holds promise as a potential therapeutic agent in many pathological scenarios of cell loss. However, TPP-IOA's target protein and organelle perform critical functions in aerobic ATP production via oxidative phosphorylation, and yet little is known about TPP-IOA's interaction with mitochondrial energetics. This is an important consideration for TPP-IOA's potential future therapeutic utility, as avoiding interference to mitochondrial energetics will be essential for many target cell types that feature a high rate of oxidative phosphorylation (e.g. neurons, cardiomyocytes). Using the purified protein target, isolated organelle target, and live cultured cells, this thesis investigated TPP-IOA's interaction with fundamental components of energetics-related mitochondrial biology.

Assessments with pure cytochrome *c* revealed that TPP-IOA can inhibit the respiration-associated reduction activity of cytochrome *c*, and that this occurred at concentrations marginally higher than those required to inhibit the protein's pro-apoptotic peroxidase activity. In isolated rat liver mitochondria, TPP-IOA impaired oxidative phosphorylation via inhibition of both ADP-phosphorylating-respiration and FCCP-uncoupled respiration, and stimulation of non-phosphorylating respiration. Critically, TPP-IOA was unable to inhibit pro-apoptotic peroxidase activity at concentrations that avoided interference to oxidative phosphorylation, suggesting it may be unable to perform its desired pharmacological activity without causing toxicity to mitochondrial energetics. In live cultured cells, TPP-IOA caused effects associated with impaired oxidative phosphorylation, including a collapsed mitochondrial membrane potential, fragmented mitochondrial

network morphology, and apparent loss of mitochondria. Furthermore, TPP-IOA effectively inhibited apoptotic death under lethal conditions in cells that preferentially utilized anaerobic glucose metabolism, but not in cells manipulated to be heavily reliant on oxidative phosphorylation and thus more sensitive to the perturbations to mitochondrial energetics. Altogether, these findings indicate that relative cellular dependence on oxidative phosphorylation is a critical factor influencing TPP-IOA's pharmacological efficacy. Furthermore, potential therapeutic applications may be limited to pathologies involving predominantly less aerobic tissues/cell types or depressed aerobic metabolism. Additionally, these findings have broader implications for mitochondrial medicine based on similar mitochondrial drug targeting strategies.

II - Keywords:

Mitochondria, bioenergetics, metabolism, oxidative phosphorylation, respiration, triphenylphosphonium, apoptosis, cytochrome *c*, glycolysis, glucose, galactose, glutamine, mitochondrial membrane potential, peroxidase activity, cell culture,

III - Acknowledgements:

I am grateful and appreciative for all of the guidance, support, and thoughtful feedback from my co-supervisors, Dr. Jeffrey Stuart and Dr. Jeffery Atkinson, as well as from the other members of my examining committee, Dr. Bob Carlone, Dr. Paul LeBlanc, and Dr. Jim Ballantyne (external examiner; University of Guelph). I am especially grateful to Dr. Jeffrey Stuart for allowing me the independence to take this thesis project entirely in the direction that I desired, for his confidence and belief in my abilities to grow as a person and scientist, and for the wonderful relationship that has grown between us.

Thank you to the numerous past and present members of the Stuart lab, most notably Shehab Selim, Joao Fonseca, and Max Merilovich, for the many great moments shared together over the years. Thank you to Andrew Valente for his interest and effort in developing the image analysis macro and the enjoyable collaborative experience that resulted. Special thanks to Dr. Ellen Robb for the wonderful mentorship, guidance and friendship that began when I entered the Stuart lab as an undergraduate in May 2011 and continues to this day. Thank you to Mikel Ghelfi and Venkata Krishna Garapati of the Atkinson laboratory for chemical synthesis and occasional purity analyses. Thank you to the numerous individuals of the Department of Biological Sciences and other departments that I have come to know over the years and have shared many memorable times together.

Thank you to Alison from the Student Development Centre for her support and guidance in times of need; the gentlemen at Machine Shop and Electrical Shop for their technical assistance and expertise; the Science Stores ladies for all of their assistance.

There are several research and equipment funding sources that allowed this research to happen, including: NSERC, BUAF Seed Grant, Canadian Foundation for Innovation. I'd also like to thank the Ontario Government (Ministry of Training, Colleges, & Universities) for supporting me with Ontario Graduate Scholarships.

I would also like to recognize the numerous funding sources that have provided me with various awards/grants/bursaries for conference-related travel, including the Faculty of Graduate Studies, Department of Biological Sciences, Graduate Student Association, Society for Free Radical Biology & Medicine, American Physiological Society, Mitochondrial Physiology Society, and International Union of Biochemistry & Molecular Biology.

Last but definitely not least, thank you to my immediate family and close friends for their unwavering support, patience, and love throughout this journey. I am forever indebted to all of you.

Table of Contents:

IV - Contributions:

I performed all experiments, data presentation, statistical analyses, and chapter writing.

Shawnnah Staples, a 2014 NSERC Undergraduate Summer Research Assistant (USRA), assisted in performing mitochondrial peroxidase activity assays under my direction and supervision.

Shehab Selim, a 2015 NSERC USRA, assisted in generating the stable SH-SY5Y-mito-mEFP cell lines under my direction and supervision.

The description of the custom-made Mitochondrial Network Analysis (MiNA V.1.0.0) tool (included within Appendix II) was modified with permission from the original manual written by its creator Andrew Valente.

V - Dissemination of Results:

The experimental findings of this thesis have been prepared as a single manuscript entitled "*The mitochondria-targeted imidazole substituted oleic acid derivative 'TPP-IOA' affects mitochondrial bioenergetics and its protective efficacy in cells is influenced by cellular dependence on aerobic metabolism.*" It has been accepted by the journal "*Biochimica et Biophysica Acta – Bioenergetics*" pending approval of minor revisions.

Experimental findings of this thesis were presented in some capacity at several academic conferences:

1) Maddalena LA, Selim SM, Atkinson JA, & Stuart JA. (November 2015). "A mitochondria-targeted anti-apoptotic inhibitor of cytochrome *c* peroxidase activity interferes with mitochondrial bioenergetics and does not prevent cell death in cultured cells reliant on oxidative phosphorylation." Poster presented at the *2015 Society for Free Radical Biology & Medicine Annual Meeting*. Boston, Massachusetts, USA.

2) Maddalena LA, Atkinson JA, & Stuart JA. (September 2015). "Interference with mitochondrial bioenergetics by TPP-IOA, a mitochondria-targeted anti-apoptotic inhibitor of cytochrome *c* peroxidase activity" Poster presented at the *2015 American Physiological Society (APS) Conference: Physiological Bioenergetics*: *From Bench to Bedside*. Tampa, Florida, USA.

3) Maddalena LA, Atkinson JA, & Stuart JA. (November 2014). "Interference with mitochondrial respiration by TPP-IOA, an anti-apoptotic inhibitor of cytochrome *c* peroxidase activity." Poster presented at the *2014 Society for Free Radical Biology & Medicine (SFRBM) Annual Meeting.* Seattle, Washington, USA.

4) Maddalena LA, Staples S, Atkinson JA, & Stuart JA. (September 2014). "Experimental considerations for evaluating bioenergetics effects of a mitochondria-targeted compound, TPP-IOA." Poster presented at *Mitochondrial Physiology (MiP) 2014 -10th Conference: Joint International Union of Biochemistry & Molecular Biology (IUBMB) / MiP Society Symposium on Mitochondrial Physiology – Methods, Concepts, and Biomedical Perspectives*. Obergurgl, Tyrol, Austria.

VI - List of Abbreviations:

Ψ_m	mitochondrial membrane potential
Ψ_p	plasma membrane potential
3HP-TPP	3-hydroxypropyl-triphenylphosphonium
Ac-DEVD-AMC	N-acetyl-L-α-aspartyl-L-α-glutamyl-L-valyl-N-(4-methyl-2-oxo-2H-1-benzopyran-7-yl)-L-α-asparagine OR N-acetyl-Asp-Glu-Val-Asp-7-amino-4-methylcoumarin
ADP	adenosine diphosphate
AMP	adenosine monophosphate
AIF	apoptosis inducing factor
AFU	arbitrary fluorescence units
ANOVA	analysis of variance
Apaf-1	apoptotic protease activating factor-1
Asp	aspartate
ATP	adenosine triphosphate
BSA	bovine serum albumin
CLAHE	contrast limited adaptive histogram equalization
CMXRos	chloromethyl-X-rosamine
Cys	cysteine
DMEM	Dulbecco's modified eagle medium
DMSO	dimethylsulfoxide
DTNB	5,5′-dithiobis(2-nitrobenzoic acid)
DTT	DL-dithiothreitol
endoG	endonuclease G
EDTA	ethylenediaminetetraacetic acid
$FADH_2$	flavin adenine nucleotide (reduced)
FBS	fetal bovine serum
FCCP	carbonylcyanide-ρ-trifluoromethoxyphenylhydrazone
FIJI	FIJI is just ImageJ
G418	geneticin
Glu	glutamate
H_2O_2	hydrogen peroxide
HEPES	((4-(2-hydroxyethyl)-1-piperazineethanesulfonic acid)
HSD	honestly significant difference
His	histidine
HtrA2	high-temperature-requirement protein A2
$I.C._{50}$	half maximal inhibitory concentration
IgG	immunoglobulin G
IOA	imidazole-substituted oleic acid
Lys	lysine
mEFP	modified emerald fluorescent protein
MEM	modified eagle medium
Met	methionine
mito-mEFP	mitochondria-targeted modified emerald fluorescent protein
NADH	nicotinamide adenine dinucleotide (reduced)
NAD+	nicotinamide adenine dinucleotide (oxidized)
OGD	oxygen/glucose deprivation
OXPHOS	oxidative phosphorylation

PBS	phosphate-buffered saline
PBS-t	phosphate-buffered saline with Tween-20
PTFE	Potter-Elvehjem polytetrafluoroethylene
p	proton motive force
Q	ubiquinone
RCR	respiratory control ratio
SEM	standard error of the mean
Smac	second-mitochondria derived activator of caspase
SDS-PAGE	sodium dodecyl sulfate polyacrylamide gel electrophoresis
tBOOH	tert-butyl hydroperoxide
TCA	tricarboxylic acid
TMRM	tetramethylrhodamine methyl ester
TNB	thionitrobenzoic acid
TPP	triphenylphosphonium
TPP-IOA	3-hydroxypropyl-triphenylphosphonium-conjugated imidazole-substituted oleic acid
TPP-OA	3-hydroxypropyl-triphenylphosphonium-conjugated oleic acid
Val	valine
VDAC	voltage-dependent anion channel
WST-1	water-soluble tetrazolium-1

VII - List of Figures:

Chapter 1.0

Chapter 2.0

Chapter 3.0

Chapter 1.0 - Introduction:

1.1 General Overview:

This thesis investigates the interaction of the novel mitochondria-targeted anti-apoptotic molecule "TPP-IOA" with the mitochondrial protein cytochrome *c*, and effects on mitochondrial energetics, morphology, and turnover. In this chapter, an overview of apoptotic cell death is provided, including general descriptions of biochemical and morphological changes, the participation of "caspases", and the role of mitochondria in apoptosis. An overview of cellular energy metabolism is given, including roles of oxidative phosphorylation and glycolysis. A brief description of the mitochondrial quality control process of mitophagy, along with changes in mitochondrial morphology relating to cellular energy metabolism, mitophagy and apoptosis are provided.

There is a growing literature describing the design and use of lipophilic cations in targeting mitochondria with pharmacologically-active molecules. Current knowledge regarding "TPP-IOA" is reviewed below, including its mechanism of anti-apoptotic action and evidence for its pharmacological efficacy. Finally, the existing knowledge of its interaction with mitochondrial energetics is covered, as well as the related existing knowledge gaps that are important to better understanding the molecule's anti-apoptotic utility.

1.2 Apoptosis, a form of programmed cell death:

The term "apoptosis" comes from a Greek word (prefix "*apo*", meaning "separation", and suffix "*ptosis*", meaning "to fall") used to describe the falling off of either leaves from a tree or petals from a flower (Kerr et al., 1972; Duque-Parra, 2005). Kerr, Wyllie, & Currie first adopted this term for scientific context in 1972 to describe a form of cell death that they and others had observed to be largely characterized by seemingly organized and distinct morphological changes

(Kerr et al., 1972). This apparent form of cell death was observed in a variety of eukaryotic cells and tissues of multi-cellular organisms under different physiological and pathological conditions, and was therefore suggested to be an active and inherently programmed or regulated form of cell death. After decades of active research, the term is presently still used to describe a main form of programmed cell death characterized by distinct morphological features shaped by regulated energy-dependent biochemical events.

Apoptotic cell death is recognized to occur under both physiological and pathological states. As a normal physiological process, apoptotic cell death occurs throughout multi-cellular organismal development and lifespan as a homeostatic mechanism to maintain cell populations. For example, during development excess neurons are produced by the embryonic brain but are degraded via apoptosis for proper brain maturation (Roth & D'Sa, 2001). Physiological apoptosis is important in opposing mitotic cell death division, and thus ensuring normal cell numbers in adult tissues (e.g. Renehan et al., 2001). However, either excessive or insufficient cell death via apoptosis can contribute to pathologies associated with various diseases. For example, the loss of quiescent cells that typically have little regenerative capacity (e.g. neurons, cardiomyocytes) occurs via excessive apoptotic cell death in affected tissues in a variety of disease states (e.g. neurodegenerative disorders of the brain or ischemia/reperfusion injury of various highly aerobic tissues; Ghavami et al., 2014; Lopez-Neblina et al., 2005). There has been great interest in understanding molecular pathways regulating apoptotic cell death in these contexts, as the prevention of cell loss and tissue degeneration is a medical goal.

1.2.1 Morphological and biochemical features of apoptosis:

Both simple light microscopy and electron microscopy have allowed for a basic understanding of the gross morphological and ultrastructural characteristics of apoptosis (Häcker, 2000). Generally, the morphological changes occurring during apoptosis include (sequentially) cell shrinkage via condensation of the nucleus and cytoplasm, fragmentation of the

nucleus, and formation and subsequent budding off of small protuberances of the cell membrane to generate many small, spheroid or ovoid plasma membrane-enclosed entities containing cytoplasmic contents. These latter structures are known as apoptotic bodies, which become phagocytosed and subsequently degraded within phagolysosomes (Kerr et al., 1972).

Intracellular biochemical and molecular changes underlie the gross morphological changes of apoptosis. These include cytosolic and nuclear protein cleavage, protein cross-linking, cytoskeleton degradation, chromatin condensation, DNA fragmentation, and plasma membrane phospholipid rearrangements (e.g. Elmore, 2007). Notably, the process of apoptosis and subsequent clearance of apoptosis cells *in vivo* generally occurs without an inflammatory response that may be otherwise generally damaging (Rock & Kono, 2008).

Generally, the distinct morphological and biochemical changes of apoptosis distinguish it from another main form of cell death known as necrosis (Kanduc et al., 2002). Morphologically, necrosis is characterized by swelling of organelles and cytoplasm that eventually leads to rupture of the plasma membrane, lysis of the cell, and the unorganized release of intracellular contents (Häcker, 2000). Necrotic cell death occurs rapidly, independent of energy, and generally without physiological regulation. As such, it is sometimes referred to as an "accidental" form of cell death and generally only occurs under catastrophic conditions (e.g. abrupt energy crisis or drastic physical damage to the cell). *In vivo*, the unorganized release of intracellular contents can damage the surrounding extracellular environment by eliciting an inflammatory response that may further exacerbate acute tissue trauma (Rock & Kono, 2008).

1.2.2 Apoptotic proteolytic activity of Caspases:

A major family of proteins involved in the regulation of apoptotic cell death are caspases (cysteine-dependent aspartate-directed proteases). These proteins are cytosolic proteases expressed as a mostly inactive proenzyme or zymogen with an inhibitory N-terminal "pro" domain. Under apoptotic conditions, regulated proteolytic processing results in release of the

inhibitory domain, initiating the enzyme's proteolytic activity (Fuentes-Prior & Salvesen, 2004). Each caspase enzyme features a cysteine amino acid residue in its active site and catalyzes proteolytic cleavage of specific target protein(s) or peptide(s) at the C-terminal side of an aspartate residue. The target substrate specificity is determined by the four amino acids that precede the cleavage site (i.e. residue-residue-residue-residue-aspartate; Thornburry et al., 1997; Talanian et al., 1997).

Members of the caspase family are categorized as either initiators or executioners of apoptosis, with Caspase-2, -8, -9, -10 fitting in the former category and Caspase-3 and to a lesser extent -6 and -7 belonging to the latter category in mammals (Cohen, 1997; Kumar, 2007). Generally, initiator caspases participate in proteolytic cascades that activate executioner caspases. In turn, active executioner caspases cleave a variety of specific protein substrates that contribute to intracellular degradation and morphological changes that are characteristic of apoptosis (e.g. Earnshaw et al., 1999; Porter & Janicke, 1999; Kumar 2007). Caspase activation contributes to cell death in a variety of human diseases (e.g. see review by McIlwain et al., 2013).

1.2.3 Mitochondrial involvement in apoptosis:

There are two main pathways of apoptotic cell death: the "extrinsic" pathway and the "intrinsic" pathway. In the extrinsic apoptotic pathway, specific extracellular cell death-inducing ligands (e.g. members of the tumour necrosis factor-α family of cytokines) bind to specific death-receptors located in the plasma membrane to initiate intracellular cascades of events that catalyze apoptotic cell death. In contrast, in the intrinsic apoptotic pathway, intracellular-derived signals derived from internal stress (e.g. intracellular dysfunction) stimulate mitochondrial release of several proteins that subsequently initiate intracellular cascades leading to apoptosis. There can be convergence of the extrinsic and intrinsic apoptosis pathways, with many of the extrinsic pathway ligands activating signals that cause mitochondrial release of pro-apoptotic

proteins (Elmore, 2007). The mitochondrial contribution to apoptotic cell death is important in a variety of pathological disease states, where it contributes to tissue degeneration and organ dysfunction (e.g. see citations in Kroemer et al., 2007).

A pivotal event in mitochondria-mediated apoptosis is the release of the mitochondrial protein cytochrome *c* into the cytosol (**Fig. 1.1**). Cytochrome *c* activates a cytosolic cascade of molecular events that culminate in the activation of apoptotic machinery leading to cell death. Cytochrome *c* release from mitochondria proceeds by a two-step process, whereby cytochrome *c* first loses its affinity for the inner mitochondrial membrane, and then translocates into the cytosol after permeabilization of the outer mitochondrial membrane (Ott et al., 2002). Cytosolic cytochrome *c* binds to the cytosolic protein apoptotic protease activating factor-1 (Apaf-1), inducing a conformational change that allows this complex to bind dATP or ATP (Li et al., 1997). Subsequently, the complex oligomerizes to form the 'apoptosome' - a multimeric complex of cytochrome *c* and Apaf-1 (Zou et al., 1999). The initiator caspase Pro-caspase 9 is then recruited to the apoptosome, and subsequently cleaved (Li et al., 1997; Zou et al., 1999). Active Caspase 9 then proteolytically activates the main executioner Caspase 3, which then catalyzes the extensive proteolysis leading to apoptotic cell death (Li et al., 1997: Zou et al., 1999; Jiang & Wang, 2004).

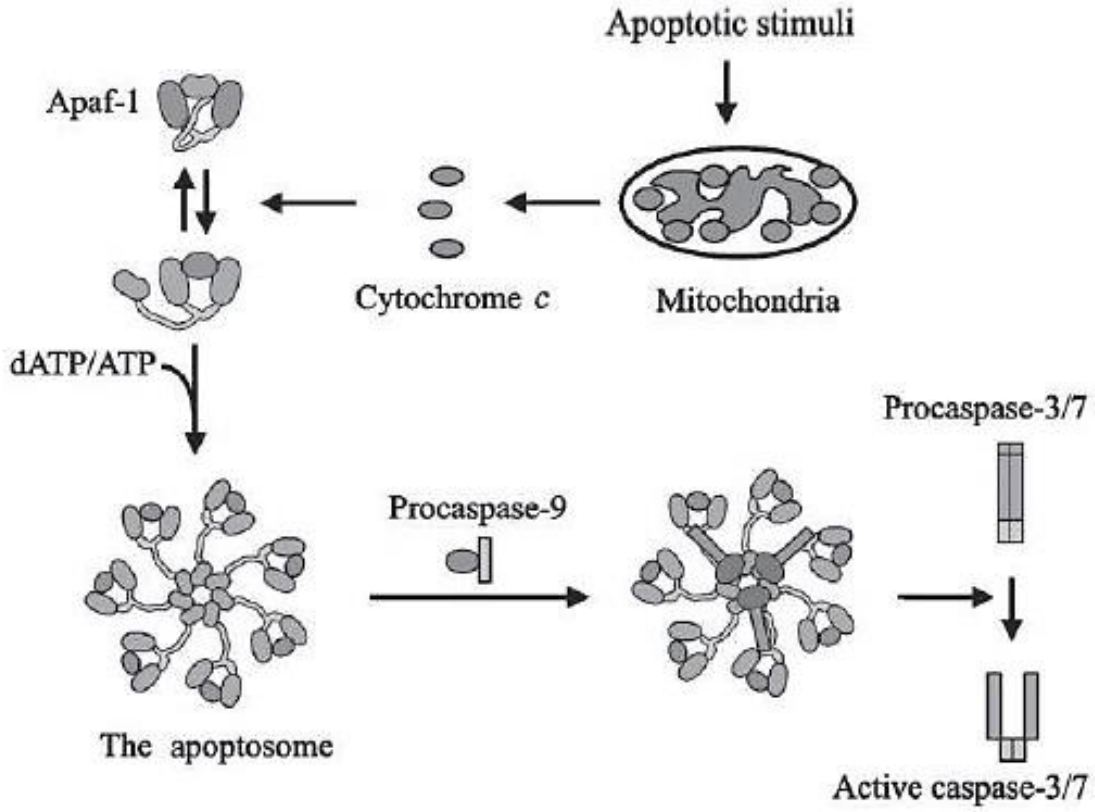

Figure 1.1: Cytochrome c released into the cytosol participates in apoptosome formation and subsequent activation of caspases (from Jiang & Wang, 2004).

In addition to cytochrome *c*, other pro-apoptotic proteins are released by mitochondria, including Smac/Diablo (second-mitochondria derived activator of caspase, or Diablo), Omi/HtrA2 (high-temperature-requirement protein A2), endoG (endonuclease G), and AIF (apoptosis inducing factor). Smac/Diablo and Omi/HtrA2 act through sequestration and/or proteolytic activity to free caspases of inhibitory interactions in the cytosol, thus increasing availability for activation (Du et al., 2000; Verhagen et al., 2000; Yang et al., 2003). EndoG and AIF each possess nuclease activity and thus catalyze DNA degradation after translocation to the nucleus (Li et al., 2001; Susin et al., 1999). Notably, the pro-apoptotic activity these proteins has been observed to occur downstream of cytochrome *c* release, after caspase activation (Adrain et al., 2001; Arnoult et al., 2002; Arnoult et al., 2003), again emphasizing the importance of cytochrome *c* release from mitochondria during apoptosis. Since cytochrome *c* release from

mitochondria is a critical early apoptotic event, there is great interest in pharmacologically inhibiting this step to prevent apoptotic cell death in certain pathological contexts.

1.2.4 Cytochrome c *– mitochondrial redox activities:*

Cytochrome *c* is an approximately 12 kDa soluble, positively charged, redox-active protein located in the inter membrane space of mitochondria in all aerobic organisms. The protein contains a single heme group that is covalently attached to the protein via two thioether bridges at Cys14 and Cys17. In the centre of the porphyrin ring of the heme is a single iron atom that is normally hexa-coordinated, with four proximal ligands provided by the porphyrin ring of the heme structure and two axial ligands provided by His18 and Met80 (see **Fig. 1.2** for a visual depiction of cytochrome *c* structure). Importantly, the heme iron can undergo one-electron transitions from $Fe2^{+}$ (reduced; ferrous) and $Fe3^{+}$ (oxidized; ferric) states. This redox transition allows the heme group to serve as a cofactor for redox activities of the protein.

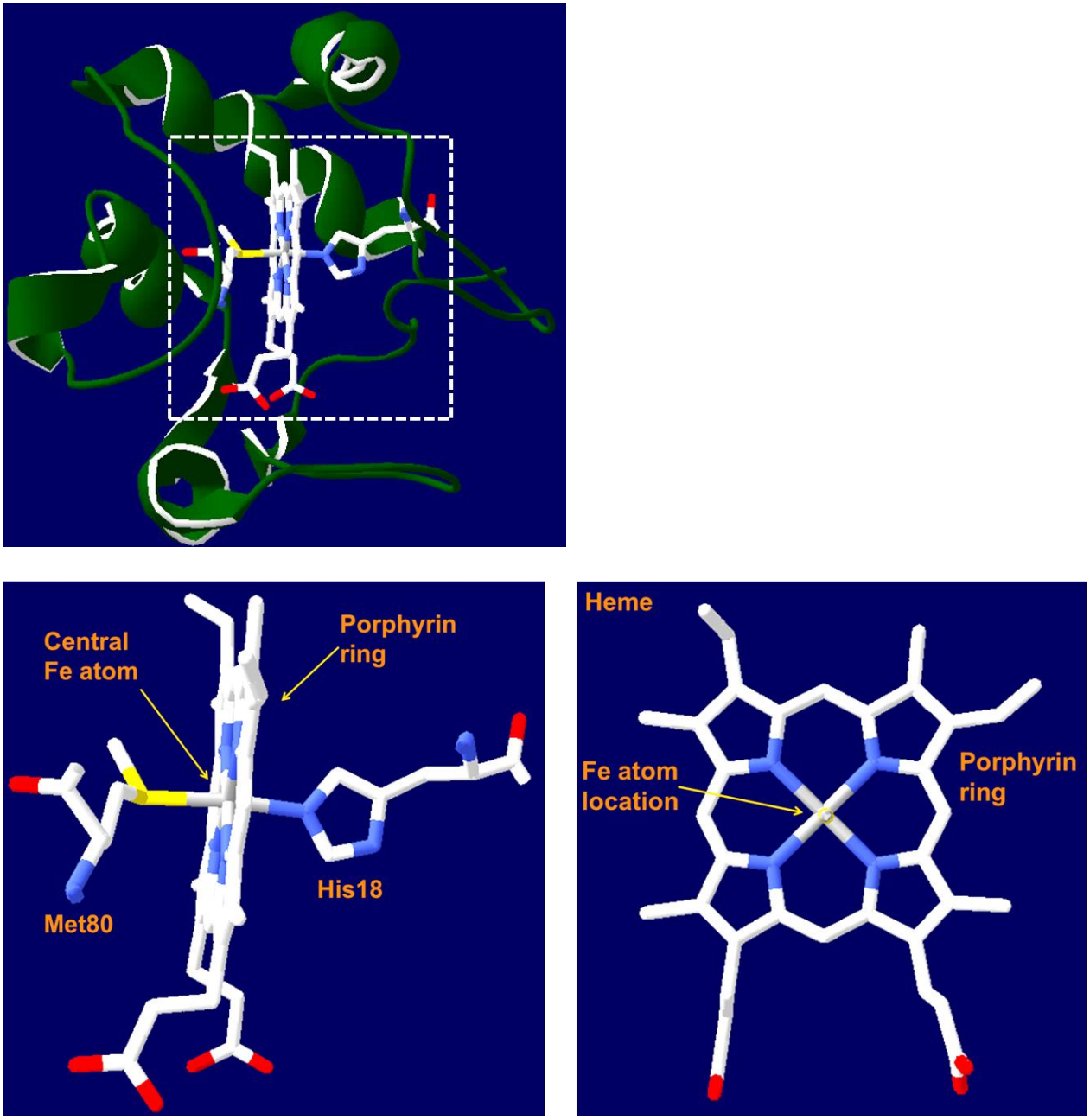

Figure 1.2: Structure of cytochrome *c* isolated from bovine heart (Protein Data Bank accession code 2B4Z; Mirkin et al., 2008).
Top panel: Ribbon backbone of cytochrome *c* (green) with stick representations of the heme group and axial Met80 and His18 ligands. ***Bottom panel:*** Stick representation of the heme group with (***left***) or without (***right***) axial Met80 and His18 ligands from alternative viewpoints. White, blue, red, and yellow sticks respectively represent the locations of carbon, nitrogen, oxygen, and sulphur atoms. Images were generated using Swiss-PDBViewer DeepView v4.1 (Guex & Peitsch, 1997).

Cytochrome *c*'s interactions with the mitochondria-specific class of phospholipids cardiolipins (also known as "diacylphosphatidylglycerol") are of importance for its biological activity. These phospholipids are predominantly localized in the inner mitochondrial membrane

(Krebs et al., 1979; Gonzalvez & Gottlieb, 2007). With a net positive charge, cytochrome *c* favourably binds the negatively charged cardiolipin head group (Kagan et al., 2006). Cardiolipin binding to cytochrome *c* is thought to involve electrostatic interactions between positively charged lysine residues of cytochrome *c* and the negatively charged phosphate groups on cardiolipin, as well as hydrophobic interactions between a polyunsaturated fatty acid residue on cardiolipin and a hydrophobic pocket of cytochrome *c* (Bayir et al, 2006). The former interaction involves a loosely bound protein conformation and is believed to necessitate electron transport activity (Yin & Zhu, 2012). Alternatively, the hydrophobic interaction is associated with a tightly bound conformation with partial unfolding of the protein and is important for mitochondrial involvement in apoptosis. This interaction with cardiolipin involves the loss of the Met80-heme iron coordination, and opens the heme iron catalytic site to be accessible to small oxidizing equivalents, like H_2O_2 (Kagan et al., 2005; Yin & Zhu, 2012). Using such oxidizing equivalents for catalysis, the heme iron exhibits measurable peroxidase activity that appears to be specific to bound polyunsaturated species of cardiolipin (Kagan et al., 2005). The accumulation of peroxidized cardiolipin species within mitochondria is recognized as an essential event for both outer mitochondrial membrane permeabilization during apoptosis, and the loss of cytochrome *c* from the inter membrane space of mitochondria (Ott et al., 2002; Nakagawa, 2004; Kagan et al., 2005; Petrosillo et al., 2005; Korytowski et al., 2011; Yin & Zhu et al., 2011).

1.3 Oxidative phosphorylation:

Mitochondria are the sites of aerobic ATP production via oxidative phosphorylation. Oxidative phosphorylation centres on the establishment of a proton electrochemical gradient across the inner mitochondrial membrane that is used to generate ATP (Mitchell, 1961). In this process, electrons derived from the catabolism of nutrients are transported through a step-wise series of reduction-oxidation (redox) reactions along protein complexes embedded in the inner

mitochondrial membrane, eventually reducing oxygen to water at Complex IV. Energy harvested from electron transfer concomitantly drives proton extrusion from the matrix into the inter membrane space by Complexes I, III, and IV. The resulting build-up of protons in this compartment creates a proton motive force (Δp; units in millivolts), which features an electrical component (an electrical gradient, or difference in electrical charge, across the inner mitochondrial membrane, "$\Delta\Psi_m$", referred to as mitochondrial membrane potential) and a chemical component (a chemical gradient, or difference in proton concentration across the inner mitochondrial membrane, "ΔpH"). This proton motive force is typically -120 to -160 mV within intact cells or -180 to -190 mV in isolated mitochondria (Kamo et al., 1979; Haffner et al., 1990; Azzone et al., 1984), and is used to drive Complex V (or the "ATP synthase") to catalyze the phosphorylation of ADP into ATP (Noji et al., 1997). Since the reduction of oxygen is the final step in the generation of the proton motive force used to synthesize ATP, oxygen consumption is said to be coupled to ADP phosphorylation (see **Fig. 1.3** below for a schematic illustration of the mitochondrial electron transport system and the accompanying description for more details).

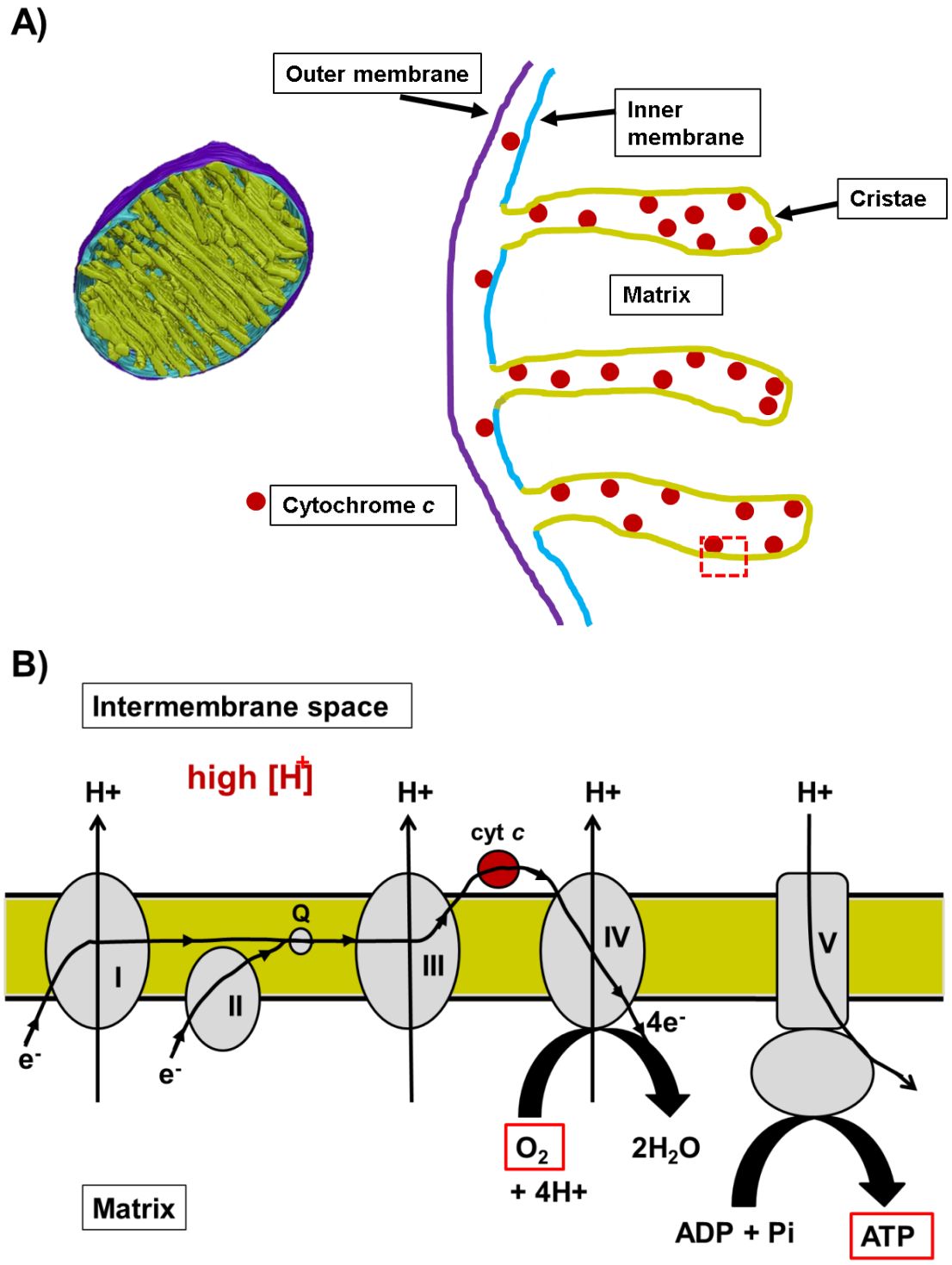

Fig 1.3: Cartoon depiction of the ultrastructure and oxidative phosphorylation system of mitochondria.
A) ***Left:*** Three-dimensional electron tomography image of a brown fat mitochondrion (taken from Frey & Mannella, 2000). ***Right:*** Cartoon depiction of mitochondrial ultrastructure. Cristae (invaginations of the inner mitochondrial membrane and the predominant site of oxidative phosphorylation) are depicted in yellow, the inner boundary membrane is depicted in blue, the outer mitochondrial membrane in purple, and the mobile electron carrier cytochrome *c* is depicted as a red-coloured circle. The interior blank space is the matrix compartment.

B) Schematic cartoon illustrating the oxidative phosphorylation system within mitochondria. Electrons derived from catabolic processes are delivered to Complex I and Complex II (from NADH and $FADH_2$, respectively) and then passed on to the mobile lipophilic electron carrier molecule ubiquinone ("Q") embedded within the membrane. Electrons from ubiquinol are delivered to Complex III and then passed on to the mobile electron carrier protein cytochrome ("cyt") *c* located in loose association with the inner membrane in the intermembrane space. Subsequently, cytochrome *c* donates electrons to Complex IV, where they are accepted by oxygen (terminal electron acceptor) in its reduction to water. The transport of electrons through the system is coupled to the extrusion of protons to the intermembrane space by Complex I, III, and IV. The resulting electrochemical gradient across the inner mitochondrial membrane yields a proton motive force. The dissipation of this force via proton flow back down the electrochemical gradient through Complex V drives ADP phosphorylation to form ATP.

Notably, mitochondrial oxygen consumption is not perfectly coupled to ATP synthesis, as protons constitutively "leak" across the inner mitochondrial membrane back into the matrix independent of Complex V. Proton leak can also be induced through physiologically-regulated processes (Divakaruni & Brand, 2011), but generally is mediated by certain inner mitochondrial membrane-spanning proteins (e.g. uncoupling proteins, adenine nucleotide translocase) with proton-translocating capability (Erlanson-Albertsson, 2003; Divakaruni & Brand, 2011). Importantly, exogenous small molecules or drugs may artificially stimulate proton leak to dissipate the proton motive force and uncouple electron transfer from ATP synthesis. For example, the chemical carbonylcyanide-ρ-trifluoromethoxyphenylhydrazone (FCCP) mediates proton transfer across membranes, and acts as a potent uncoupler of oxidative phosphorylation (Terada, 1990). Generally, such protonophoric action can be detrimental to oxidative phosphorylation, as ATP synthesis is impaired when there is an insufficient proton motive force.

Oxidative phosphorylation is a major contributor to oxygen consumption in mammals. In the basal state, it is estimated that approximately 90% of total mammalian oxygen consumption is by mitochondria (Rolfe & Brown, 1997). Of this percentage, approximately 80% is estimated to be coupled to ATP synthesis, whereas approximately 20% is uncoupled by proton leak (Rolfe & Brown, 1997). Based on estimates with humans and rats, the brain, heart, liver, and kidney are the major oxygen-consuming tissues in the basal state, and largely contribute to whole-

organismal basal oxygen consumption rate when considering the relatively low proportion of their individual mass to total body mass (Rolfe & Brown, 1997). Generally, oxidative phosphorylation is the preferred metabolic pathway for ATP production in quiescent or differentiated cells (e.g. Lunt & Vander Heiden, 2011). In highly aerobic tissues or cell types, disruptions to oxidative phosphorylation can be potentially detrimental to their ability to perform their normal function(s), and may even lead to cell death if too severe (e.g. if there is prolonged oxygen depletion; Kalogeris et al., 2012). Notably, dissipation of mitochondrial membrane potential by drugs is being increasingly recognized as a major mode of drug toxicity that can limit drug utility in these tissues (Nadanaciva & Will, 2009).

Given the importance of oxidative phosphorylation to ATP synthesis, it is important to test the functional integrity of this system under experimental conditions of interest (e.g. in the presence of a drug candidate). Since electron transport is coupled to proton extrusion across the inner mitochondrial membrane in both mitochondria and cells, the rate of mitochondrial oxygen consumption can serve as an accurate measure of total proton current (Brand & Nicholls, 2011). With the use of an oxygen-sensitive electrode, experiments can be designed to measure proton current in isolated mitochondria, permeabilized cells, intact cells, and tissue slices to assess basic processes of oxidative phosphorylation, and thus characterize mitochondrial energetic (dys)function (Chance & Williams, 1955; reviewed in Brand & Nicholls, 2011). Other ways to assess potentially impaired oxidative phosphorylation can include measurements of mitochondrial membrane potential, which can be achieved using fluorescent membrane permeant-cationic dyes whose mitochondrial uptake/fluorescence are dependent on mitochondrial membrane potential (e.g. Perry et al., 2011; Brand & Nicholls, 2011; Nicholls, 2012).

1.4 Glucose metabolism:

Glucose is a major substrate fueling mammalian energy metabolism. Glucose is catabolised by glycolysis, which converts glucose into pyruvate through a series of ten enzyme-catalyzed reactions within the cytosol. In total, the completion of the pathway generates a net yield of two ATP molecules via substrate-level phosphorylation, two molecules of the reduced coenzyme nicotinamide adenine dinucleotide (NADH), and two molecules of pyruvate per molecule of glucose. The end-product pyruvate can be imported into mitochondria and enter the TCA cycle, which generates the reduced intermediates NADH and $FADH_2$ (reduced flavin adenine nucleotide) that provide electrons for oxidative phosphorylation for aerobic ATP production. Alternatively, pyruvate can remain in the cytosol, where it may be enzymatically converted to lactic acid. This latter pathway utilization is referred to as "lactate fermentation", and additionally results in NAD^+ regeneration necessary to sustain cytosolic ATP production via substrate-level phosphorylation. From the perspective of ATP yield, the cellular ATP yield from glycolysis alone is relatively low (i.e. 2 net ATP molecules produced per glucose molecule) compared to oxidative phosphorylation (i.e. up to approximately 36 ATP molecules per glucose molecule) (Pape et al., 2012). Importantly, however, glycolysis intermediates can branch into other metabolic pathways (e.g. pentose phosphate shunt) to provide carbon to be used for the biosynthesis of macromolecules (e.g. nucelotides, amino acids, lipids) rather than ATP (Lunt & Vander Heiden, 2011).

1.5 Proliferating mammalian cells predominantly utilize aerobic glycolysis:

Proliferating mammalian cells, whether they are cancerous or normal, tend to preferentially direct glycolysis-derived pyruvate to lactate rather than to mitochondria for oxidative phosphorylation (Vander Heiden et al., 2011). This fermentative metabolism is termed "aerobic glycolysis", as it occurs even in the presence of oxygen. The predominant usage of

aerobic glycolysis by such cell types is in contrast to the energy metabolism of non-proliferative, differentiated cell types (e.g. neurons, cardiomyocytes), which generally are more reliant on oxidative phosphorylation to meet the ATP demands. Mitochondria of proliferative cells generally are still fully functional (Vander Heiden et al., 2009; Zheng, 2012). Thus, the increased usage of aerobic glycolysis has been proposed to be a metabolic adaptation of proliferative cells to serve needs other than ATP production. This is thought to predominantly involve the incorporation of glycolytically-derived carbon intermediates into biomass (e.g. nucleotides, amino acids, lipids), which is required for the production of daughter cells during cell division (Vander Heiden et al., 2009; Mulukutla et al., 2010; Lunt & Vander Heiden, 2011).

1.6 Manipulation of cellular energy metabolism of cultured cells:

Cell lines are useful tools for studying biological phenomena and in drug development. Cultured cells are usually grown under conditions stimulating high rates of proliferation. Under these conditions, cultured cells preferentially utilize aerobic glycolysis rather than oxidative phosphorylation. This renders them less sensitive to perturbations of oxidative phosphorylation than cells with a more aerobic metabolic phenotype (Marroquin et al., 2007). This characteristic has important ramifications – prospective drug molecules that perturb oxidative phosphorylation may be better tolerated by cells utilizing primarily aerobic glycolysis to meet ATP demand.

Since glucose is catabolized primarily by aerobic glycolysis in cultured cells, providing an alternative carbohydrate source in culture media can influence cellular energy metabolism. With this in mind, replacement of glucose with galactose has been used to increase reliance on oxidative phosphorylation (e.g. Marroquin et al., 2007). Galactose can be converted to glucose for subsequent entry into glycolysis, however, the conversion of a galactose molecule to a glucose molecule consumes ATP and therefore prevents a net ATP gain from the glycolytic production of pyruvate (Holden et al., 2004). As a result, cells are forced to utilize other

metabolic substrates provided in the culture medium for ATP generation. This predominantly involves enhanced mitochondrial catabolism of the amino acid glutamine (Meister, 1956; Reitzer et al., 1979; Zielke et al., 1976; Kovacevic & McGivan, 1983; Rossignol et al., 2004; DeBerardinis et al., 2007). For example, when galactose replaced glucose as the main carbohydrate source in the culture medium for HeLa cells, greater than 98% of cellular ATP was provided by glutamine oxidation through the TCA cycle (Reitzer et al., 1979). Enhanced glutamine utilization for ATP production has been similarly observed with other proliferative cells in culture provided with a non-fermentable carbohydrate source, and has been proposed as a general phenomenon with proliferative cell types (Zielke et al., 1984; Neerman & Wagner, 1996).

With forced reliance on oxidative phosphorylation from enhanced glutamine utilization, cells display an elevated aerobic metabolism that includes measurably higher rates of cellular oxygen consumption and lowered glycolytic activity (e.g. Rossignol et al., 2004; Marroquin et al., 2007; Aguer et al., 2011; Gusdon et al., 2012; Swerdlow et al., 2013). This renders cells more dependent on the functional integrity of the mitochondrial energetics system, and consequently more sensitive to disrupted oxidative phosphorylation (Marroquin et al., 2007). With this in mind, glucose-free, galactose/glutamine-containing media has been used in cell culture studies to identify defective mitochondrial respiratory function in cultured cells derived from patients with mitochondrial disorders or other diseases (Robinson et al., 1992; Aguer et al., 2011), as well as to screen small molecules or drug candidates for mitochondrial energetic toxicity (Marroquin et al., 2007; Dykens et al., 2008; Rana et al., 2011).

1.7 Mitophagy – process of selective mitochondrial degradation:

Autophagy (from the Greek words *auto* “self”, and *phagein* “to eat”) is a physiological process that involves the orderly degradation of intracellular contents for recycling purposes (De

Duve, 1966; Levine & Klioncky, 2004). The process features a program of sequential events that includes sequestration of intracellular proteins and organelles by double-membrane vesicles (termed "autophagosomes") and delivery to acidic lysosomes, where hydrolytic degradation takes place to liberate products that may be recycled for use in anabolic or catabolic processes (Mizushima, 2007). In addition to the bulk degradation of intracellular contents (termed 'macroautophagy"), autophagy may be selective for specific organelles, including mitochondria. The mitochondria-selective form of autophagy is termed "mitophagy" (Lemasters, 2005).

Mitophagy has been increasingly recognized as an important process for homeostatic quality control of mitochondria. It is involved in routine mitochondrial turnover, and can also be stimulated when mitochondria are defective or have impaired function (Ashrafi & Schwarz, 2012). For example, depolarization of the mitochondrial membrane potential by chemical uncoupling can lead to the selective recruitment of mitophagy machinery and subsequent lysosomal degradation of mitochondria within cells (Narendra et al., 2008; Narendra et al., 2010; Sun et al., 2012). In this context, mitophagy serve as an important coordinated role with other cellular processes (e.g. mitochondrial biogenesis) that ensure necessary mitochondrial content is maintained within the cell (Detmer & Chan, 2007). Experimentally, mitophagy can be identified in a number of ways, including co-localization of mitochondria with autophagosome machinery and delivery into lysosomes (Ding & Yin, 2012). Additionally, mitophagy can be reflected as an apparent decrease in mitochondria-specific content (e.g. mitochondrial proteins, mitochondrial DNA, cardiolipin, etc) within cells (Ding & Yin, 2012).

1.8 Mitochondrial dynamics in energetics, mitophagy, and cell death:

Due in large part to static, electron microscopy techniques, mitochondria have been classically looked upon as singular, discrete organelles. However, the advent of live-cell confocal microscopy has yielded a more accurate depiction of mitochondrial morphology. It is

now apparent that mitochondria exist in a complex network representing a dynamic equilibrium between fusion and fission (reviewed in McBride et al., 2006). Generally, their morphology can fluctuate between a highly fused, interconnected reticulum or network and a fragmented state with smaller networks and/or discrete, individual puncta or rod-like structures. The ongoing shaping of mitochondrial network morphology is tightly controlled by various proteins that catalyze pro-fusion or pro-fission events on either the outer or inner mitochondrial membranes (e.g. reviewed in Soubannier & McBride, 2009). Interestingly, mitochondrial morphology appears to be closely associated with function in energy metabolism, their own quality control processes that cooperates with intracellular machinery, cell death, and other cellular activities (Babbar & Sheikh, 2013).

Energetic status of mitochondria within cells has been observed to be associated with different morphologies. In human ovarian cancer HeLa cells forced to have increased reliance on oxidative phosphorylation for ATP production, a more highly fused, elongated mitochondrial network existed in comparison to when cultured in a glucose-containing, fermentable medium (Rossignol et al., 2004). In rat kidney epithelial cells, elevated ATP production was observed when the mitochondrial network was present in a highly fused state at the G1-S transition phase of the cell cycle (Mitra et al., 2009). Conversely, a more fragmented mitochondrial network has generally been observed in cultured cells exposed to chemical uncouplers of oxidative phosphorylation or inhibitors of respiratory chain components that disrupt mitochondrial membrane potential and ATP production (e.g. Legros et al., 2002; Ishihara et al., 2003; Benard et al., 2004; De Vos et al., 2005; Barsoum et al., 2006; Liot et al., 2009; Liu & Hajnóczky, 2011; Toyama et al., 2016). These findings suggest that fused mitochondrial network is more conducive for increased ATP production, whereas a fragmented network is associated with decreased energetic efficiency and lowered ATP production. The exact functional advantage(s) to explain increased mitochondrial ATP production when mitochondria are in a more fused state

are unclear, but may involve increased efficiency (i.e. coupling) of the system as a result of greater complementation of biomaterials involved in oxidative phosphorylation (e.g. metabolites) and electrical continuity (e.g. Youle & van der Bliek, 2012). Regardless of the exact reason(s), identifying changes in mitochondrial morphology can be useful indices of possible changes to energetic properties of mitochondria within a cell. For example, observing fragmentation of mitochondria in response to an exogenously applied drug candidate of interest may be indicative that the molecule exerts toxicity to mitochondrial bioenergetics.

Other examples of mitochondrial morphology changes within cells can include both processes of mitochondrial quality control and apoptotic cell death. The fission of mitochondria with sufficiently impaired energetics (e.g. prolonged dissipation of membrane potential) enables selective degradation of mitochondria from the network, possibly to maintain a healthy pool of proper functioning mitochondria (Twig et al., 2008; Ashrafi & Schwarz, 2012). Under lethal conditions, fragmentation of the mitochondrial network facilitates events that stimulate apoptotic cell death (Karbowski & Youle, 2003; Suen et al., 2008). The involvement of mitochondrial morphology under these two processes is presently an active area of research. Nonetheless, identifying mitochondrial shape changes under conditions of interest can provide useful clues that such processes are potentially occurring.

1.9 Targeting small molecules to mitochondria:

Given the importance of mitochondrial events in apoptosis, directly targeting mitochondrial apoptotic processes with small molecules could be a way to prevent cell death where appropriate. The mitochondrial membrane potential resulting from a functioning electron transport system causes the interior compartment of mitochondria to be substantially more negatively charged with respect to the extra-mitochondrial environment (Kamo et al., 1979;

Azzone et al., 1984; Haraldsdóttir et al., 2012). This membrane potential is a potentially exploitable property for drug delivery to mitochondria.

A general class of molecules that feature chemical properties conducive for mitochondrial targeting is lipophilic cations. These molecules possess a positive charge and yet are relatively lipid soluble. Consequently, they can essentially be "electrophoresed" across biological membranes through simple diffusion rather than protein-mediated import. The accumulation of a singly positively charged lipophilic cation is proportional to membrane potential (Ψ) (Ross & Murphy, 2011), as described by the Nernst equation:

$$\Delta\Psi = 61.5 log_{10}\left(\frac{[cation\ in]}{[cation\ out]}\right) \qquad at\ 37°C$$

This relationship translates to an approximate ten-fold accumulation of the cation for every approximate 60 mV difference in electrical potential across a membrane. The plasma membrane typically possesses a membrane potential of -30 to -60 mV (negative inside; Azzone et al., 1984), meaning that lipophilic cations will accumulate approximately five-to-ten-fold within the cytosol. Since the mitochondrial membrane potential in live cells is typically -120 to -160 mV (Kamo et al., 1979), lipophilic cations further accumulate several-hundred-fold within mitochondria (Ross & Murphy, 2011).

One lipophilic cation that has been well-utilized for mitochondrial targeting is triphenylphosphonium (TPP), which features a single positive charge that is screened or delocalized over a large hydrophobic surface area (see **Fig. 1.4** for schematic depiction of cellular and mitochondrial uptake of a prototypical TPP-containing molecule). The first use of a TPP molecule in mitochondrial biology came in the late 1960's by Vladimir Skulachev and colleagues, who showed that a TPP-cation accumulated within mitochondria during respiration due to the large mitochondrial membrane potential (Liberman et al., 1969; Bakeeva et al., 1970). Over the next several decades, TPP-cations were often used in conjugation with TPP-compatible

electrodes as a tool to investigate mitochondrial membrane potential (e.g. Kamo et al., 1979; Nobes et al., 1990). However, the use of TPP cations in biomedical applications was pioneered beginning in the mid-1990's by Mike Murphy, who reasoned that attachment of bioactive compounds to TPP cations could be used to deliver mitochondria-targeted therapeutics (Murphy, 1997). His research group later synthesized a mitochondria-targeted antioxidant consisting of a TPP-moiety attached to the antioxidant ubiquinone – termed "MitoQ" (Kelso et al., 2001). The interactions with mitochondria of this molecule and other similar derivatives have been well-characterized (e.g. Kelso et al., 2001; Asin-Cayuela et al., 2004; Murphy & Smith, 2011). These molecules are able to effectively limit both oxidant levels within mitochondria and accumulation of mitochondria/intracellular oxidative damage, and can exert protective effects in a variety of pathological contexts both *in vitro* and *in vivo* (reviewed in Smith & Murphy, 2010). The proof of efficacy of this small molecule, together with a growing understanding of fundamental mitochondrial biochemical processes in mammalian health and disease, have subsequently garnered vast interest in developing novel TPP-cation based mitochondrial therapeutics with potentially greater target specificity and enhanced modulatory properties.

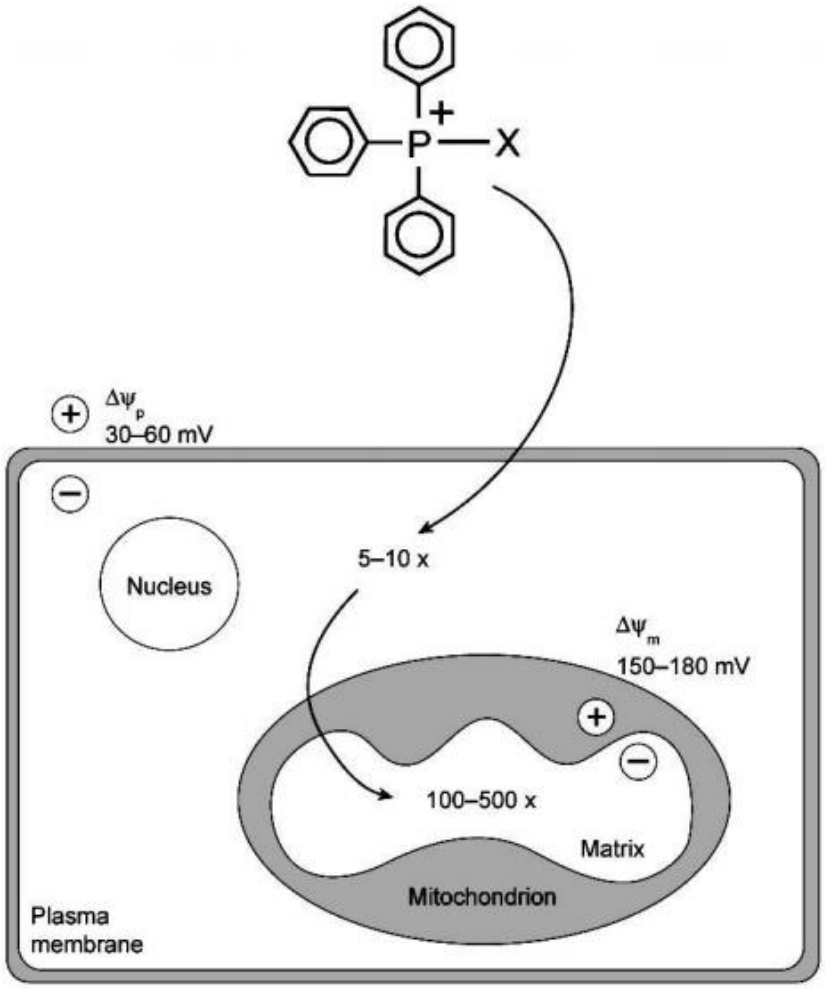

Figure 1.4: Uptake of a prototypical TPP-conjugated compound. The prototypical TPP-molecule conjugated to an "X" bioactive moiety first accumulates 5-10-fold in the cytosol as a result of the plasma membrane potential ($\Delta\Psi_p$), and then further accumulates several h undred-fold in mitochondria as a result of the mitochondrial membrane potential ($\Delta\Psi_m$). Figure taken from Ross et al. (2005).

1.10 TPP-IOA is a mitochondria-targeted inhibitor of apoptosis:

Considering that the peroxidase activity exhibited by cytochrome *c*/cardiolipin complexes is crucial to the release of pro-apoptotic factors, the design of inhibitory agents to disrupt this complex has been proposed to be a promising novel strategy for modulating apoptosis (Kagan et al., 2009b). Once cytochrome *c* and cardiolipin are tightly bound, peroxidase activity in cytochrome *c* is induced through partial unfolding of the protein and weakening of the heme-iron coordination bond to Met80. This structural change allows for improved access of the heme

catalytic site to small molecules, like H_2O_2, that can provide oxidizing equivalents that feed catalysis (Kagan et al., 2005; Kagan et al., 2009b). With this in mind, blocking the availability of the heme catalytic site has been proposed as one strategy to diminish the peroxidase function of this complex (Kagan et al., 2009b; Atkinson et al., 2011).

Imidazole-substituted long chain fatty acids have been invented for this purpose (Kagan et al., 2009b; Atkinson et al., 2011). These molecules were initially intended for potential use as radioprotectors or radiomitigators, as lethal γ–irradiation exposure *in vivo* can cause massive cell death through the mitochondrial apoptotic pathway (Macia i Garau et al., 2011). They were designed on the basis of their carboxyl group being able to interact with Lys residues on cytochrome *c*, and the hydrophobic acyl chain being able to protrude into the hydrophobic pocket within the protein that provides accessibility to the heme iron site. Consequently, the imidazole attached to the oleate chain could potentially interact with the heme-iron of the catalytic site, thus fulfilling heme-iron hexa-coordination and lessening the catalytic site's availability (Kagan et al., 2009b; Atkinson et al., 2011). Indeed, imidazole-substituted oleic (IOA) and stearic acids (ISA) with the imidazole moiety located 7 carbons away from the terminal methyl group were able to interact with the haem-iron of cytochrome *c* (Atkinson et al., 2011). Furthermore, these imidazole-fatty acid derivatives were shown to be effective inhibitors of the peroxidase activity of pure cytochrome *c*/tetra-oleoyl-cardiolipin complexes (Atkinson et al., 2011).

To achieve mitochondrial targeting of these inhibitors, they were chemically conjugated to a TPP moiety (specifically a *3-hydroxypropyl-triphenylphosphonium* molecule). Indeed, TPP-IOA (*3-hydroxypropyl-triphenylphosphonium-conjugated imidazole substituted oleic acid*; **Fig. 1.5a**) administration to cultured mouse embryonic cells via addition to culture medium resulted in rapid accumulation of TPP-IOA within mitochondria (Atkinson et al., 2011). Notably, in addition to the fully intact molecule being present, the two hydrolysis products, 3-

hydroxypropyl-TPP (**Fig. 1.5b**) and the imidazole oleic acid moiety (**Fig. 1.5c**), were each also detectable (the relative abundances are unclear from this report), indicating TPP-IOA can undergo intracellular endogenous hydrolytic processing (Atkinson et al., 2011). Additionally, a single bolus intraperitoneal injection of TPP-IOA to live mice resulted in rapid detectable accumulation within radiosensitive tissues of interest (bone marrow, small intestine; Atkinson et al., 2011), indicating successful *in vivo* uptake.

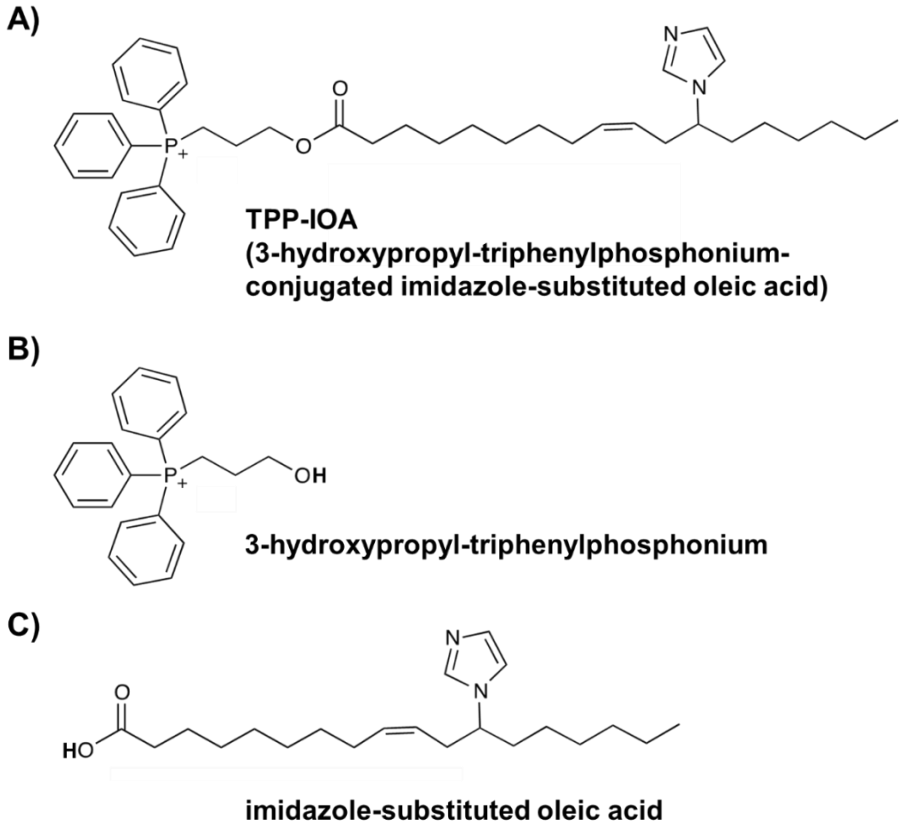

Figure 1.5: Chemical structures of the mitochondria-targeted imidazole fatty acid derivative *a*) TPP-IOA (*3-hydroxypropyl-triphenylphosphonium-conjugated imidazole substituted oleic acid),* and its hydrolysis products *b*) 3-hydroxypropyl-triphenylphosphonium and *c*) imidazole-substituted oleic acid.

Notably, IOA conjugation to the TPP-moiety via esterification (therefore free anionic carboxyl group is not available) did not affect proximity of the imidazole ligand to the heme iron, and nor did it significantly affect the ability for inhibition of peroxidase activity of pure cytochrome *c*/cardiolipin complexes (Atkinson et al., 2011). This suggests that electrostatic

interactions with Lys residues of cytochrome *c* are actually not important for binding of the molecule, while the hydrophobic interaction predominates. Subsequently, in cultured mouse embryonic fibroblasts exposed to lethal doses of γ–irradiation, TPP-IOA suppressed cytosolic cytochrome *c* accumulation, Caspase-3 cleavage, phosphatidylserine externalization, and increased the overall survival (Atkinson et al., 2011). TPP-IOA also limited the abundance of apoptotic mouse lung endothelial cells in response to the mitochondrial respiratory poison and apoptotic trigger rotenone, suggesting the possibility that the anti-apoptotic capabilities may not be stimulus- or cell-type specific. Importantly, the protective effects observed *in vitro* successfully translated *in vivo*, as TPP-IOA profoundly increased whole-organism survival in a rodent model of lethal γ–radiation exposure (Atkinson et al., 2011).

Subsequently, Maddalena (2012) investigated whether TPP-IOA has the potential to limit cell loss resulting from ischemia/reperfusion-like injury (e.g. akin to neuronal cell death following brain ischemia/reperfusion), which involves apoptotic cell loss through the mitochondrial pathway of apoptosis (e.g. Honda et al., 2005; Kalogeris et al., 2012). Here, an *in vitro* cell culture model was utilized in which SH-SY5Y human neuroblastoma cells were transiently deprived of both oxygen and glucose (oxygen/glucose deprivation model; OGD). With TPP-IOA addition following the insult, a detectable prevention of cell loss was observable after a recovery period in comparison to vehicle control-treated cells (**Fig. 1.6**).

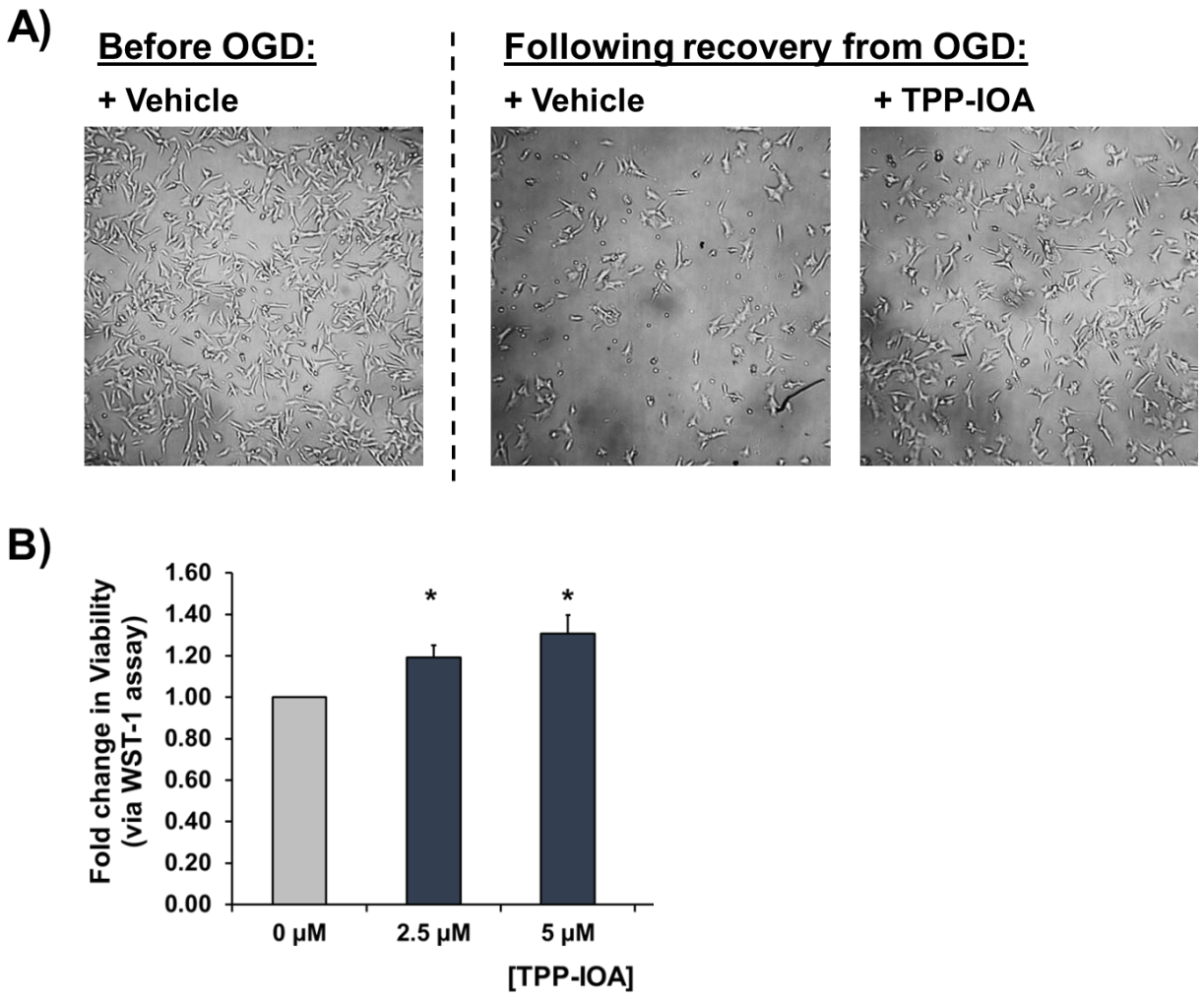

Figure 1.6: TPP-IOA limits the extent of cell loss induced from a transient ischemia-reperfusion-like injury (oxygen/glucose deprivation (OGD) model) in cultured SH-SY5Y human neuroblastoma cells.
A) Brightfield microscopy images of SH-SY5Y cells in culture under basal culture conditions either immediately prior to (***left panel***) or 24 hours after recovery (***right panel***) from eight hours of oxygen- and glucose-deprivation (OGD) reveal that TPP-IOA (5 µM; administered immediately upon restoration of both oxygen and glucose levels) can prevent cell loss resulting from a transient period of OGD. Images are representative fields of views under 100x total magnification. **B)** Water-soluble tetrazolium-1 (WST-1)-based viability assay (performed 24 hours from the onset of OGD recovery) reveals that TPP-IOA improves viability of cells subjected to OGD. Data were standardized to the vehicle control group. * represents p-value < 0.05 (Student's t-test). Figure was adapted from Maddalena (2012).

1.11 TPP-IOA's interaction with energetics:

In the only previous assessment of TPP-IOA's impact on mitochondrial energetics, total cellular ATP levels were measured 48 hours from the addition of TPP-IOA to proliferative

mouse embryonic cells under standard culture conditions. Here, an absence of an effect was reported (*Note:* TPP-IOA concentrations and data not provided; Atkinson et al., 2011). However, considering the predominant use of aerobic glycolysis/lactate fermentation of proliferative cells and resultant decreased sensitivity to toxins affecting mitochondrial energetics (Marroquin et al., 2007), the interpretation of TPP-IOA's impact on mitochondrial energetics from the existing data is limited. The interpretation may be further limited by the long duration between TPP-IOA addition and measurements (48 hours), as compensatory transcriptional adaptations to decreased mitochondrial ATP output are possible in this timeframe (e.g. proliferation of mitochondria or downregulation of ATP consuming processes, etc, caused via activation of the major intracellular energy sensing protein AMP-kinase; Hardie, 2011). Thus, TPP-IOA's interaction with mitochondrial energetics is unclear from existing data.

Crucially, many cell types of great biomedical interest with limited regenerative capability are typically highly aerobic and reliant on mitochondria to meet their ATP demand. With this in mind, it is important to note that the existing *in vitro* data for TPP-IOA's protective effects comes from proliferative cells cultured under standard conditions that are heavily glycolytic. Additionally, the existing *in vivo* protective data comes from a pathological state (radiation poisoning) in which the predominantly affected cells are highly proliferative and predominantly utilize aerobic glycolysis (Macia i Garau et al., 2011; Lunt & Vander Heiden, 2011). Therefore, there is no definitive evidence that TPP-IOA can be effective at limiting cell death in highly aerobically-active cell types that are otherwise more sensitive to acute drug-induced toxicities to mitochondrial energetics. With this in mind, understanding TPP-IOA's interaction with mitochondrial energetics is important for potentially expanding its anti-apoptotic utility to other *in vivo* pathological states affecting highly aerobic tissues (e.g. heart, brain).

1.12 Project Objectives, Proposed Approaches, and General Hypothesis:

Given the prevention of cell death previously observed in various *in vitro* and *in vivo* models, the mitochondria-targeted small molecule TPP-IOA has potential as an effective therapeutic agent in other pathologies involving cell death through the mitochondrial pathway of apoptosis. The pathological contexts in which TPP-IOA has been demonstrably effective to date have involved pathologies and/or experimental models where the predominantly affected cell types (i.e. proliferative gastrointestinal tract cells, hematopoietic cells, and various cells in culture) meet their ATP demands through fermentative metabolic pathways rather than oxidative phosphorylation. Crucially, many cell types of great biomedical interest (e.g. neurons, cardiomyocytes) feature a highly aerobic energy metabolism, and are reliant on oxidative phosphorylation. Since TPP-IOA is targeted to mitochondria and interacts directly with cytochrome *c*, it has the potential to directly interfere with oxidative phosphorylation. However, TPP-IOA's direct interaction with oxidative phosphorylation is unknown. If TPP-IOA does indeed perturb activity of mitochondrial energetics, its protective efficacy may be limited in cell types that are heavily reliant on oxidative phosphorylation, which could limit potential future therapeutic applications. With this in mind, the overall general aim of this thesis was to investigate the anti-apoptotic utility of TPP-IOA from a bioenergetics perspective. The experimental objectives and accompanying *in vitro* approaches are as follows:

1) Since the target protein, cytochrome *c*, also possesses an electron transfer activity that is critical for oxidative phosphorylation, does the interaction of TPP-IOA with cytochrome *c* affect this activity? Furthermore, if this occurs, then does it occur at concentrations similar to those required to inhibit cytochrome *c*'s pro-apoptotic oxidative activity? For investigations aimed at the direct effects of TPP-IOA on its target protein, biochemical assay systems containing purified cytochrome *c* were used. A spectrophotometry-based

assay measuring reduction activity and a spectrofluorometry-based assay of peroxidase activity were each utilized.

2) Since the target organelle, the mitochondrion, is the major site of ATP generation through oxidative phosphorylation, can TPP-IOA interfere with mitochondrial oxidative phosphorylation? Furthermore, if such disruption occurs, then does it occur at concentrations similar to those required for inhibition of pro-apoptotic oxidative activity? For investigations aimed at elucidating the direct effects of TPP-IOA on its target organelle, closed-system respirometry measuring mitochondrial respiratory states and a spectrofluorometry-based assay of pro-apoptotic oxidative activity were utilized with isolated rat liver mitochondria.

3) Does TPP-IOA interfere with energetics or related mitochondrial physiology in intact cells? If there is any such impact, then does cellular reliance on mitochondrial oxidative phosphorylation limit TPP-IOA's ability to prevent cell death in response to apoptotic stimuli? A cell culture approach was used to address these questions. To assess energetics, a combination of closed-system respirometry for metabolic rate measurements and confocal imaging-based qualitative assessment of mitochondrial membrane potential were performed. Additionally, a combination of confocal microscopy, immunoblot, and a spectrophotometric enzyme activity assay were used to determine effects of TPP-IOA and related molecules on mitochondrial network morphology. Finally, apoptotic cell death was studied in cells cultured with different culture media compositions to increase reliance on oxidative phosphorylation. Cell death was evoked by an apoptotic stimulus and cell viability was assessed using a Trypan blue exclusion assay together with a spectrofluorometric activity assay of the apoptosis marker Caspase-3.

Overall, it is hypothesized that TPP-IOA can interfere with energetic processes of mitochondria, and that this could limit its protective efficacy in cells that are reliant on mitochondrial oxidative phosphorylation.

Chapter 2.0 - Experimental Methodology:

2.1 Materials:

3-hydroxypropyl-triphenylphosphonium (Catalogue #S860166), cytochrome *c* (from bovine heart; Cat. # C3131), cardiolipin solution (from bovine heart; ≥80% polyunsaturated fatty acid content, primarily linoleic acid; in ethanol Cat. #C1649), ascorbic acid, tert-butyl hydroperoxide aqueous solution (70% w/w; Cat. #B2633), Dulbecco's Modified Eagle Medium powdered media with glucose (4500 mg/L), L-glutamine, and sodium pyruvate (Cat. #D7777), supplement-free Dulbecco's Modified Eagle Medium powdered media (Catalogue #5030), fetal bovine serum (Cat. #F1051), nonessential amino acids, penicillin/streptomycin solution, 0.25% trypsin/EDTA solution, and bovine serum albumin (BSA) were obtained from Sigma-Aldrich (St. Louis, USA).

Dimethylsulfoxide (DMSO), DL-dithiothreitol (DTT), Bradford reagent, D-galactose, L-glutamine, HEPES ((4-(2-hydroxyethyl)-1-piperazineethanesulfonic acid), and Trypan Blue were obtained from BioShop (Burlington, ON, Canada).

Amplex Red reagent (10-Acetyl-3,7-dihydroxyphenoxazine; Item 10010469) was obtained from Cayman Chemical (Ann Arbor, MI, USA).

The Caspase-3 fluorogenic substrate Ac-DEVD-AMC (Cat. #556449) and Caspase-3 inhibitor Ac-DEVD-CHO (Cat. #556465) were both obtained from BD Biosciences (Franklin Lakes, NJ, USA).

Tissue culture dishes (100x20 mm & 60x15 mm) and cell scrapers were obtained from Sarstedt, Inc (Newton, SC, USA).

MitoTracker Red CMXRos and Lipofectamine 2000 transfection reagent were purchased from Life Technologies Incorporated (Burlington, ON, Canada).

Goat (C-11) polyclonal Actin antibody (Product #sr-1615) raised against a peptide fragment of the C-terminus of human Actin was purchased from Santa Cruz Biotechnology, Inc. (Dallas, TX, USA).

Rabbit polyclonal VDAC antibody (Product #600-401-882) raised against a synthetic peptide corresponding to amino acids 185 – 197 of human VDAC1 and infrared dye-conjugated secondary (IgG) antibodies to rabbit (Cat. # 611-132-122) and goat (Cat. #605-732-125) were all purchased from Rockland Immunochemicals (Gilbertsville, PA, USA).

Unless otherwise indicated, all other chemicals, reagents, and solutions were purchased from Sigma-Aldrich (St. Louis, MO, USA), BioSHOP (Burlington, ON, Canada), or Fisher Scientific (Mississauga, ON, Canada).

2.2 Preparation of reagents, stock solutions, and buffers:

TPP-IOA and TPP-OA were obtained from Dr. Jeffrey Atkinson (Brock University; see Atkinson et al., 2011 for chemical synthesis of TPP-IOA). TPP-IOA, TPP-OA, and 3-hydroxypropyl-TPP (**Fig. 2.1** below) were dissolved in sterile-filtered DMSO. Stock solutions of each were made via serial dilutions and stored as small volume aliquots (typically 35 µL) at -20°C and protected from light. Phosphate-buffered saline (PBS; 1X) consisted of 137 mM NaCl, 2.7 mM KCl, 10 mM Na_2HPO_4, 2 mM KH_2PO_4, pH adjusted to 7.4. PBS-t (1X) consisted of PBS with 0.1% (v/v) Tween-20 detergent. For isolation of mitochondria (section 2.2.5 below), SHE buffer consisted of 250 mM sucrose, 10 mM HEPES, and 1mM EGTA, final pH adjusted to 7.5, and SHE+BSA buffer consisted of SHE buffer with 0.5% (*w/v*) bovine serum albumin (delipidated, fraction V), final pH adjusted to 7.5. Mitochondrial respiration buffer consisted of 125 mM sucrose, 65 mM KCl, 10 mM HEPES, and 2 mM KH_2PO_4, pH adjusted to 7.2. Trypan blue solution (0.4% *w/v*) was prepared in 0.81% NaCl and 0.06% K_2HPO_4. Cell lysis buffer (1X) consisted of 10 mM Tris-HCl, 10 mM NaH_2PO_4, 130 mM NaCl, 1% Triton-X-100, 10 mM

sodium pyrophosphate, pH 7.5. Caspase-3 activity assay buffer (1X) consisted of 20 mM HEPES (pH 7.5), 10% glycerol, 2 mM DTT. MitoTracker Red CMXRos, and TMRM each at 1 mM were made using DMSO and stored at -20 in small aliquots. All aqueous buffers/solutions were prepared using ultrapure deionized water obtained from a Milli-Q water purification system (MilliPore Ltd, Etobicoke, ON, Canada).

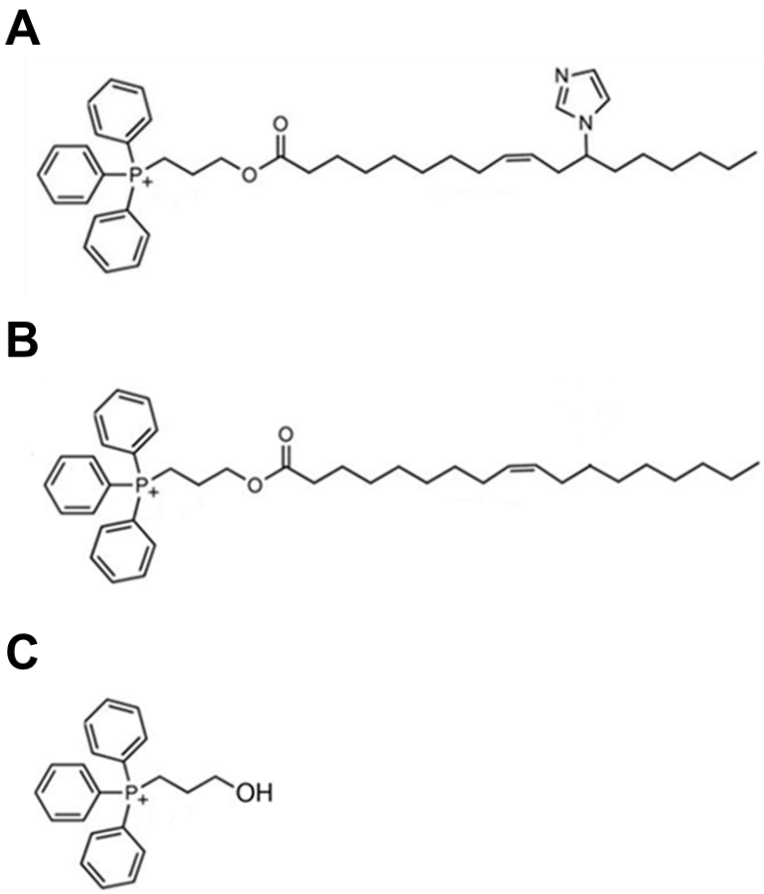

Figure 2.1: Chemical structures of *A)* TPP-IOA, *B)* TPP-OA (TPP-IOA devoid of an imidazole group), and *C)* 3-hydroxypropyl-TPP.

2.3 Cytochrome c/cardiolipin complex peroxidase activity:

Peroxidase activity of pure cytochrome *c* in the presence of cardiolipin was assessed with Amplex Red reagent [similarly to as described in Atkinson et al., (2011) and Birk et al., (2013)] using a Varian Cary Eclipse fluorescence spectrophotometer equipped with microplate reader (Agilent Technologies, Santa Clara, CA, USA). This spectrofluorometric assay measures the

formation of resorufin – the fluorescent oxidation product of Amplex Red reagent generated in the presence of peroxidase enzymatic activity (Zhou et al., 1997). To perform the assay, cytochrome *c* (1 μM; from bovine heart) was incubated within HEPES buffer (20 mM, pH 7.4) with purified cardiolipin (15 μM; ≥80% polyunsaturated fatty acid content, primarily linoleic acid, from bovine heart) with or without the TPP-conjugated molecules for 10 minutes while hidden from light, before addition of hydrogen peroxide and Amplex Red reagent each at a final concentration of 50 μM. The formation rate of resorufin was continuously measured over approximately 10 minutes following peroxide and Amplex Red additions using excitation and emission wavelengths of 525 nm and 590 nm, respectively. Maximal reaction rates [Arbitrary Fluorescence Units (AFU) per minute] were calculated from the initial linear range of resorufin formation using the instrument software Cary Eclipse Kinetics (Walnut Creek, USA). The final amount of DMSO in each assay was 0.1%. The assay was performed at room temperature with protection from light.

2.4 Isolation of liver mitochondria:

Mitochondria from liver tissue of 10 - 12 month old female Long Evans rats (obtained from Charles River Laboratories, Sherbrooke, QE, Canada; whole body weight ranged from approximately 350 grams – 450 grams) were isolated essentially as described in Stuart et al., (2005). Animals were euthanized in accordance with protocols approved by Brock University Animal Care Committee, which involved overdose by isoflurane inhalation and subsequent heart excision. All steps of mitochondria isolations were completed on ice or at 4°C. Liver tissue was immediately excised, washed several times with PBS, then finely minced using a straight edge razor blade, and transferred to a 50 mL centrifuge tube before being rinsed several times with PBS to remove blood. Minced tissue was then re-suspended in SHE + BSA buffer and centrifuged at 1,000 *x g* for 10 minutes. The resulting blood-containing supernatant was

discarded, and the pellet was re-suspended in fresh SHE+BSA buffer. The tissue suspension was then homogenized by hand using a pre-chilled Potter-Elvehjem polytetrafluoroethylene (PTFE) pestle and glass tube. Tissue homogenate was centrifuged at 500 *x g* for 12 minutes, and the resulting supernatant was subsequently transferred to a fresh centrifuge tube and centrifuged at 9,500 *x g* for 10 minutes. The pellet containing the mitochondrial fraction was gently re-suspended in SHE buffer and centrifuged again at 9,500 *x g* for 10 minutes. The resulting pellet containing the final mitochondrial fraction was gently re-suspended in SHE buffer. Protein concentration of the final mitochondrial suspension was then determined spectrophotometrically using the Bradford reagent/method with BSA as the protein standard. The entire isolation process from tissue harvest to protein concentration determination was performed within approximately 120 minutes. The final mitochondria-containing suspension was stored on ice throughout the duration of subsequent experiments (i.e. peroxidase activity and respiration assays) that were performed within 10 hours of the isolation.

2.5 Mitochondrial peroxidase activity:

Measurements of peroxidase activity of freshly isolated mitochondria were performed essentially as in Atkinson et al. (2011) using an Amplex-based assay. Here, the organic peroxide tert-butyl hydroperoxide (tBOOH) was used as both an inducer of cytochrome *c* peroxidase (interacts similarly as cardiolipin; Belikova et al., 2006; Belikova et al., 2009; Yanamala et al., 2014) and a source of oxidizing equivalents rather than hydrogen peroxide to avoid decomposition by endogenously high levels of the hydrogen peroxide-detoxifying enzyme catalase within liver mitochondria. Mitochondria (0.25 mg/mL) freshly isolated from rat liver were incubated in HEPES buffer (20 mM, pH 7.4) with or without the TPP-conjugated molecules for ten minutes before addition of 2mM tBOOH and 50 μM Amplex Red reagent. The final amount of DMSO in each assay was 0.05%. The maximal formation rate of resorufin as a

proxy for peroxidase activity was calculated as in section 2.2.3, above. All peroxidase activity assays were performed with 96-well microplates maintained at room temperature under ambient and dark conditions.

2.6 Reduction of cytochrome c *by ascorbate:*

Ascorbate was used to reduce cytochrome *c* due to it possessing a lower redox potential than cytochrome *c* (Lide, 1994) and thus a propensity to readily reduce the heme iron. Cytochrome *c* (1 μM final concentration), and immediately thereafter TPP-IOA, 3HP-TPP, or TPP-OA, were added to a 1.5 mL polystyrene cuvette containing HEPES buffer (20 mM, pH 7.4). The final amount of DMSO present in each assay cuvette was 0.1%. The mixture was briefly vortexed and then allowed to incubate protected from light at room temperature under ambient conditions for 10 minutes. The cuvette was subsequently placed inside a Varian Cary-100 Bio UV-Vis spectrophotometer, wherein 1 μM ascorbic acid was added and the entire solution was rapidly mixed using a micropipette. The formation of an absorption peak at 550 nm, the characteristic peak of reduced heme iron of cytochrome *c* (Moore & Pettigrew, 1990), was recorded over approximately 10 minutes. The maximal rate of reduction (ΔAbsorbance per minute) was calculated from the initial linear range of 550 nm peak formation using the instrument software Cary WinUV Kinetics (Walnut Creek, USA).

2.7 Mitochondrial respiration measurements:

Oxygen consumption rates of freshly isolated rat liver mitochondria were measured at 25°C within a thermostatically-controlled closed chamber using a Clark-type oxygen electrode (Rank Brothers Dual Digital Model 20 Respirometer; Bottisham, United Kingdom) attached to a polygraph recorder. Prior to commencing measurements, the device was calibrated using air-saturated mitochondrial respiration buffer warmed to the experimental temperature. One

milligram per millilitre suspension of mitochondria in respiration buffer was first added to the respirometer chamber, followed by addition of TPP-IOA or 3HP-TPP. The final percentage of DMSO in the chamber was 0.1%. After 5 minutes of being open to atmosphere, the chamber was capped and a stable reading of baseline oxygen consumption rate was obtained.

To subsequently assess mitochondrial respiratory states, an experimental paradigm similar in principle to the classic experiments of Chance and Williams (1955) was followed. Briefly, the respiratory substrates glutamate and malate (5 mM final concentration of each) were each added to the closed chamber to achieve State 2 respiration. After reaching a stable rate of oxygen consumption, a finite amount of ADP (250 μM final) was added to stimulate State 3 respiration (representative of ADP-phosphorylating respiration or oxidative phosphorylation capacity). State 4 respiration (representative of non-phosphorylating respiration) was determined from the stable slowed rate apparent following State 3 respiration. Notably, oxygen levels in the chamber were ensured to not drop below approximately 20% saturation in order to avoid potential back diffusion of oxygen into the chamber and a resultant artefactual slowed respiration rate. To measure fully uncoupled respiration rates (representative of electron transport system capacity), the same experimental paradigm was followed except the chemical protonophore FCCP at a final concentration of 2 μM was added to the chamber after a steady State 2 respiration rate was reached. All chart slope values from the polygraph recordings were converted to nanomol O_2 consumed · $minute^{-1}$ · milligram mitochondrial $protein^{-1}$.

2.8 Cell culture:

SH-SY5Y human neuroblastoma cells, and in some instances C2C12 murine myoblasts, were used for experiments. SH-SY5Y neuroblastoma cells (ATCC, Manassas, VA, USA) and C2C12 myoblasts were grown in Dulbecco's Modified Eagle Medium (DMEM) supplemented with 10% fetal bovine serum (FBS), 4500 mg/L glucose, 4 mM L-glutamine, 1 mM sodium

pyruvate, 2x MEM nonessential amino acid solution, and penicillin (50 I.U./mL) / streptomycin (50 µg/mL) solution. Cells were cultured in a humidified 5% CO_2 atmosphere within a Thermo Forma Series II water-jacketed CO_2 incubator maintained at 37°C. Cells were grown and expanded in culture on 100 mm diameter culture plates and subcultured at a split ratio of 1:5 once approximately 80% confluence was reached. To subculture, growth medium was removed, plates were rinsed with PBS, and then 0.25% Trypsin/EDTA solution was added to plates for approximately 3 minutes to detach cells from the plates. Once cells were visibly detached, FBS-containing culture media was added to neutralize trypsin action. Cell suspensions were then collected into conical tubes, and centrifuged for 5 minutes at 240 *x g*. The resulting supernatant was discarded, and the cell pellet was re-suspended with fresh growth media. One millilitre of the resulting cell suspension was added throughout the growth surface of each new culture plate already containing freshly added growth media, and plates were placed back into the culture incubator.

For experiments involving galactose-containing culture medium, SH-SY5Y cells grown in glucose-containing media (as above) were harvested using the splitting procedure above and were seeded onto 100 mm culture plates containing medium that consisted of glucose-free DMEM supplemented with 10% fetal bovine serum, 10 mM galactose, 6 mM L-glutamine, 10 mM HEPES, 1 mM sodium pyruvate, 2x MEM nonessential amino acid solution, and penicillin (50 I.U/mL) / streptomycin (50 µg/mL) solution. These cells were cultured under the same ambient conditions as cells grown in glucose-containing medium for five-to-six days prior to harvest for subsequent experiments (i.e. respiration or cell death assays).

For all cell culture work, any buffers, solutions, or media used were pre-warmed to 37°C in an Isotemp 110 water bath (Fisher Scientific, Mississauga, ON, Canada) for at least 1 hour prior to use. All cell culture work was performed under sterile conditions inside of a Class II Type A2 biological safety cabinet (Esco Inc., Hatboro, PA, USA).

2.9 Measurements of total and apoptotic cell death:

2.9.1 Induction of cell death/apoptosis with hydrogen peroxide:

SH-SY5Y cells were harvested from 100 mm culture plates via trypsinization and seeded onto either 6-well plates for measurements of total cell death or 60 mm plates for measurements of Caspase-3 activity following exposure to hydrogen peroxide. To evoke cell death, culture medium on plates was replaced with same culture medium containing freshly added hydrogen peroxide with or without freshly added TPP-IOA or other experimental compounds of interest. The hydrogen peroxide/TPP-IOA addition was made by adding freshly diluted stock solution to culture media within a conical tube, which was then immediately mixed by gentle inversion, before addition to culture plates. The final percentage of DMSO in the media was 0.1%. A set of preliminary dose-response experiments were performed to determine the concentration of hydrogen peroxide that evoked approximately 50% total cell death (assessed by the Trypan blue exclusion assay and performed as indicated the proceeding section) in cells cultured within both types of media (glucose-containing or glucose-free/galactose-/glutamine-containing DMEM).

2.9.2 Trypan Blue exclusion assay for total cell death:

Twenty-four hours from the onset of hydrogen peroxide exposure, measurements of the number of living SH-SY5Y cells were made using the Trypan Blue exclusion assay. Floating cells present within the culture media and adherent cells harvested via trypsinization were combined into conical tubes and the cell pellet resulting from centrifugation (5 minutes at 240 *x g*) was re-suspended in 100 µL of media. Ten µL of this cell suspension was then diluted with 190 µL of 0.4% (*w/v*) Trypan Blue solution (dilution factor = 20), which was then briefly vortexed and allowed to incubate for 3 minutes at room temperature. Subsequently, the mixture was briefly re-suspended and 10 µL was loaded onto a hemocytometer (Hausser Scientific, Horsham, PA, USA) with a cover slip in place. The hemocytometer was viewed with a Hund

Wetzlar Wilovert Inverted Phase-Contrast microscope (Fisher Scientific, Mississauga, ON, Canada), and the number of cells in the four large corner squares and large middle square were counted. Cells that appeared stained blue were considered non-viable/dead, while cells excluding the Trypan Blue dye appeared colourless/opaque and were recorded as living. The concentration of living cells in the initial 100 µL cell suspension was calculated by the following equation:

 # Live cells/mL = (mean number of live cells per square) x (dilution factor) x (10,000)

The total number of living cells in the initial 100 µL cell suspension was then determined by multiplying the amount of live cells per millilitre by the total volume of the initial cell suspension. In every independent experiment performed, the calculated values for each experimental sample were normalized to the mean value of the non-treated control samples.

2.9.3 Caspase-3 activity assay for apoptosis:

Cells were harvested 12 hours from the onset of hydrogen peroxide exposure for measurements of Caspase-3 activity in whole-cell lysates using the fluorogenic Caspase-3 proteolytic substrate N-acetyl-Asp-Glu-Val-Asp-7-amino-4-methylcoumarin (Ac-DEVD-AMC).

To first harvest cells, medium containing floating cells was collected into conical tubes that were then centrifuged at 500 *x g* for 3 minutes, while ice-cold PBS was added the culture plates containing adherent cells that were then immediately collected via scraping the plate surface with a plate scraper. Both scraped cells and the corresponding pelleted floating cells were combined within microcentrifuge tubes kept on ice that were then centrifuged at 500 *x g*, 4°C for 3 minutes with an IEC Micromax RF refrigerated microcentrifuge (Fisher Scientific). The resulting cell pellets were flash frozen in liquid nitrogen and stored at -80°C.

To prepare whole-cell lysates, cell pellets were re-suspended in a small volume (120 µL) of ice-cold cell lysis buffer and allowed to incubate on ice for 30 minutes with routine vortexing (5 seconds in duration at setting 5; VWR Mini Vortexer) every 5 minutes. Subsequently, lysates

were centrifuged at 10,000 *x g*, 4°C for 10 minutes and the resulting supernatants were used for subsequent assays. Protein concentrations of lysates were determined via the Bradford reagent/assay with BSA as the protein standard using a UV-Vis spectrophotometer.

Prior to performing assays of Caspase-3 activity, all samples were diluted to a concentration of 1.5 µg/µL so that equal volume of each assay reagent could be used between samples. Twenty-five micrograms of whole-cell lysate was used per Caspase-3 activity measurement performed within 96-well spectrofluorometric microplates. To each assay well, freshly prepared protease assay buffer (consisting of 20 mM HEPES (pH 7.5), 10% glycerol, and 2 mM DTT), 25 µg sample lysate, and 20 µg Ac-DEVD-AMC were added in succession and the microplate was incubated for 3 hours at 37°C protected from light within a microplate warmer. After this period, the microplate was scanned using a Varian Cary Eclipse fluorescence spectrophotometer with set excitation and emission wavelengths of 360 nm and 445 nm, respectively. Emitted AMC fluorescence, which becomes spectrofluorometrically detectable when AMC is released from the Ac-DEVD peptide as a result of characteristic Caspase-3-catalyzed proteolytic cleavage (Talanian et al., 1997), was used as a quantifiable measure of Caspase-3 activity for each sample. Each sample lysate was assayed in quadruplicate wells that were averaged together to obtain a single value of Caspase-3 activity (arbitrary AMC fluorescence intensity units) per experimental treatment. Each assay performed included a measure of background fluorescence emission in lysate-free wells that was subtracted from all sample readings.

2.10 Establishment of a stable SH-SY5Y cell line expressing modified emerald fluorescent protein-labelled mitochondria:

The plasmid mEmerald-Mito-7 encoding a gene for modified emerald fluorescent protein (mEFP) targeted to the mitochondrial matrix compartment via N-terminal mitochondrial

targeting sequence from subunit VIII of human Complex IV/cytochrome *c* oxidase (Planchon et al., 2011) was a gift from Michael Davidson (Florida State University). The plasmid contained a kanamycin-resistance gene for bacterial selection and geneticin (G418)-resistance gene for mammalian cell selection. The plasmid was obtained from Addgene (plasmid # 54160) as an *E. coli* agar stab culture. To recover the plasmid DNA, the bacteria were streaked onto an agar plate containing 50 mg/mL kanamycin, which was then kept overnight within a 37°C incubator. Single colonies were then selected and amplified in overnight liquid cultures at 37°C in a C25KC shaker incubator (New Brunswick Scientific, Edinson, NJ, USA). Eighteen hours later, these cultures were removed and plasmid DNA was isolated and purified using a plasmid DNA Miniprep Kit (Norgen Biotek, Thorold, ON, Canada). Both purity (260 nm/280 nm absorbance ratio) and concentration of the resulting isolated plasmid mEmerald-Mito-7 DNA were assessed using a NanoPhotometer instrument.

A stably transfected SH-SY5Y cell line expressing mEmerald-Mito-7 was created, herein referred to as "SH-SY5Y-mito-mEFP". For this, a 24-well plate was seeded with 90,000 SH-SY5Y cells per well. Approximately 36 hours later, at which point wells were approximately 80% confluent, cells were transfected using Lipofectamine 2000 reagent following the manufacturer's instructions. Briefly, Lipofectamine 2000 reagent and plasmid DNA were each diluted in serum-free/antibiotic-free DMEM (transfection media) and then combined to form plasmid DNA-lipid complexes. After a 5 minute incubation period, the diluted mixture was added to wells. Five different combinations of plasmid DNA:Lipofectamine reagent in quadruplicate wells were used (µg:µL): 0.5:0.5, 1:1, 1.5:1.5, 1:3, 1:1.5. Approximately 24 hours after the transfection procedure, transfection media was replaced with selection media (DMEM with 10% FBS, 2x nonessential amino acids, and G418 at 400 µg/mL; the G418 concentration was determined in a prior screening experiment to be the minimum lethal dose for SH-SY5Y cells in 24-well plates). Selection medium was refreshed every other day. After approximately 10

days of selection, the concentration of G418 in culture media was dropped to100 µg/mL. Culture media with 100 µg/mL G418 freshly added was used thereafter to maintain selection. The stable cell line generated using the transfection combination of 1 µg plasmid DNA / 3 µL Lipofectamine 2000 reagent was used for all subsequent imaging experiments. To confirm mitochondrial localization of the mEFP, colocalization of mEFP signal with the mitochondria-targeted fluorescent dye MitoTracker RedCMXRos was detected using confocal microscopy (see **Appendix I Fig. AI.5.1**; protocols for imaging and staining are described below).

2.11 Fluorescence microscopy:

Confocal images of both live and fixed cells were obtained using a Carl Zeiss Axio Observer.Z1 inverted light/epifluorescence microscope equipped with ApoTome.2 optical sectioning and a Hamamatsu ORCA-Flash4.0 V2 digital camera. Cells were cultured on MatTek 35 mm poly-D-lysine-coated glass bottom culture dishes with culture media devoid of phenol red for imaging and plates were viewed with a Plan-Apochromat 63x/1.40 Oil DIC M27 microscope objective. For live cell imaging, the microscope stage and objectives were maintained at 37°C, with temperature control achieved through TempModule S-controlled stage heater and objective heater (PeCon, Erbach, Germany). A humidified 5% CO_2 environment was also maintained on the stage through tubing connected to a humidified CO_2 culture incubator. Fixed cells were imaged under ambient conditions. Blue fluorescence (i.e. for Hoechst 33342 signal) was detected using a fluorescence channel possessing excitation and emission wavelength filter sets of 335 – 383 nm and 420 – 470 nm, respectively, with set excitation and emission wavelengths of 353 nm and 465 nm, respectively (Zeiss Item# 411003-0002-000). Green fluorescence (i.e. for mito-mEFP signal) was detected using a fluorescence channel possessing excitation and emission wavelength filter sets of 450 – 490 nm and 500 – 550 nm, respectively, with set excitation and emission wavelengths of 488 nm and 509 nm, respectively (Zeiss Item# 411003-0004-000). Red

fluorescence (i.e. for TMRM and MitoTracker Red CMXRos signals) was detected using a fluorescence channel with excitation and emission wavelength filter sets of 540 – 552 nm and 590 – 660 nm, respectively, with set excitation and emission wavelengths of 587 nm and 610 nm, respectively (Zeiss Item# 411003-0010-000). Both the intensity of fluorescence illumination achieved via an X-Cite 120LED light source and camera exposure times were held constant between experimental groups across experiments. Z-stack series consisted typically of 30 – 40 slices, each 0.25 – 0.3 μm apart, and were rendered into single 2D images using the "extended depth of focus" processing tool using Zeiss Zen 2 (blue edition) microscopy software.

2.12 Mitochondrial and nuclear labelling:

Mitochondria and nuclei were labelled with MitoTracker Red CMXRos and Hoechst 33342, respectively, by following manufacturer's protocols. Briefly, to label mitochondria and nuclei in some experiments, cells were incubated within their culture incubator for 30 minutes with phenol red-free DMEM containing freshly added 50 nM MitoTracker Red CMXRos with or without 500 ng/mL Hoechst 33342. Immediately after staining, plates were washed three times with dye-free culture media to remove excess dye before imaging.

2.13 Measurements of mitochondrial membrane potential:

Tetramethylrhodamine methyl ester (TMRM) dye was used to semi-quantitatively assess mitochondrial membrane potential in SH-SY5Y cells through confocal microscopy. Plates of cells were given imaging media containing freshly added 30 nM TMRM and then placed back in the culture incubator for 45 minutes to allow for dye equilibration before imaging. Images of individual cells were obtained before and after experimental treatments at several time points. To quantify changes in mitochondrial membrane potential, changes in fluorescence intensities that took into account cytosolic background fluorescence were measured using ImageJ/FIJI software.

2.14 Quantitative analysis of mitochondrial morphology:

To quantitatively analyze mitochondrial morphology in live-cell confocal microscopy images, a custom-made image processing algorithm compiled into ImageJ macro format ("Mitochondrial Network Analysis, Version 1.0.0", Valente 2016, unpublished; see **Appendix II** for more details) was used. Components of the processing algorithm were inspired by that of Leonard et al., (2015) and consisted of freely-available ImageJ image processing tools compiled into a series of automated steps to allow for an objective and automated process. The processing steps ultimately generated a skeletonized depiction of mitochondria in single live cell images that was compatible for quantitative analysis.

Briefly, the raw confocal microscopy images were subjected to deconvolution using the Diffraction Point Spread Function 3D plugin together with the DeconvolutionJ plugin. To improve contrast between all mitochondrial structures and background in the deconvolved image, contrast limited adaptive histogram equalization (CLAHE) was subsequently performed. Through preliminary analysis trials, it was determined that use of deconvolution and CLAHE together as processing tools rather than each tool alone ultimately yielded the most accurate mitochondrial skeleton, and therefore both tools were included in the processing step. In the resulting processed image, using the default black and white threshold algorithm of ImageJ, fluorescent mitochondrial signal was subjected to thresholding in order to eliminate relatively weak signal capable of generating artifact. The resulting image was then made binary, such that mitochondrial signal became uniformly white and everywhere else uniformly black. Using the Skeletonize 3D plugin, the binary image was subsequently converted to a skeleton image in which mitochondrial signal was converted to lines of one pixel in width. From the skeletonized mitochondrial signal, skeleton structures were classified as either individuals or networks. Individuals were considered skeletons that did not demonstrate any sort of branching (i.e. either

puncta or rods, or extended tubules), whereas networks were considered skeletons containing at least one branching point. All resulting quantitative mitochondrial measures were analyzed on a "per cell" basis.

2.15 Cellular respiration measurements:

Respiration measurements of intact SH-SY5Y cells were performed using a Clark-type oxygen electrode (Rank Brothers Dual Digital Model 20 Respirometer; Bottisham, UK) attached to a polygraph recorder, essentially as in Robb et al., (2012). Briefly, cells from one 100 mm culture plate were harvested via trypsinization, centrifuged at 240 *x g* for 3 minutes, re-suspended in 1 mL of culture media (serving as respiration buffer), and then placed into a thermostatically-controlled chamber maintained at 37°C attached to the respirometer. The chamber was capped and the rate of oxygen consumption was measured over a 5-10 minute period. All respiration rates were converted to nmol O_2 consumed·minute^{-1}·10^6 cells^{-1}. Immediately following measurements, the cell suspension was recovered in a 1.5 mL microcentrifuge tube. A small volume (20 µL) of sample was taken to determine the total number of living cells using the Trypan blue exclusion assay, while the remainder of the sample was centrifuged for several minutes at approximately 2200 *x g* using a Fisher Scientific benchtop minicentrifuge. The supernatant was discarded and the resulting cell pellet was flash frozen in liquid nitrogen and then stored at -80°C for later lysate preparation and experimental analysis (i.e. protein concentration determination, citrate synthase activity measurements and immunoblot experiments; below).

2.16 Whole-cell lysate preparation:

Harvested cell pellets were lysed by incubation in freshly prepared ice-cold lysis buffer (10 mM Tris pH 8.0, 150 mM NaCl, 2 mM EDTA, 2 mM dithiothreitol, 0.4 %

phenylmethylsulfonyl fluoride, 40 % (v/v/) glycerol, 0.5 % (v/v) Nonident P40 detergent) with periodic sonication (Ultrasonic Inc., Sonicator W-375; setting 5) for one hour on ice. Following this, the resulting suspensions were centrifuged at 10 000 *x g* at 4°C for ten minutes using a benchtop minicentrifuge. The resulting supernatants (i.e. the whole-cell lysates) were kept and protein concentrations were determined using the Bradford method using BSA as the protein standard. All whole-cell lysates were stored at -80°C.

2.17 Citrate synthase activity assay:

Maximal citrate synthase activity of whole-cell lysates was measured using a Bio-Tek PowerWave Microplate UV-Vis spectrophotometer (Winooski, VT, USA) at 30°C, essentially as in Brown et al., (2007). The activity assay was based on coupling the rate-limiting activity of citrate synthase to the irreversible formation of thionitrobenzoic acid (TNB) from 5,5′-dithiobis(2-nitrobenzoic acid) (DTNB; Sere, 1969). Assay buffer consisted of 50 mM Tris pH 8.0, 500 μM DTNB, 100 μM acetyl-coenzyme A, and 1 μg lysate protein. Citrate synthase activity was monitored at 412 nm. After measuring background activity over a period of 3 minutes, 500 μM oxaloacetate was added to initiate the reaction and the absorbance at 412 nm was followed over approximately 10 minutes.

***2.18 Immunoblots*:**

Equal amounts of protein (30 μg) from each whole-cell lysate were separated by sodium dodecyl sulfate polyacrylamide gel electrophoresis (SDS-PAGE; gels consisted of a 4% polyacrylamide top stacking layer and 12% polyacrylamide bottom resolving layer) within a Bio-Rad Mini-PROTEAN Tetra Cell apparatus. Prior to running the gel, whole-cell lysates were mixed 1:1 (*v/v*) with loading dye containing 10% (*v/v*)/200 mM DTT and were heated at 90°C for 5 minutes. Following electrophoresis, the separated proteins were blotted from the gel onto a

polyvinylidene fluoride membrane using a Bio-Rad Trans-Blot semi-dry transfer apparatus. Blotted membranes were blocked for one hour at room temperature with a 5% (*w/v*) non-fat skim milk/PBS-t solution to limit non-specific antibody binding. For antibody incubation, membranes were separately incubated with anti-VDAC (1:500; *w/v*) overnight on a rotisserie at 4°C, washed with PBS-t (5 cycles of 5 minutes duration), then incubated with an infrared fluorophore-conjugated rabbit antibody (1:2500; *w/v*) for 2 hours at room temperature. The same membranes were later probed with anti-Actin (1:250; *w/v*) overnight 4°C as a protein loading/transfer control, washed with PBS-t (5 cycles of 5 minutes duration), and subsequently incubated with an infrared fluorophore-conjugated goat antibody (1:2500; *w/v*) for 2 hours at room temperature. After each secondary antibody incubation, the membranes were visualized using an Odyssey infrared imaging system (LI-COR Biosciences). Densities of protein bands were quantified using the "Gel Analysis" tool of ImageJ software and were standardized to the value of one experimental sample.

2.19 Statistical Analyses:

All statistical analyses were performed using GraphPad Prism 5 software (San Diego, USA). T-tests (one-tailed) were performed on data sets containing two experimental groups, whereas one-way ANOVAs were performed for data sets containing three or more experimental groups. Paired t-tests or repeated measures one-way ANOVAs were used whenever possible, as indicated in figure descriptions. A p-value of < 0.05 was considered significant for all statistical tests. When statistical significance in data sets was observed from one-way ANOVAs, post-hoc analysis was performed using Tukey's honestly significant difference (HSD) test. Non-linear regression with least squares fit was used for determination of $I.C._{.50}$ values from concentration-response curves with log-transformed concentration values.

Chapter 3.0 – Results:

3.1 Inhibition of cytochrome c/cardiolipin complex and mitochondrial peroxidase activities:

To independently verify TPP-IOA's (**Fig. 2.1A**) previously reported ability to inhibit the pro-apoptotic peroxidase activity of cytochrome *c* (Atkinson et al., 2011), peroxidase activities of purified cytochrome *c*/cardiolipin complexes and isolated mitochondria were determined (**Fig. 3.1**). In the absence of cardiolipin, cytochrome *c* (1 μM) catalyzed resorufin formation at a rate of 2491 ± 187 arbitrary fluorescence units (A.F.U.) per minute (**Fig. 3.1A,B**). In the presence of tetralinoleoylcardiolipin (15 μM), the rate of cytochrome *c* (1 μM)-catalyzed resorufin formation increased to 9210 ± 444 A.F.U. per minute (**Fig. 3.1A,B**). The enhancement of cytochrome *c* peroxidase activity observed here in the presence of tetralinoleoylcardiolipin is consistent with the well-established mechanism by which cardiolipin binding to cytochrome *c* causes structural changes within the protein that result in greater accessibility of the heme iron catalytic site for catalysis (e.g. Kagan et al., 2005, Belikova et al., 2006).

As expected, TPP-IOA dose-dependently diminished the rate of resorufin formation of the cytochrome *c*/cardiolipin solution, indicating inhibition of peroxidase activity (**Fig. 3.1C**). This finding is consistent with initial published reports (Atkinson et al., 2011) showing that TPP-IOA is an effective inhibitor of cytochrome *c* peroxidase activity.

To determine that the cytochrome *c* peroxidase inhibition of TPP-IOA is due to the strategically placed imidazole group of the oleic acid moiety, measurements were repeated with one of two control molecules. TPP-oleic acid has identical structure but lacks the inhibitory imidazole group along the fatty acyl chain (**Fig. 2.1B**). 3-hydroxypropyl-TPP (3HP-TPP) is the mitochondria-targeting moiety of TPP-IOA that remains after endogenous cleavage (**Fig. 2.1C**; Atkinson et al., 2011). Both molecules were tested at the concentrations at which TPP-IOA elicited approximately half maximal (0.5 μM; or TPP-IOA to cytochrome *c* ratio of 0.5:1) and

maximal (10 μM; or TPP-IOA to cytochrome *c* ratio of 10:1) inhibition (**Fig. 3.1D**). If the imidazole group placed on the acyl chain of TPP-IOA is indeed responsible for conferring inhibition of cytochrome *c*/cardiolipin peroxidase activity, then there should be no inhibition when the imidazole group is absent. Compared to the vehicle control (0.1% DMSO), TPP-OA did not exert significant inhibition of peroxidase activity at the two concentrations tested (both p-values > 0.05 versus non-treated control, one-way ANOVA with Tukey's HSD post-hoc test). These findings confirm that the imidazole group of TPP-IOA is indeed the major component driving inhibition of cytochrome *c*'s peroxidase activity. Additionally, 3HP-TPP did not inhibit peroxidase activity at either concentration (both p-values > 0.05 versus non-treated control, one-way ANOVA with Tukey's HSD post-hoc test), indicating that the TPP-containing moiety resulting from endogenous processing of TPP-IOA does not interfere with cytochrome *c* peroxidase activity at concentrations equivalent to those at which TPP-IOA is effective. Altogether, these findings indicate that TPP-IOA, by virtue of the strategically placed inhibitory imidazole along its oleic acyl chain, is a potent and direct inhibitor of the peroxidase activity of cytochrome *c*.

The ability of TPP-IOA to inhibit peroxidase activity in freshly isolated intact liver mitochondria was also assessed using an Amplex red-based assay system. Resorufin formation was significantly suppressed by TPP-IOA at both 5 μM (corresponding to 20 nmol TPP-IOA per mg mitochondrial protein; 2418 ± 502 resorufin formed per minute) and 10 μM (corresponding to 40 nmol TPP-IOA per mg mitochondrial protein; 1548 ± 245 resorufin formed per min) compared to the non-treated control group (3505 ± 601 resorufin formed per minute; **Fig. 3.1E**; p-values both < 0.05, repeated measures one-way ANOVA with Tukey's HSD post-hoc test). On the basis of prior reports indicating cytochrome *c* to be present in adult rat liver mitochondria at approximately 0.21 nmol per mg mitochondrial protein (Wainio, 1970; Petrosillo et al., 2003),

these findings indicate that higher amounts of TPP-IOA are required to inhibit peroxidase activity in isolated mitochondria than with the purified protein.

The effect of 3-hydroxypropyl-TPP on peroxidase activity of isolated mitochondria was also tested over a similar concentration range (0.5 – 10 μM; or 10 - 40 nmol per mg mitochondrial protein). Compared to the non-treated control group, resorufin formation was not significantly inhibited at any of the concentrations tested (p-values > 0.05 for each concentration, repeated measures one-way ANOVA with Tukey's HSD post-hoc test; **Fig. 3.1E**). This, along with the lack of inhibitory effect in the above experiments with purified cytochrome c, suggests that 3-hydroxypropyl-TPP does not inhibit peroxidase activity of mitochondria. Moreover, these findings further indicate that the imidazole-containing oleic moiety of TPP-IOA is responsible for the inhibition of mitochondrial peroxidase activity.

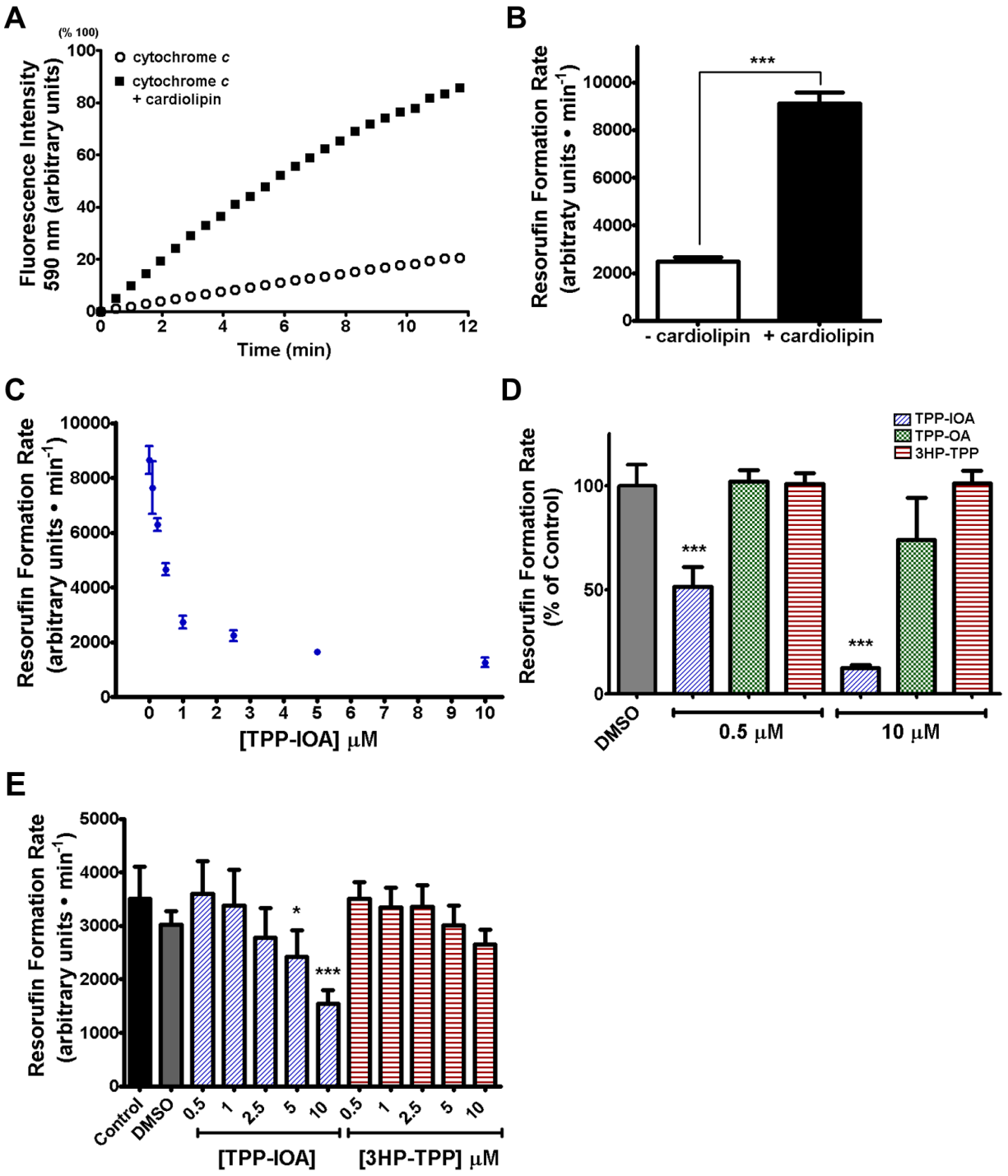

Figure 3.1: Inhibition of purified cytochrome *c* and mitochondrial peroxidase activity by TPP-IOA and related TPP-containing molecules.

A) Representative spectrofluorometric kinetic traces of resorufin formation catalyzed by cytochrome *c* in the absence or presence of cardiolipin. **B)** Quantification of maximal resorufin formation rate from initial linear range of kinetic traces indicates that cardiolipin induces peroxidase activity of purified cytochrome *c*. Bars represent means + SEM from 27 or 29 total replicates from ten separate experimental trials performed over two independent experiments. *** = p-value < 0.001 (unpaired Student's t-test). **C)** TPP-IOA dose-dependently inhibits peroxidase activity of cardiolipin-induced cytochrome *c* peroxidase activity. Data points represent means ± SEM from six replicates from two independent experimental trials. **D)** At

effective inhibitory concentrations of TPP-IOA against cytochrome *c* peroxidase activity, 3HP-TPP and TPP-OA each do not elicit inhibition. Bars represent means + SEM from 6 -12 total replicates from two independent experimental trials. Data were standardized to Vehicle control (0.1% DMSO) values. *** = p-value < 0.001 compared to Vehicle control (one-way ANOVA with Tukey's HSD post-hoc test). **E)** TPP-IOA inhibits peroxidase activity of isolated mitochondria from rat liver, while 3HP-TPP does not over the same concentration range. Bars represent means + SEM from four independent mitochondrial preparations each measured in at least sextuplicate. * = p-value < 0.05, *** = p-value < 0.001 compared to Control (repeated measures one-way ANOVA with Tukey's HSD post-hoc test). In A – E, peroxidase activity (F.A.U./minute) was spectrofluorometrically determined from the initial linear formation rate of the fluorescent oxidation product of Amplex Red reagent, resorufin (ex. 525 nm/ em. 590 nm). ***Note:*** In C & D, the concentrations on the x-axis also correspond to the molar ratio of TPP-IOA to cytochrome *c*.

3.2 Interference with cytochrome c *reduction:*

Beyond its role as the catalytic site for cytochrome *c*'s pro-apoptotic peroxidase activity, the heme iron within cytochrome *c* serves as the redox active site for electron transfer from Complex III to Complex IV of the mitochondrial electron transport system. Given that TPP-IOA physically interacts with cytochrome *c* and presents a ligand (i.e. imidazole) to the heme iron, TPP-IOA may also interfere with the protein's normal electron transfer activity in oxidative phosphorylation. To determine whether TPP-IOA interferes with the reduction activity of cytochrome *c*, a spectrophotometric assay measuring the reduction of purified (ferri)cytochrome *c* ($Fe3^{+}$) to (ferro)cytochrome *c* ($Fe2^{+}$) was performed (**Fig. 3.2A**; representative experimental spectrophotometric trace). In this assay, the rate of cytochrome *c* reduction by ascorbate in the presence of DMSO was 0.0218 ± 0.0004 arbitrary absorbance units per minute. The rate of cytochrome *c* reduction by ascorbate was increasingly inhibited by increasing concentrations of TPP-IOA (**Fig. 3.2B**), indicating that TPP-IOA can interfere with the ability of cytochrome *c*'s heme iron to accept electrons.

To determine if either 3-hydroxypropyl-TPP (3HP-TPP) or TPP-oleic acid (TPP-OA) exhibits similar interference, the rates of cytochrome *c* reduction by ascorbate in the presence of either of these molecules at the approximate half maximal inhibitory TPP-IOA dose (5 µM) were compared. The rate of cytochrome *c* reduction was slowed in the presence of either 3HP-TPP or

TPP-OA, however the magnitudes of interference also significantly differed between TPP-IOA, TPP-OA, and 3HP-TPP (**Fig. 3.2C**; p-values < 0.001 between each group; one-way ANOVA with Tukey's HSD post-hoc test). 3HP-TPP appeared to elicit minor inhibition of cytochrome *c* reduction rate (0.0169 ± 0.0016 arbitrary absorbance units per minute), while both TPP-OA (0.00304 ± 0.0002 arbitrary absorbance units per minute) and TPP-IOA (0.0123 ± 0.0005 arbitrary absorbance units per minute) significantly inhibited this activity. TPP-OA, devoid of an imidazole ligand along its oleic acyl chain, evoked the strongest inhibition of cytochrome *c* reduction. Taken together, these findings reveal that TPP-IOA can disrupt the electron accepting activity of cytochrome *c* that is required for its function in oxidative phosphorylation. Moreover, such interference is likely driven by the oleic acyl chain of the molecule, since TPP-OA alone was a highly effective inhibitor of this activity.

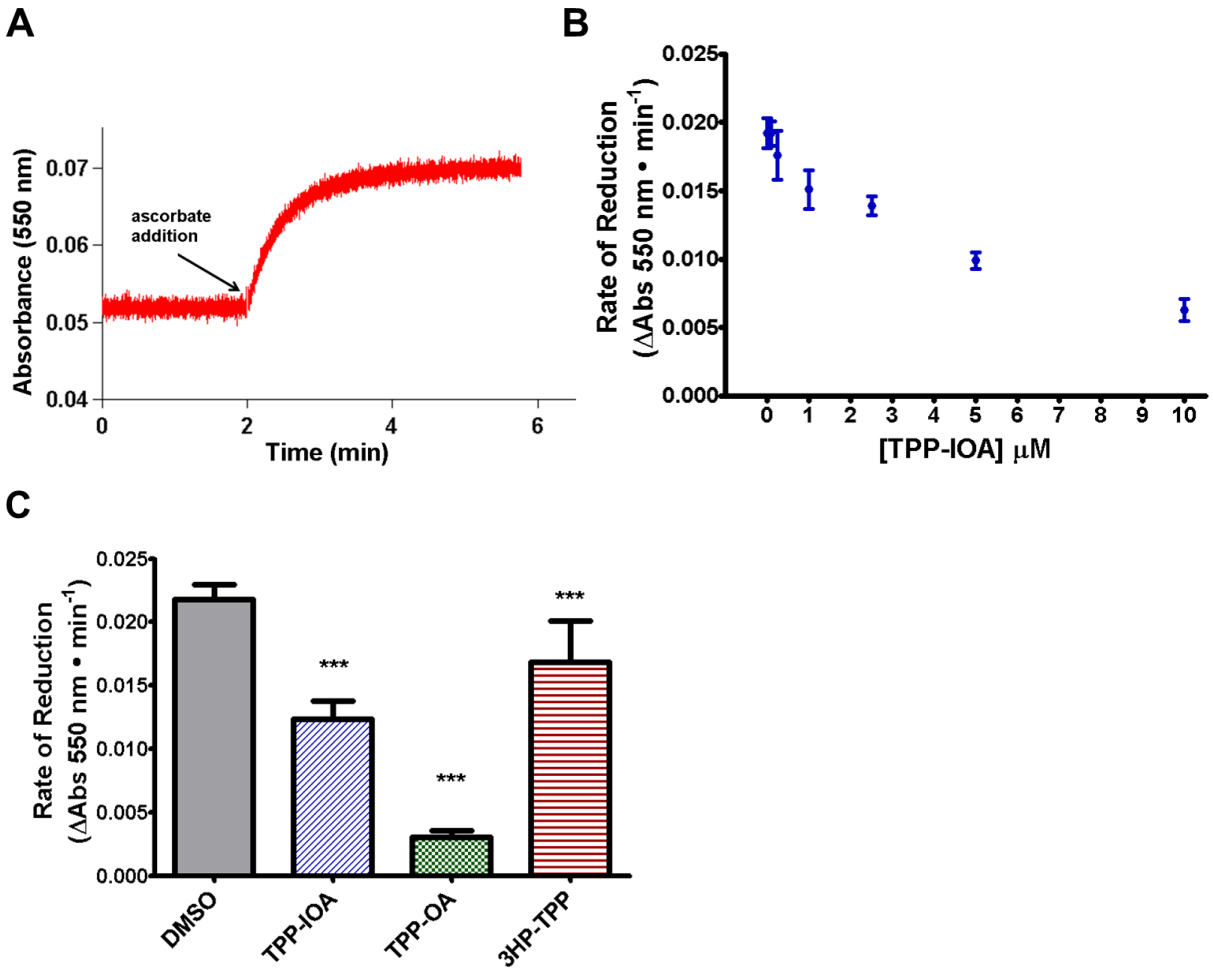

Figure 3.2: Interference by TPP-IOA and related TPP-containing molecules with reduction of purified cytochrome *c* by ascorbate.

A) Representative spectrophotometric kinetic trace (550 nm) of the reduction of purified (ferri)cytochrome *c* by ascorbate. Ascorbate (1 μM) was added to cytochrome *c* (1 μM) within HEPES buffer after approximately two minutes to initiate reduction, and the reaction was allowed to proceed for several subsequent minutes. The assay shown was performed in the presence DMSO (0.1 %; Vehicle control for TPP- conjugated molecules). **B)** TPP-IOA dose-dependently interferes with the rate of reduction of cytochrome *c* by ascorbate. Reduction rates were calculated from the initial linear range after ascorbate addition. Data points represent means ± SEM from 4 – 9 total replicates from two independent experiments. **C)** At the approximate $I.C._{50}$ value of TPP-IOA, TPP-OA elicits greater interference to cytochrome *c* reduction by ascorbate while 3HP-TPP elicits a less intense effect. Bars represent means + SEM from 4 -9 total replicates from two independent experimental trials. *** = p-value < 0.001 compared to DMSO (one-way ANOVA with Tukey's HSD post-hoc test). All groups had significantly different mean values from one another (not shown on graph; p-value < 0.001 for each comparison, one-way ANOVA with Tukey's HSD post-hoc test) ***Note:*** in both B & C, the concentrations also correspond to the molar ratio of TPP-IOA to cytochrome *c*.

3.3 Therapeutic efficacy of TPP-IOA at the level of its isolated protein target:

For drug candidates, the dose ratio between therapeutic and toxic effects is known as the therapeutic index. It can be the ratio of the respective doses that cause 50% inhibition of the effects of interest (Muller & Milton, 2012). Since the above findings demonstrated inhibition of both the cardiolipin-induced peroxidase activity and the electron accepting activity of cytochrome *c* by TPP-IOA, it is instructive to compare the relative dose-dependencies of these two effects to determine TPP-IOA's therapeutic index. Therefore, $I.C._{.50}$ values were determined as 0.65 ± 0.06 μM or nmol TPP-IOA per nmol cytochrome *c* (R^2 = 0.9711; non-linear regression with least squares fit) and 5.28 ± 1.12 μM or nmol TPP-IOA per nmol cytochrome *c* (R^2 = 0.9768; non-linear regression with least squares fit) for peroxidase activity inhibition (**Fig. 3.3A,B** red squares) and reduction inhibition (**Fig. 3.3A,B** blue circles), respectively. Additionally, these respective $I.C._{.50}$ values differed significantly from one another (p-value <0.0001; extra-sum-of-squares F-test). From these values, an approximate therapeutic index of 8.12 was calculated. Although no universally acceptable "safe" therapeutic index value exists (Muller & Milton, 2012), this result nonetheless indicates that, at the level of its specific protein target, there is a protective window for TPP-IOA when considering its potentially therapeutic anti-apoptotic effect and its presumably undesired interference with bioenergetics activity.

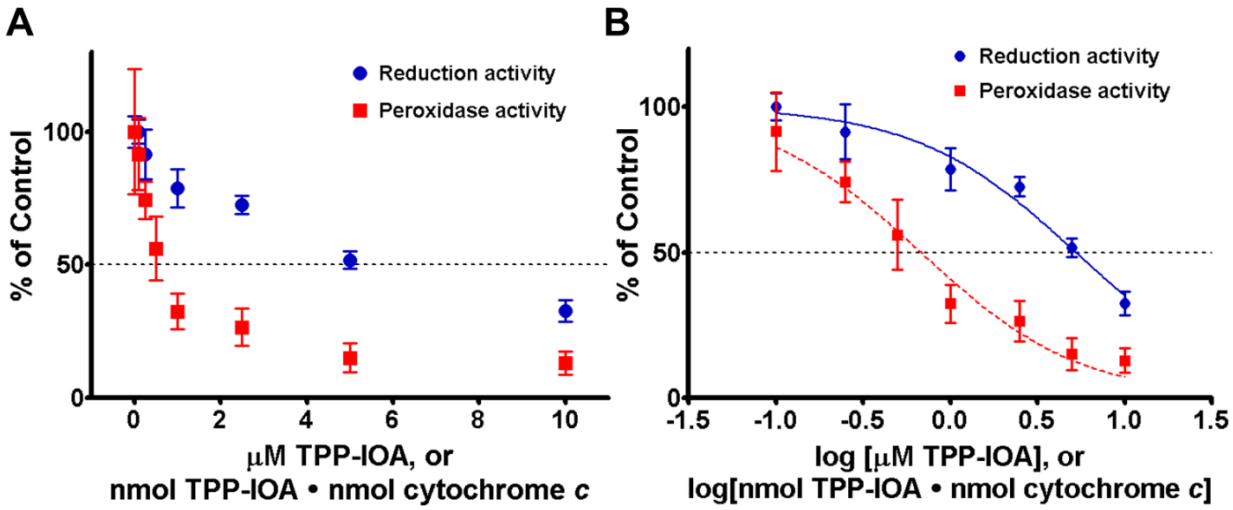

Figure 3.3: Merged dose-response relationships for TPP-IOA's inhibitory effects on both peroxidase activity and reduction of purified cytochrome *c* reveal the existence of a therapeutic window.
A) Non-transformed and **B)** semi-log transformed dose-response curves for TPP-IOA's inhibition of both peroxidase activity (squares) and reduction activity (circles) of purified cytochrome *c*. Red squares represent means ± SEM of cardiolipin-induced cytochrome *c* peroxidase activity from six replicates performed over two independent experiments (data derived from Fig. 3.1B. Blue circles represent reduction of cytochrome *c* by ascorbate in the presence of TPP-IOA from 4 – 9 total replicates performed over two independent experiments (data derived from Fig. 3.2B). Data points within each set were standardized to respective vehicle (0.1% DMSO) control group values. Non-linear regression analysis revealed $I.C._{50}$ values for the two responses differed significantly (p-value <0.0001; extra-sum-of-squares F-test). ***Note:*** the micromolar concentrations of TPP-IOA indicated on the x-axes are equivalent to the ratio of nmol TPP-IOA to nmol cytochrome *c*.

3.4 Interference with mitochondrial respiration:

There is no information regarding TPP-IOA's effect on mitochondrial respiration, however, previous studies have demonstrated that molecules with similar chemical structure to TPP-IOA, such as oleic acid and TPP-containing linker molecules, can perturb mitochondrial respiration (Schönfeld et al., 1989, see refs in Wojtczak & Schönfeld, 1993, see refs in Di Paolo & Lorusso, 2006, Reily et al., 2013, & Trnka et al., 2015). Given these reports and the finding above that TPP-IOA can interfere with cytochrome *c*'s reduction activity, it was hypothesized that TPP-IOA could affect oxidative phosphorylation. To test this hypothesis, respiratory states of freshly isolated mitochondria from rat liver were measured using closed-system respirometry

(**Fig. 3.4**). The respiratory control ratio (RCR; State 3 respiration divided by State 4 respiration) takes into account all functional aspects of oxidative phosphorylation components, and is indicative of the extent to which oxygen consumption and ATP production are coupled. If TPP-IOA interferes with any functional component of oxidative phosphorylation, then a reduction in the RCR would be observed. In the presence of vehicle control (DMSO), isolated liver mitochondria exhibited an RCR of 5.69 ± 0.34. TPP-IOA reduced the RCR (**Fig. 3.4A**), with significantly lower values observed at both 5 µM and 10 µM TPP-IOA (3.79 ± 0.24 and 2.56 ± 0.16, respectively; p-value <0.05 for both, one-way ANOVA with Tukey's HSD post-hoc test). 3-hydroxypropyl-TPP also significantly reduced the RCR, but only at a concentration of 10 µM (4.33 ± 0.03; p-value <0.05, one-way ANOVA with Tukey's HSD post-hoc test).

To avoid possible overestimation bias that is inherently associated with statistical analysis of RCRs, values were mathematically converted to the related linear function termed "oxidative phosphorylation coupling efficiency", where a value of 1.0 represents a perfectly coupled system (Gnaiger, 2014; **Fig. 3.4B**). The oxidative phosphorylation coupling efficiency in the presence of the vehicle control was 0.82 ± 0.01, compared to 0.72 ± 0.02 and 0.61 ± 0.02 for 5 µM and 10 µM TPP-IOA, respectively (p-value < 0.05 for both doses compared to vehicle control, one-way ANOVA with Tukey's HSD post-hoc test). The oxidative phosphorylation coupling efficiency was also significantly reduced by 10 µM 3-hydroxypropyl-TPP (0.77 ± 0.0; p-value < 0.05 compared to vehicle control, one-way ANOVA with Tukey's HSD post-hoc test). Thus, through either metric it can be concluded that TPP-IOA significantly decreases the efficiency of oxidative phosphorylation in isolated mitochondria, and that its free mitochondria-targeting chemical moiety 3-hydroxypropyl-TPP can also elicit this response at higher concentrations. The larger absolute changes observed for TPP-IOA compared to 3-hydroxypropyl-TPP at lower doses suggests that the IOA moiety is required to decrease the coupling efficiency of mitochondria exposed to TPP-IOA, and that this moiety may be

negatively interacting with some functional component(s) of oxidative phosphorylation to drive the dysfunction. Additionally, at higher concentrations there may be a potentially minor contribution from the mitochondria-targeting moiety.

To elucidate the functional processes of oxidative phosphorylation affected by TPP-IOA that contribute to the limited respiratory control/oxidative phosphorylation coupling of mitochondria, mitochondrial respiratory states defined by Chance and Williams (1955) were assessed. State 3 respiration represents capacity for phosphorylating respiration (saturating levels of exogenous substrates and ADP provided), and encompasses components of both the phosphorylating system and electron transport system. If TPP-IOA interferes with any component of these two systems, then a reduction in the State 3 respiration rate would be observed. State 3 respiration was decreased by TPP-IOA, with significant reductions compared to the vehicle control observed at both 5 µM and 10 µM (16.32 ± 2.24, 12.39 ± 1.27, and 9.18 ± 1.33 nmol O_2 consumed · min^{-1}· mg $protein^{-1}$, respectively; p-values < 0.05 for both doses, one-way ANOVA with Tukey's HSD post-hoc test; **Fig. 3.4C**). Respiration rates in response to 5 µM and 10 µM TPP-IOA were approximately 76 ± 7.79 % and 56 ± 8.16 % that of the vehicle control, respectively. Therefore, TPP-IOA can reduce the capacity for phosphorylating respiration by disrupting some functional component of the phosphorylating system or electron transport system. In contrast, similar concentrations of 3-hydroxypropyl-TPP did not alter State 3 respiration, indicating that the free TPP-moiety does not contribute to the observed effects on oxidative phosphorylation.

The rates of fully uncoupled respiration were also measured in the presence of the protonophore FCCP and absence of any ADP to allow for maximal electron transport activity with an inactive phosphorylation system (**Fig. 3.4D**). If TPP-IOA perturbs any functional component(s) of the mitochondrial electron transport system, then the capacity for fully uncoupled respiration would be lessened. The mean fully uncoupled respiration rate in the

presence of the vehicle control was 24.33 ± 2.57 nmol O_2 consumed · min^{-1}· mg $protein^{-1}$. At 5 µM and 10 µM TPP-IOA fully uncoupled respiration rates were significantly decreased (16.22 ± 5.67 nmol O_2 consumed · min^{-1}· mg $protein^{-1}$, or 66 ± 23.3 % and 16.42 ± 2.57 nmol O_2 consumed · min^{-1}· mg $protein^{-1}$, or 67 ± 10.56 % that of the vehicle control, respectively). Therefore, at concentrations of 5 µM and above, TPP-IOA interferes with the electron transport system of isolated mitochondria. In contrast, FCCP-uncoupled respiration was not affected by 3-hydroxypropyl-TPP (p-value > 0.05 for all doses tested, one-way ANOVA with Tukey's HSD post-hoc test).

State 4 respiration is a measure of oxygen consumption not coupled to ADP phosphorylation, and is generally affected by processes that may stimulate the flow of protons from the intermembrane space back into the matrix independent of the ATP synthase (e.g. proton leak). If TPP-IOA exerts an effect on proton leak, then an increase in State 4/non-phosphorylating respiration rate would be observed. Indeed, there was a general trend of increased State 4 respiration in the presence of TPP-IOA, with statistical significance observed at 10 µM compared to the vehicle control (4.08 ± 0.52 nmol O_2 consumed · min^{-1}· mg $protein^{-1}$ and 2.79 ± 0.19 nmol O_2 consumed · min^{-1}· mg $protein^{-1}$, respectively; p-value < 0.05, one-way ANOVA with Tukey's HSD post-hoc test; **Fig. 3.4E**). Therefore, TPP-IOA significantly stimulates non-phosphorylating respiration, but only at relatively high concentrations. Additionally, 3-hydroxypropyl-TPP caused a general trend of elevated State 4 respiration rates (e.g. 3.37 ± 0.37 nmol O_2 consumed · min^{-1}· mg $protein^{-1}$ at 10 µM TPP-OA versus 2.79 ± 0.19 nmol O_2 consumed · min^{-1}· mg $protein^{-1}$ for the vehicle group), however, this did not reach statistical significance (p-value > 0.05 versus the vehicle, one-way ANOVA with Tukey's HSD post-hoc test).

Taken together, these findings reveal that, at concentrations of 5 µM and greater, TPP-IOA causes mitochondrial bioenergetic dysfunction, through interference with some

component(s) of the oxidative phosphorylation/electron transport system machinery and stimulation of some leak-inducing process(es). Both effects appear to require the IOA moiety of TPP-IOA, since the effects of the endogenously freed mitochondria targeting TPP-containing moiety manifest only at the highest concentrations tested, and even then with lower severity.

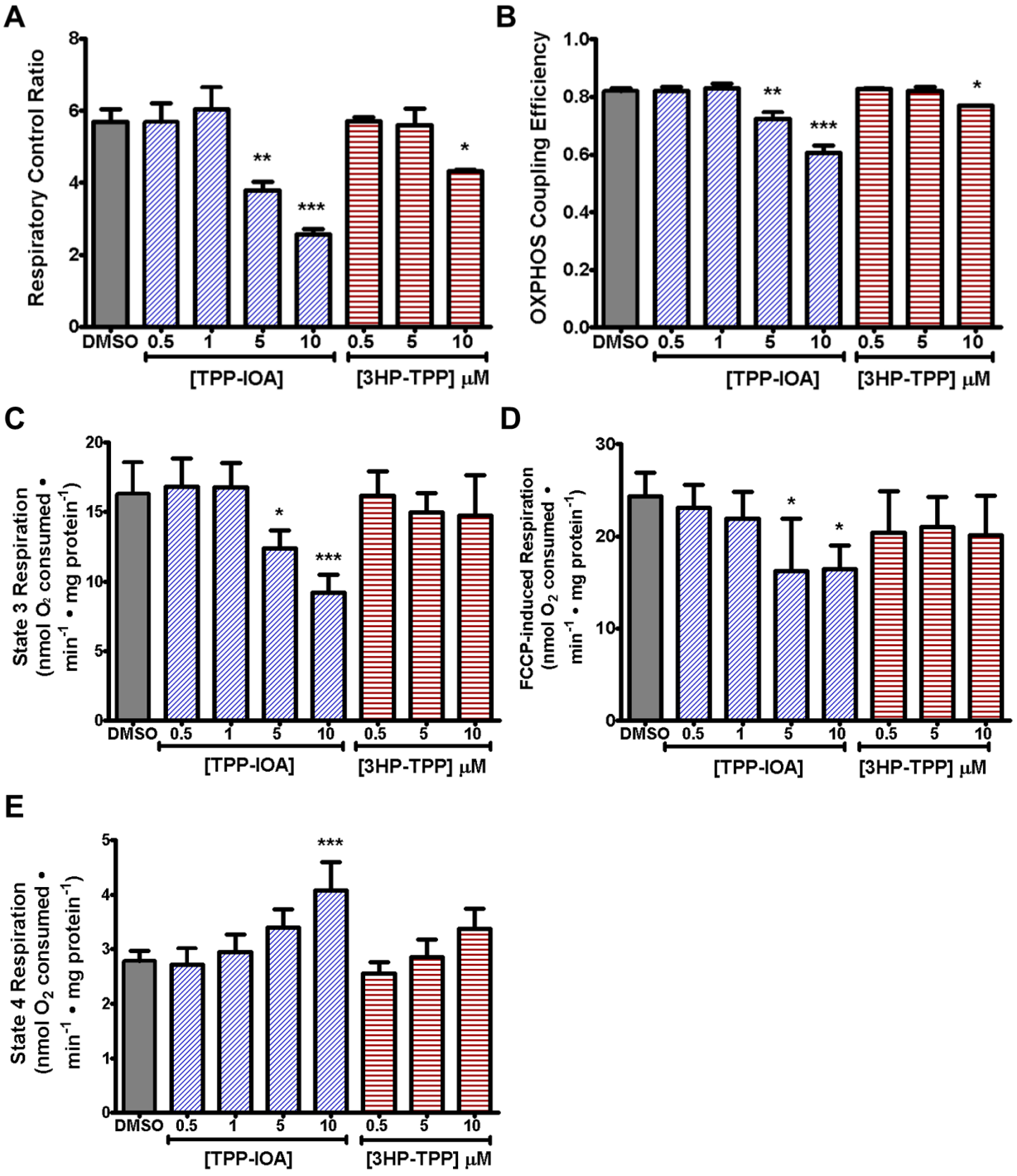

Figure 3.4: Inhibitory effects of TPP-IOA and its TPP-containing moiety on respiration of isolated mitochondria.

A) Respiratory control ratio (RCR; State 3/State 4). **B)** Oxidative phosphorylation coupling efficiency ($1 - RCR^{-1}$). **C)** State 3 respiration, or oxidative phosphorylation capacity (250 μM ADP addition). **D)** Fully uncoupled respiration, or electron transport system capacity (2 μM FCCP). **E)** State 4 respiration, or non-phosphorylating respiration. In A – E, measurements were made using isolated rat liver mitochondria provided with glutamate and malate (5 mM each) as respiratory substrate within a closed-chamber containing a Clark-type electrode. Blue diagonally-striped bars represent TPP-IOA treatment and red horizontally-striped bars represent 3HP-TPP treatment. All bars represent means + SEM from at least three independent

mitochondrial preparations each measured in at least duplicate. * = p-value < 0.05, ** = p-value < 0.01, *** = p-value < 0.001 compared to Vehicle control (one-way ANOVA with Tukey's HSD post-hoc test).

3.5 Therapeutic efficacy of TPP-IOA at the level of isolated mitochondria:

Since TPP-IOA could directly cause dysfunction to components of oxidative phosphorylation in isolated mitochondria, it is crucial to determine whether it can exert desired inhibition to pro-apoptotic oxidative events at concentrations that avoid such toxicity. To identify this, the dose-responses for inhibition by TPP-IOA to both peroxidase activity and oxidative phosphorylation function (via measures of both RCR and oxidative phosphorylation coupling efficiency) of isolated mitochondria were plotted together (**Fig. 3.5**). Generally, concentrations of TPP-IOA required for appreciable inhibition of peroxidase activity elicited an even stronger reduction to the RCR (**Fig. 3.5A,C**). Additionally, the oxidative phosphorylation coupling efficiency appears to have been concomitantly inhibited with peroxidase activity over the concentration range of TPP-IOA tested (**Fig. 3.5B,D**). Together, these measures indicate that TPP-IOA is unable to inhibit peroxidase activity without concomitantly disrupting oxidative phosphorylation of mitochondria.

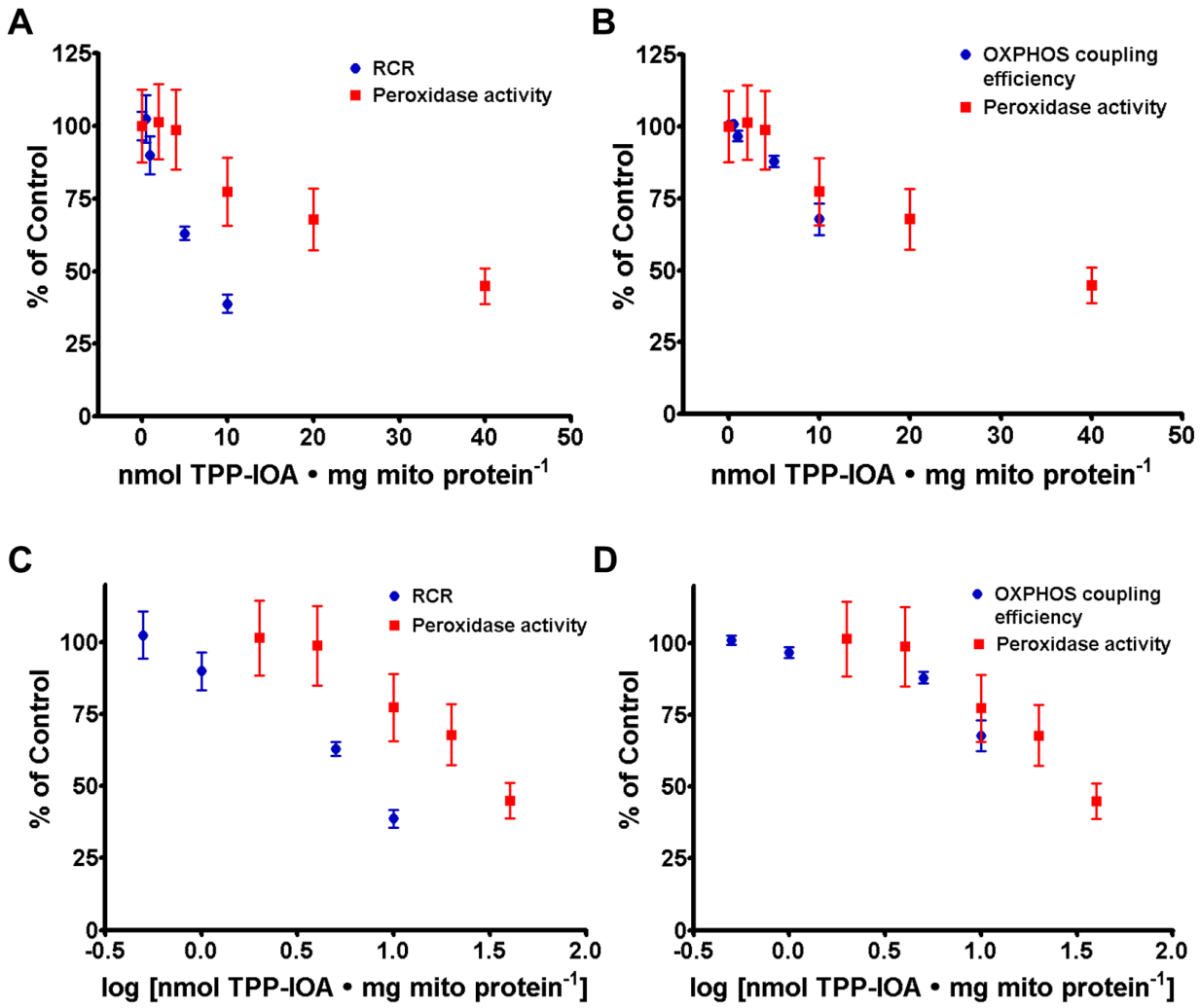

Figure 3.5: Merged dose-response relationships for TPP-IOA's inhibitory effects on peroxidase activity and respiration of isolated mitochondria.
A,B) Non-transformed and **C,D)** semi-log transformed dose-response curves for TPP-IOA's inhibition of both peroxidase activity and either respiratory control or oxidative phosphorylation coupling of isolated mitochondria. Solid red boxes represent means ± SEM of peroxidase activity, whereas solid blue dots represent respiratory control ratio (RCR) in (**A,C**) and oxidative phosphorylation efficiency in (**B**,**D**) of isolated rat liver mitochondria. Data points represent means ± SEM from three (RCR and oxidative phosphorylation efficiency) or four (peroxidase activity) independent mitochondrial preparations each measured in at least duplicate. Data points in each data set were derived from data shown in Fig. 3.1D and Fig. 3.4A,B and were standardized to respective vehicle (0.1% DMSO) control values.

3.6 Impact of TPP-IOA on mitochondrial bioenergetics in intact cultured cells:

Although the cell-free experimental approach provides useful insights into TPP-IOA's interactions with basic molecular or biochemical processes underlying cell function(s) of interest,

it has translational limitations owing to the absence of a fully physiological intracellular environment. Therefore, additional investigations were conducted in live cultured cells.

It was hypothesized that changes in bioenergetic parameters observed in isolated mitochondria would be evident also in intact cells exposed to TPP-IOA. To address this hypothesis, mitochondrial membrane potential and respiration rates, indicative of mitochondrial proton motive force and proton current, respectively, were assessed in cultured SH-SY5Y human neuroblastoma cells. Mitochondrial membrane potential is the major component of the proton motive force that drives ATP production from oxidative phosphorylation. This was semi-quantitatively assessed in SH-SY5Y-mito-mEFP cells using confocal fluorescence imaging with the lipophilic membrane-permeant red fluorescent cation TMRM (**Fig. 3.6**), whose mitochondrial uptake is proportional to membrane potential (Scadutto Jr. and Grotyohann, 1999). TMRM was used in non-quench mode whereby a decrease in mitochondrial membrane potential corresponds to decreased TMRM fluorescence intensity (Nicholls, 2012, Perry et al., 2011). FCCP treatment was used as a control to confirm that TMRM fluorescence intensity decreased when the mitochondrial membrane potential was dissipated (personal observations from preliminary assay optimization experiments; data not shown). In SH-SY5Y cells exposed to TPP-IOA (1 µM), mitochondrial TMRM fluorescence intensity was decreased compared to that of vehicle control-treated cells (37155 ± 3514 arbitrary fluorescence units per cell versus 54421 ± 2608 arbitrary fluorescence units per cell, respectively; p-value < 0.001, Student's t-test; **Fig. 3.6A middle panel** for representative images depicting TMRM fluorescence signal, and **Fig. 3.6B** for TMRM fluorescence signal quantification), indicating TPP-IOA can dissipate the mitochondrial membrane potential in intact cells.

Oxygen consumption rates (nmol O_2 consumed · min^{-1}) of intact SH-SY5Y human neuroblastoma cells were measured using closed-system respirometry (**Fig. 3.7**), and were initially standardized to cell number (**Fig. 3.7A**). The basal oxygen consumption rate of intact

cells acutely exposed to TPP-IOA (1 µM; 3 hours) remained unchanged compared to that of vehicle control-treated cells (1.46 ± 0.06 nmol O_2 consumed · min^{-1} · million $cells^{-1}$ versus 1.47 ± 0.33 nmol O_2 consumed · min^{-1} · million $cells^{-1}$, respectively; p-value < 0.05), suggesting that TPP-IOA does not exert a detectable effect on any processes that exert major control over the basal respiration rate.

The protonophore FCCP was subsequently used to chemically uncouple oxygen consumption from ATP synthesis, thereby allowing for fully uncoupled respiration rates and an indication of potential impairments to functional components of the electron transport system. Expectedly, both vehicle-treated and TPP-IOA (1 µM)-treated cells exhibited significantly elevated fully uncoupled respiration rates compared to their respective basal respiration rates (p-values < 0.05 and < 0.001 compared to basal rates for DMSO and TPP-IOA groups, respectively; Student's t-test). However, the fully uncoupled respiration rate was significantly attenuated in the presence of TPP-IOA compared to the vehicle-treated cells (2.06 ± 0.02 nmol O_2 consumed · min^{-1} · million $cells^{-1}$ versus 2.66 ± 0.33 nmol O_2 consumed · min^{-1} · million $cells^{-1}$; p-value < 0.05, Student's t-test), suggesting that TPP-IOA decreases the aerobic capacity of SH-SY5Y cells.

Respiration rates standardized to cell number do not take into account any changes in the abundance of mitochondria that may underlie experimental trends, such as in the results above. It was later determined that TPP-IOA (1 µM for 3hrs) elicited changes consistent with reduced mitochondrial abundance (see section **3.7** below for this data). Therefore, to account for differences in mitochondrial content between treatment groups at the time of respiration measurements, all oxygen consumption rates (nmol O_2 consumed · min^{-1}) were also standardized to activity of citrate synthase (e.g. as in Picard et al., 2008; **Fig. 3.7B**), a mitochondrial matrix enzyme whose expression level and maximal activity correlate strongly with mitochondrial content (Larsen et al., 2012).

Compared to the vehicle control, TPP-IOA caused elevated basal oxygen consumption rates per unit citrate synthase (0.03622 ± 0.00391 nmol $O_2 \cdot min^{-1} \cdot$ unit citrate synthase^{-1}, versus 0.0503 ± 0.0057 nmol O_2 consumed $\cdot min^{-1} \cdot$ unit citrate synthase^{-1} respectively; p-value 0.06, Student's t-test). As expected, respiration rates standardized to citrate synthase activity were elevated in the fully uncoupled state (FCCP addition) compared to the basal state of cells receiving the vehicle control (0.0533 ± 0.00698 nmol O_2 consumed $\cdot min^{-1} \cdot$ unit citrate synthase^{-1} versus 0.03622 ± 0.00391 nmol $O_2 \cdot min^{-1} \cdot$ unit citrate synthase^{-1}, respectively; p-value < 0.05, Student's t-test). In contrast, fully uncoupled oxygen consumption rates per unit citrate synthase in TPP-IOA treated-cells were not significantly increased compared to under the basal state (0.05301 ± 0.01354 nmol O_2 consumed $\cdot min^{-1} \cdot$ unit citrate synthase^{-1} versus 0.0503 ± 0.00573 nmol O_2 consumed $\cdot min^{-1} \cdot$ unit citrate synthase^{-1}, respectively). Therefore, while basal respiration rates standardized to cell number were unchanged in response to TPP-IOA, rates of basal respiration standardized to a proxy for mitochondrial content were elevated from the control treatment to near the uncoupled rates. Together, these findings indicate that TPP-IOA influences some component(s) of cellular or mitochondrial bioenergetics in intact cells that exerts control over the basal oxygen consumption rate.

Additionally, fully uncoupled oxygen consumption rates per unit citrate synthase did not differ between vehicle control and TPP-IOA groups (0.05301 ± 0.01354 nmol O_2 consumed $\cdot min^{-1} \cdot$ unit citrate synthase^{-1} and 0.05331 ± 0.00698 nmol O_2 consumed $\cdot min^{-1} \cdot$ unit citrate synthase^{-1}, respectively; p-value 0.9837, Student's t-test), suggesting that by this measure TPP-IOA does not significantly interfere with component(s) affecting proton current capacity (e.g. respiratory chain activity of the electron transport system).

Taken together with the above respirometry findings, it can be concluded that TPP-IOA impacts mitochondrial bioenergetics within intact cells by depolarizing the mitochondrial membrane potential and stimulating respiration. This, together with the shared similarity to the

responses to FCCP, are consistent with a possible mitochondrial uncoupling effect by TPP-IOA in live cells.

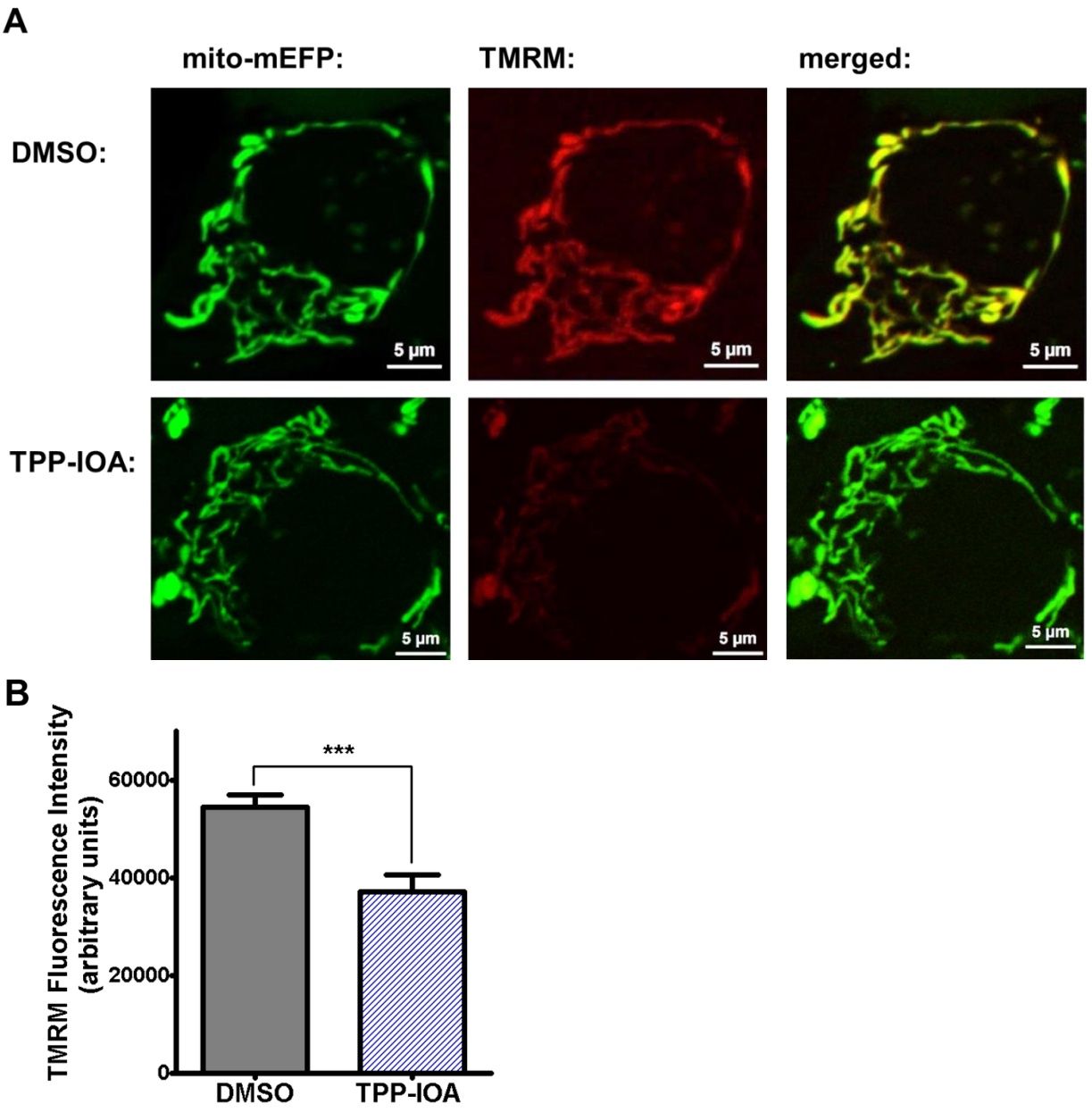

Figure 3.6: TPP-IOA dissipates mitochondrial membrane potential in intact SH-SY5Y human neuroblastoma cells.
A) Representative fluorescence images of TMRM-stained (40 nM; non-quench mode) single SH-SY5Y-mito-mEFP cells at 30 minutes of exposure to DMSO (**top**) or 1 µM TPP-IOA (**bottom**). ***Left panel:*** mito-mEFP signal (green; visual reference for mitochondrial location). ***Middle panel:*** membrane potential-dependent TMRM signal (red). ***Right panel:*** Overlay of mEFP and TMRM fluorescence signals. **B)** TMRM fluorescence signal intensity per cell is lowered in response to 1 µM TPP-IOA. Bars represent means + SEM of 12 cells per group from two independent experiments. *** = p-value < 0.001 (Student's t-test).

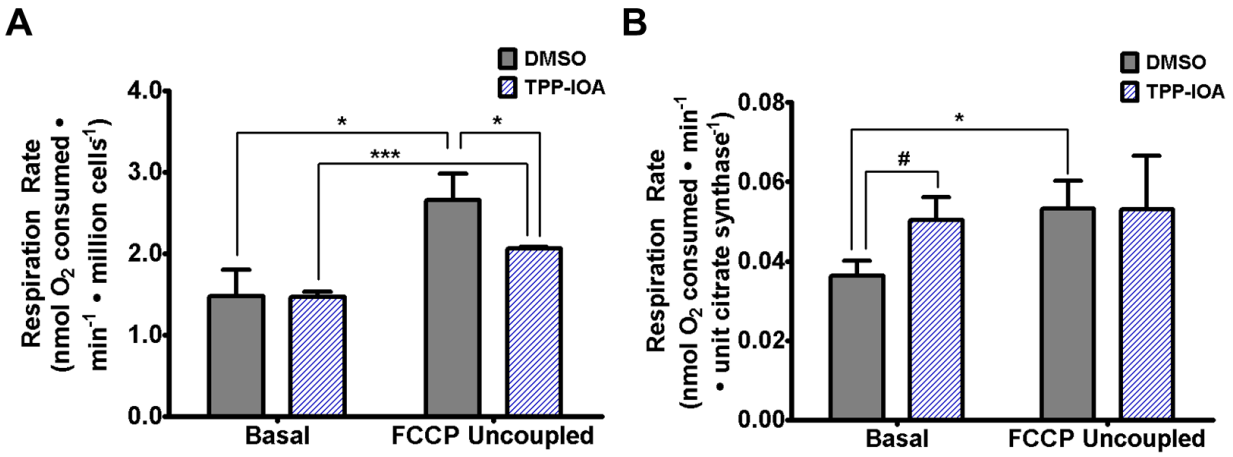

Figure 3.7: TPP-IOA interferes with cellular respiration in intact SH-SY5Y cells.
A) Basal and FCCP-uncoupled (2 µM FCCP addition) respiration rates (nmol O_2 consumed per minute) standardized to cell count (per million cells). **B)** Basal and FCCP-uncoupled (2 µM FCCP addition) respiration rates standardized to mitochondrial content (nmol O_2 consumed per minute per unit citrate synthase). SH-SY5Y cells cultured in glucose-containing DMEM were harvested for measurements at 3 hours of exposure to 1 µM TPP-IOA or an equivalent amount of DMSO (0.1%; vehicle control). Bars represent means + SEM from either two or three independent experimental replicates. * = p-value < 0.05, # = p-value < 0.06, *** = p-value < 0.001 (unpaired Student's t-test).

3.7 Impact of TPP-IOA on mitochondrial dynamics in intact cultured cells:

Components of mitochondrial dynamics, including morphology of the mitochondrial network and intracellular abundance of mitochondria, are intimately associated with bioenergetics. Generally, a fused and interconnected mitochondrial network is associated with increased bioenergetic efficiency (i.e. O_2 consumption strongly coupled to ATP synthesis), whereas the opposite has been reported for a fragmented network containing more punctate mitochondria. Since TPP-IOA disrupted mitochondrial membrane potential, it was predicted that TPP-IOA would also promote fragmentation of the mitochondrial network. To address this, confocal microscopy was used to image SH-SY5Y-mito-mEFP cells (**Fig. 3.8**). In these cells, a less interconnected, more fragmented mitochondrial network, was visually apparent at 3 hours of TPP-IOA (1 µM) exposure compared to control cells (**Fig. 3.8A**). These morphological changes

were evident as early as 45 minutes following TPP-IOA addition to media and were fully manifested by approximately 90 minutes (personal observations). A similar morphological change was also observed in C2C12 mouse myoblasts and SH-SY5Y cells not expressing mito-mEFP but labelled with MitoTracker Red CMXRosamine dye (see **Appendix I Fig. AI.5.2** and **Fig. AI.5.3**). These observations indicate that the fragmentation effect of TPP-IOA on the mitochondrial network is neither specific to SH-SY5Y cells, nor artifactually mediated by the mitochondrial labelling technique used. Additionally, FCCP was included as a positive control for the fragmentation response to chemical uncoupling of oxidative phosphorylation. FCCP (1 µM)-treated cells also contained an extensively fragmented mitochondrial network (**Fig. 3.8A**). Thus, changes to mitochondrial network morphology caused by TPP-IOA (1 µM) appear to be generally similar to those caused by a known chemical uncoupler of oxidative phosphorylation.

Additionally, the morphological changes to the mitochondrial networks within the SH-SY5Y-mito-mEFP cells were quantitatively analyzed using the custom-developed "Mitochondrial Analysis V1.0.0" ImageJ tool (Valente, unpublished – see **Appendix II** for detailed description). Both the number of mitochondrial networks (i.e. mitochondrial structures with at least one branching point) per cell and mean number of branches per mitochondrial network were quantified from the skeletonized depiction of mitochondrial signal (see both middle and top panels of **Fig. 3.8A**). TPP-IOA (1 µM) significantly increased the number of individual mitochondrial networks in cells (14.67 ± 1.42 mitochondrial networks per cell versus 9.07 ± 1.38 mitochondrial networks per cell in DMSO-treated cells; p-value < 0.05; one-way ANOVA with Tukey's HSD post-hoc test). This was similar to the response to FCCP (19.13 ± 1.42 mitochondrial networks per cell; p-value < 0.001 compared to DMSO cells; one-way ANOVA with Tukey's HSD post-hoc test). Additionally, there was a significantly lesser mean number of branches per mitochondrial network in response to TPP-IOA (11.07 ± 0.87) than in control cells (25.98 ± 3.16; p-value < 0.001, one-way ANOVA with Tukey's HSD post-hoc test).

This too was similar to the response to FCCP (7.26 ± 0.41; p-value < 0.001 compared to control, one-way ANOVA with Tukey's HSD post-hoc test). Altogether, the quantitative analysis indicates that TPP-IOA can cause mitochondrial networks to fragment into a greater number of individual networks with less extensive branching. This fragmentation response is similar to that caused by a potent chemical uncoupler. This fact, combined with the observed changes to energetics (section **3.6** above), further suggests that TPP-IOA can act as an uncoupler of oxidative phosphorylation in live cells.

Mitochondria with disrupted bioenergetics (e.g. possessing a sufficiently decreased membrane potential) can be selectively removed and degraded through mitophagy. Such degradation has been observed in cultured cells exposed to chemical disruptors of oxidative phosphorylation (e.g. McLelland et al., 2014). Since TPP-IOA caused both a disrupted mitochondrial membrane potential and a fragmented mitochondrial network in cells, it was hypothesized that TPP-IOA could be a stimulator of mitophagy. Since mitophagy can be reflected as a loss of apparent mitochondrial content in cells (e.g. Dolman et al., 2013, Ding and Yin, 2012), a reduction in mitochondrial content was predicted to occur following TPP-IOA treatment if mitophagy had occurred. To address this, two mitochondrial-specific content markers - maximal activity of the TCA cycle enzyme citrate synthase and the protein level of outer mitochondrial membrane protein voltage-dependent anion channel (VDAC) - were measured in whole-cell lysates of SH-SY5Y cells harvested 3 hours following the addition of TPP-IOA (1 µM) treatment (**Fig. 3.9**). Maximal citrate synthase activity levels were significantly lower in lysates of TPP-IOA-treated cells than of vehicle-control treated cells (184.8 ± 16.55 nmol TNB formed · min^{-1} · mg cellular $protein^{-1}$ versus 268.5 ± 12.18 nmol TNB formed · min^{-1} · mg cellular $protein^{-1}$ in vehicle control cells; p-value 0.0164, Student's t-test; **Fig. 3.9A**). Additionally, VDAC protein expression levels were significantly lower in lysates from TPP-IOA-treated cells compared to vehicle control cells, as determined by immunoblot (relative

protein band densities of 0.736 ± 0.0050 and 0.91 ± 0.0900, respectively; p-value 0.0408, Student's t-test; **Fig. 3.9B**). Together, these two measures indicate that TPP-IOA stimulated a reduction in mitochondrial content in cultured cells.

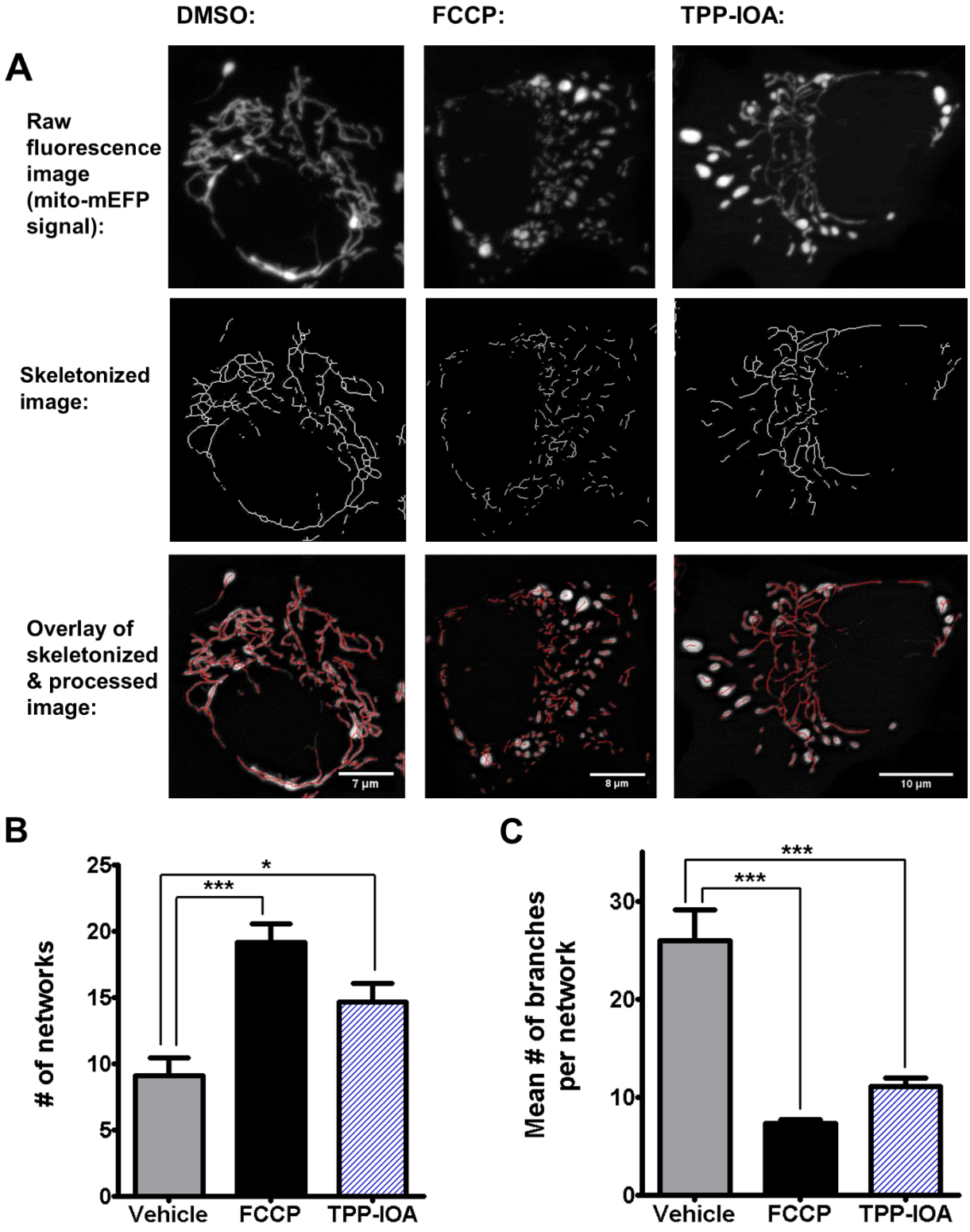

Figure 3.8: TPP-IOA alters mitochondrial network morphology in intact SH-SY5Y cells. **A)** TPP-IOA (1µM) causes fragmentation of mitochondria in SH-SY5Y-mito-mEFP cells, but to an apparent lesser degree than FCCP (1µM). ***Top panel:*** Raw confocal images of SH-SY5Y-mito-mEFP cells at 3hrs of indicated treatment (1 µM or equivalent volume of DMSO. Images were acquired using a Zeiss Axio Observer.Z1 inverted epifluorescence microscope (ex. 488 nm, em. 509 nm) equipped with ApoTome.2 optical sectioning, a 63x oil objective, and Hamamatsu camera, and are maximum intensity projections of z-stack series (≥ 25 slices, 0.25 – 0.30 µm

apart). ***Middle panel:*** Corresponding skeletonized depiction of mito-mEGP signal, as generated by post-acquisition processing with the "Mitochondrial Network Analysis, V1.0.1" ImageJ macro. ***Bottom panel:*** Overlay of the processed mito-mEFP signal with the skeleton depiction. **B)** TPP-IOA and FCCP (1µM each) increase the mean number of mitochondrial networks per cell. **C)** TPP-IOA and FCCP (1µM each) increase the mean number of branches per mitochondrial network. In **(B)** and **(C)**, measures were obtained from the "Mitochondrial Network Analysis, V1.0.1" ImageJ macro. Bars represent means + SEM from 15 total individual cells from two independent experiments. * = p-value < 0.05, *** = p-value < 0.001 compared to vehicle control (one-way ANOVA with Tukey's HSD post-hoc test).

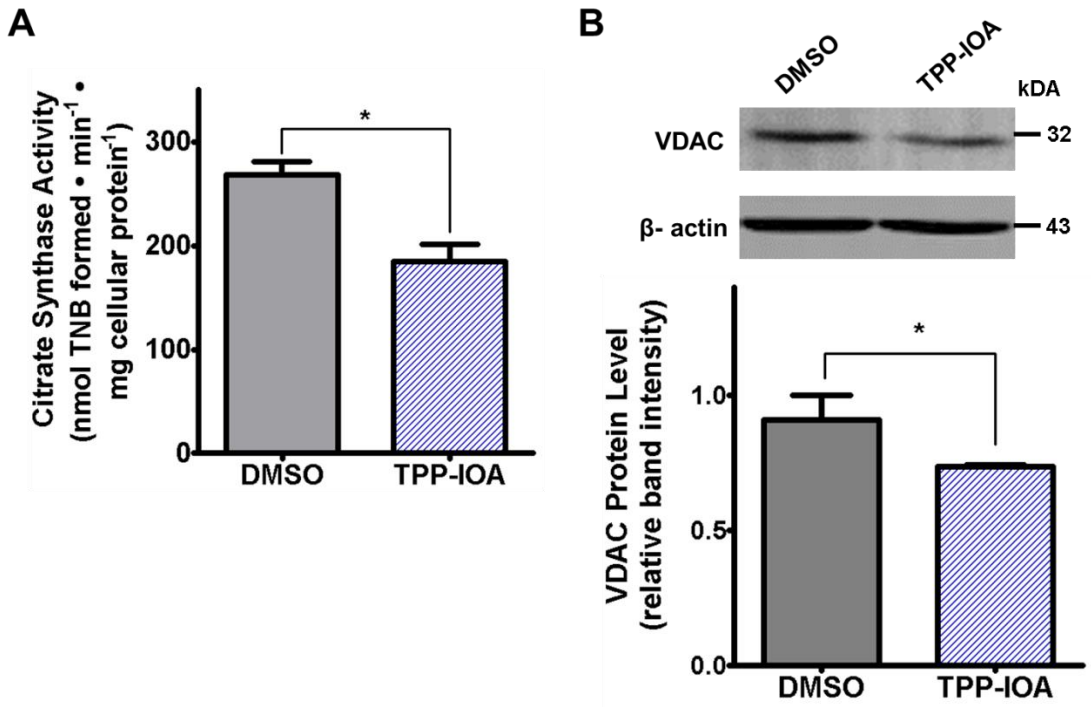

Figure 3.9: TPP-IOA reduces mitochondrial content in SH-SY5Y cells.
A) TPP-IOA (1µM) decreases maximal citrate synthase activity (nanomol TNB formed·min^{-1}·milligram cellular protein^{-1}). **B**) TPP-IOA (1µM) decreases VDAC protein levels (expression relative to an internal standard). Top inset depicts representative VDAC (~32 kDa) and β-actin (~43 kDa; probed as a loading control) immunoblot bands of indicated sample proteins separated by SDS-PAGE. In both figures, measurements were made with whole-cell lysates prepared from SH-SY5Y cells cultured in glucose-containing medium and harvested immediately after 3 hours of exposure to 0.1% DMSO (Vehicle control) or 1 µM TPP-IOA. Bars represent means + SEM from two or three experimental replicates. * = p-value < 0.05 (unpaired Student's t-test).

3.8 Influence of oxidative phosphorylation dependency on TPP-IOA's protective efficacy in intact cultured cells

Having observed changes that are associated with reduced mitochondrial ATP output in cells, as well as a narrow-to-non-existent therapeutic window between peroxidase inhibition and oxidative phosphorylation coupling measures with isolated mitochondria, it was hypothesized that TPP-IOA's protective capability in cells would be influenced by the relative reliance on oxidative phosphorylation. To investigate this, SH-SY5Y cells were cultured in either a glucose-free/galactose-&glutamine-containing medium (hereafter 'galactose medium') to promote reliance on oxidative phosphorylation, or a glucose-containing medium that preferentially allows for ATP generation via glycolysis (Reitzer et al., 1979, & Rossignol et al., 2004; Gusdon et al., 2012). The metabolic adaptation of SH-SY5Y cells to a galactose medium results in higher oxygen consumption rates and increased sensitivity to impaired ATP output from impaired mitochondrial energetics (Gusdon et al., 2012, Swerdlow et al., 2013). Consistent with these previous studies, SH-SY5Y cells cultured here in a galactose medium exhibited a significant increase in basal respiration rate compared to cells cultured in a glucose-containing medium (**Fig. 3.10**; 4.463 ± 0.5036 nmol $O_2 \cdot min^{-1} \cdot$ million $cells^{-1}$ versus 1.473 ± 0.3263 nmol $O_2 \cdot min^{-1} \cdot$ million $cells^{-1}$, respectively; p-value 0.0038, Student's t-test).

To assess TPP-IOA's anti-apoptotic effectiveness under each culture condition, the oxidant H_2O_2, which is a robust stimulator of the mitochondrial pathway of apoptosis (e.g. Singh et al., 2007), was used at doses that evoked approximately 50% cell loss (**Fig. 3.11**). In SH-SY5Y cells cultured in glucose-containing media, 300 µM H_2O_2 evoked 45.6 ± 1.9 % cell loss after 24 hours, as determined from cell viability counts using a Trypan blue exclusion assay (corresponding to 54.4 ± 1.9% total viability; **Fig. 3.11A**). In the presence of a wide range of TPP-IOA concentrations, (0.25 – 2.5 µM), the extent of total cell death was significantly reduced compared to non-treated controls (**Fig. 3.11A**). This improvement in cell viability was not

observed at higher concentrations of TPP-IOA, as 5 µM and 10 µM failed to exert a protective effect (see **Appendix I Fig. AI.5.4**). Furthermore, liberated AMC fluorescence resulting from characteristic cleavage of the peptide substrate Ac-DEVD-AMC by active Caspase-3 (Talanian et al., 1997) was used as a proxy for Caspase-3 activity in cell lysates and a marker for apoptosis. AMC fluorescence was elevated 3.26 ± 0.43-fold in response to 300 µM H_2O_2 exposure (**Fig. 3.12A**), thus indicating active Caspase-3 activity and involvement of apoptotic cell death under these lethal conditions. The induction of Caspase-3 activity was also lowered by TPP-IOA over a similar concentration range compared to non-treated controls, with statistically significant inhibition at 1 µM (**Fig. 3.12A**). Additionally, TPP-IOA (at 1 µM and 2.5 µM, but not at either 5 µM or 10 µM) limited H_2O_2-induced cell loss in C2C12 murine myoblasts cultured in a similar glucose medium, suggesting that its protective effect is not cell-type specific (see **Appendix I Fig. AI.5.5**). Altogether, these results indicate that TPP-IOA can prevent total cell death by inhibiting apoptosis in cells that are glycolytic and relatively less aerobic.

When grown in galactose medium, SH-SY5Y cells were generally more sensitive to H_2O_2, as 45.6± 1.929 % cell loss was evoked by only 200 µM H_2O_2 (corresponding to 53.41 ± 2.95 % total viability; **Fig. 3.11B**). At this concentration, Caspase-3 activity was similarly elevated compared to non-treated controls (3.39 ± 0.44 -fold increase; **Fig. 3.12B**). However, TPP-IOA (tested as low as 0.25 µM and up to 5 µM) failed to significantly prevent cell death or Caspase-3 activation in comparison to non-treated control groups under the same culture conditions (**Fig. 3.11A** and **Fig. 3.12B**). Together with the above findings, these results indicate that TPP-IOA can exert anti-apoptotic effects in cultured cells that utilize primarily glucose fermentation, but not in cells that are reliant on oxidative phosphorylation. Therefore, a lack of cellular dependence on oxidative phosphorylation is an important factor contributing to TPP-IOA's anti-apoptotic/cytoprotective effectiveness in cells.

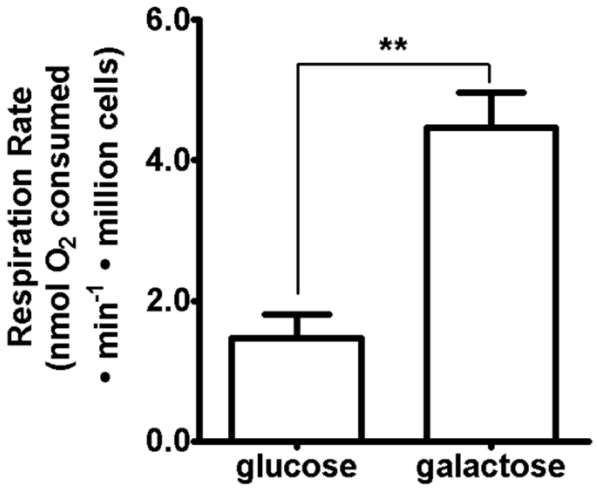

Figure 3.10: Replacing glucose-containing culture medium with glucose-free/galactose-containing culture medium enhances the basal oxygen consumption rate of SH-SY5Y human neuroblastoma cells.

Measurements of cells in glucose-free/galactose-containing culture media were performed five days after switching from glucose-containing culture media. Bars represent means + SEM from three individual replicates per condition. ** = p-value < 0.01 (one-tailed Student's t-test).

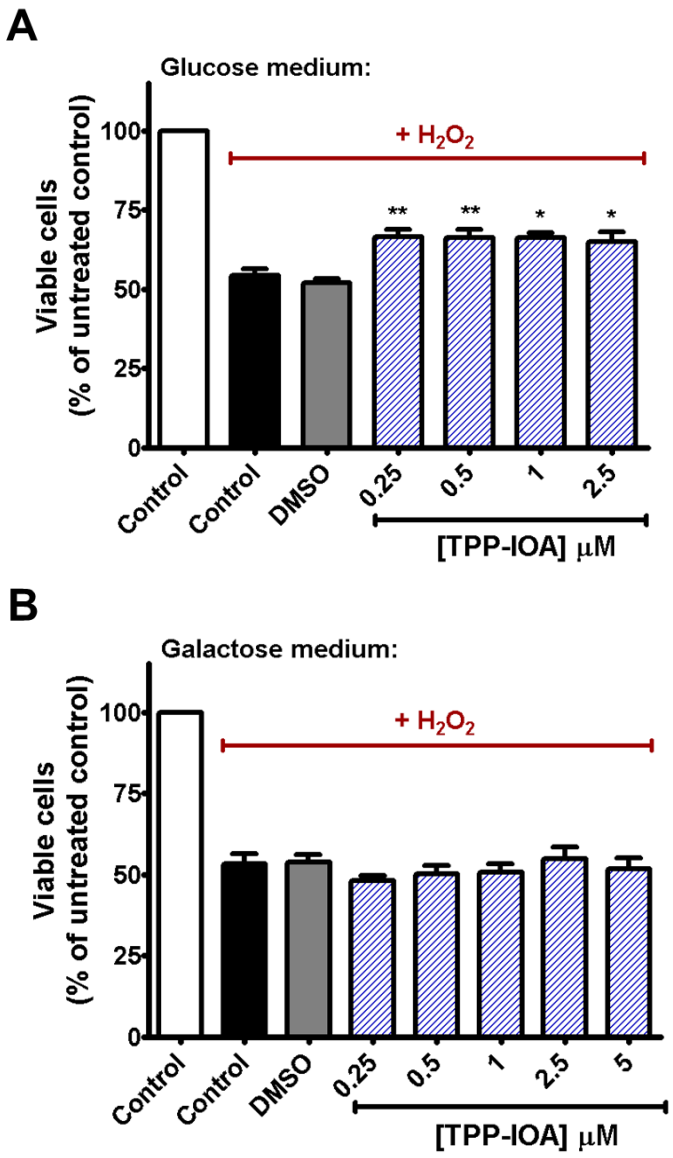

Figure 3.11: TPP-IOA inhibits H_2O_2-induced total death in SH-SY5Y cells allowed to ferment glucose but not in cells reliant on mitochondrial oxidative phosphorylation for ATP production.

A) TPP-IOA reduces the amount of total cell death caused by H_2O_2 in SH-SY5Y cells cultured in high glucose-containing media. Bars represent means + SEM from 7 – 14 total replicates from 3 – 5 independent experiments. ** = p-value < 0.01, *** = p-value < 0.001 compared to H_2O_2 control (black bar; one-way ANOVA with Tukey's HSD post-hoc test). **B)** TPP-IOA does not protect against cell death caused by H_2O_2 in SH-SY5Y cells cultured in glucose-free/galactose-containing media. Bars represent means + SEM from 6 – 11 total replicates from 3 – 5 independent experiments. No significant differences between H_2O_2-treated groups were observed (one-way ANOVA). Total cell death was assessed using the Trypan blue exclusion assay. All data were standardized to untreated-treated controls (white bar). TPP-IOA (blue diagonally-striped bars) was administered at the same time as H_2O_2. Doses of H_2O_2 previously determined to cause approximately 50% total cell death under each culture regime were used (300 μM in **(A)** and 200 μM in **(B);** dose-response data not shown).

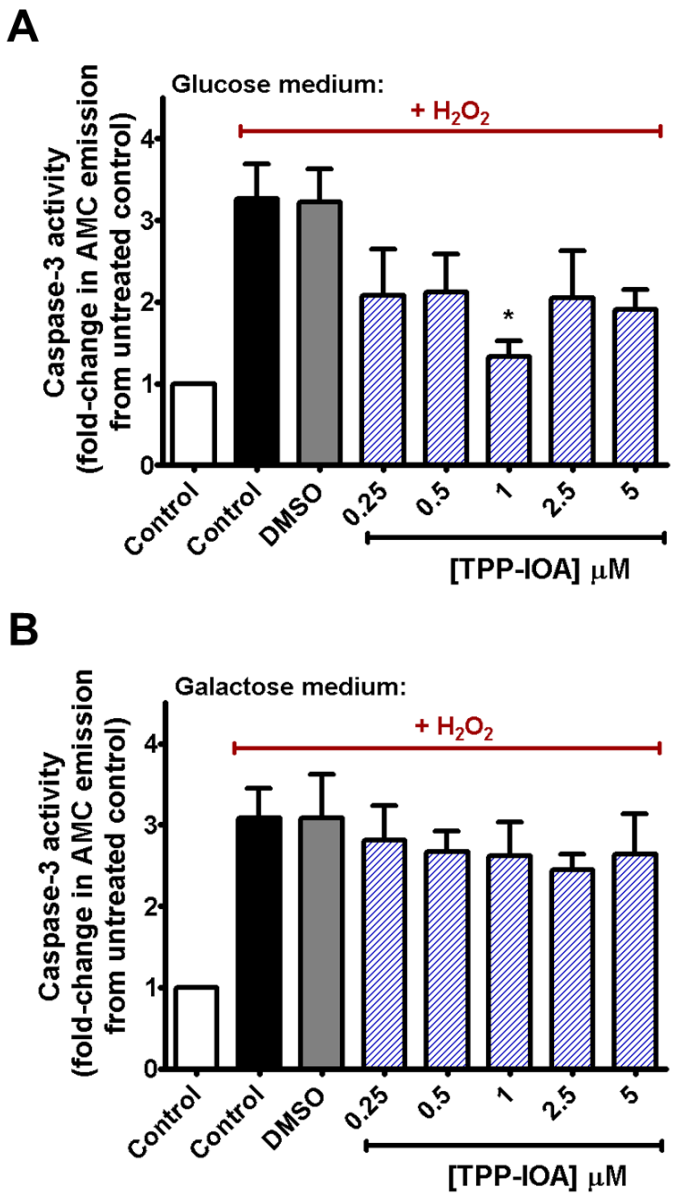

Figure 3.12: TPP-IOA prevents induction of Caspase-3 activity by H_2O_2 exposure in SH-SY5Y cells allowed to ferment glucose but not in cells that are reliant on mitochondrial oxidative phosphorylation.

A) TPP-IOA suppresses H_2O_2-induced Caspase-3 activation in SH-SY5Y cells cultured in high glucose-containing media. Bars represent means + SEM from 5 – 7 total replicates from 3 – 5 independent experiments. * = p-value < 0.05 compared to H_2O_2 control (black bar; one-way ANOVA with Tukey's HSD post-hoc test). **B)** TPP-IOA does not prevent H_2O_2-induced Caspase-3 activation in SH-SY5Y cells cultured in glucose-free/galactose-containing media. Bars represent means + SEM from 5 – 7 total replicates from 3 – 4 independent experiments. No significant differences between H_2O_2-treated groups were observed (p-value > 0.05, one-way ANOVA). All data were standardized to untreated-treated controls. TPP-IOA (blue diagonally-striped bars) was administered at the same time as H_2O_2. Caspase-3 activity [AMC fluorescence intensity (ex. 360 nm, em. 445 nm) per 25 μg cellular protein] were measured in cell lysates prepared from cells harvested immediately at 12 hours from the onset of 200 μM (**B**) or 300 μM (**A**) H_2O_2 exposure.

Chapter 4.0 – Discussion:

4.1 Effects of TPP-IOA on the reduction of purified cytochrome c*:*

Prior to the current study, TPP-IOA's effect on cytochrome *c*'s respiration-associated electron transfer activity had not been investigated. Here, it was discovered that TPP-IOA can inhibit reduction of cytochrome *c*'s heme iron, which is essential for electron chain activity during oxidative phosphorylation. Since the imidazole group of TPP-IOA acts as a ligand for the heme iron (Atkinson et al., 2011), it is possible that this is a direct effect of the imidazole group. Consistent with this notion is the fact that exogenously added imidazole can also inhibit cytochrome *c* reduction by replacing the iron-binding sulphur of the native Met80 ligand in cytochrome *c* (Babul & Stellwagen, 1971; Schejter & Aviram, 1969). However, the observation that TPP-oleic acid, which is devoid of an imidazole ligand, also slowed cytochrome *c* reduction kinetics suggests that the disruptive effect of TPP-IOA may have been caused by a different interaction.

It has been shown that binding of oleic acid to cytochrome *c* can cause conformational changes or partial unfolding of the protein that includes a weakening or loss of native Met80-heme iron coordination (Stewart et al., 2000, Sinibaldi et al., 2005, Patriarca et al., 2009). Such disruptions to the heme environment appear to have been reported at concentration ratios as low as 1:2 oleate to cytochrome *c* (Stewart et al., 2000), which is smaller than the ratio at which TPP-oleic acid caused major disruption to cytochrome *c*'s reduction activity here. This, coupled with the fact that the reduction activity of cytochrome *c* is sensitive to general structural/heme environment changes in the protein (Moore and Pettigrew, 1990), suggests that the disruption to cytochrome *c*'s reduction activity by TPP-IOA could be due to structural disruptions resulting from the oleate's interaction with the protein.

4.2 Effects of TPP-IOA on isolated mitochondria:

Much higher levels of TPP-IOA were required to achieve inhibition of peroxidase activity with isolated rat liver mitochondria (40 nmol TPP-IOA per mg mitochondrial protein) than with purified cytochrome *c* (0.5 nmol TPP-IOA per nmol cytochrome *c*; c.a. 1:1). Using the reported value of approximately 0.21 nmol cytochrome *c* per mg mitochondrial protein in adult rat liver (Wainio, 1970; Petrosillo et al., 2003), it can be estimated that approximately 190-fold higher ratio of TPP-IOA:cytochrome *c* was required to achieve 50% reduction of its peroxidase activity in isolated mitochondria. This requirement for an excessive amount of TPP-IOA may be reconciled by the fact that there are greater molecular barriers to TPP-IOA's interaction with cytochrome *c*, which is located within the inter-membrane space (e.g. Scoranno et al., 2002).

Although much higher concentrations of TPP-IOA were required, it nonetheless had significant effects on respiratory control and oxidative phosphorylation coupling efficiency in isolated mitochondria at concentrations similar to those needed to inhibit cytochrome *c*'s peroxidase activity. TPP-IOA adversely affects some functional component(s) of both the phosphorylating system, which may include ATP synthase, ANT, and/or the phosphate carrier, the electron transport system and/or substrate transporters. The elevated State 4 respiration rates in the absence of State 3 stimulation suggest that TPP-IOA stimulates proton leak. This could be due to direct effects on the phospholipid bilayer, or effects on membrane protein-mediated activities (e.g. uncoupling proteins), or a combination of both. The data do not allow for discernment between the two possibilities.

It is possible that the effects of TPP-IOA on oxidative phosphorylation are mediated partly by the long chain fatty acid structure. Long chain fatty acids have been shown to affect mitochondrial respiratory states in much the same manner as TPP-IOA (i.e. elevated State 4/non-phosphorylating respiration rates, and decreased State 3 and fully uncoupled respiration rates in isolated mitochondria; e.g. see citations in Wojtczak, 1976, Wojtczak & Schönfeld, 1993, and Di

Paola and Lorusso, 2006). There is evidence for interactions of long chain fatty acids with some transporter proteins of the phosphorylation and electron transport systems, including ANT (Wojtczak & Zaluska, 1967; Andreyev et al., 1989), phosphate carrier (Záková et al., 2000, Engstová et al., 2001), aspartate/glutamate antiporter (Samartsev et al., 1997), and the dicarboxylate carrier (Wieckowski et al., 1997). These various substrate transporters have been reported to mediate the uncoupling and/or protonophoric activity of long chain fatty acids, and the interactions could also perturb their proper functioning and lead to impaired State 3 and/or fully uncoupled respiration. Similar interactions between these transporter proteins and the long chain fatty acid moiety of TPP-IOA may be possible, the functional outcome of which would be consistent with the perturbations to mitochondrial respiration elicited by TPP-IOA.

The imidazole group on the acyl chain of TPP-IOA may also contribute to perturbations of oxidative phosphorylation. Molecules belonging to the imidazole class of antimycotics can cause uncoupling of oxidative phosphorylation and/or dissipation of membrane potential in isolated rat liver mitochondria and cultured mammalian cells (Kawahi et al., 1983; Andreux et al., 2014). A future comparison of the absolute rates of various mitochondrial respiratory states in the presence of TPP-IOA versus that in the presence of TPP-OA may directly clarify this. Whether perturbed mitochondrial respiration is a fundamental effect of imidazole fatty acid derivatives could be of importance to the development of imidazole-fatty acid molecules, particularly since a number of TPP-conjugated stearic acid derivatives with imidazole present at different parts of the acyl chain have already been synthesized and tested for their anti-apoptotic effectiveness (Jiang et al., 2014). Though the location of the imidazole group is reportedly important for the anti-apoptotic effectiveness of these molecules (Jiang et al., 2014), this may not matter for perturbations of oxidative phosphorylation.

Others have reported that lipophilic TPP-containing linker moieties devoid of any active chemical group may not be bioenergetically inert and can interfere with mitochondrial energy

coupling processes (Reily et al., 2013; Trnka et al., 2015). In the current study, the decreased RCR and oxidative phosphorylation coupling efficiency of isolated rat liver mitochondria in the presence of 3-hydroxypropyl-TPP indicate that the free TPP-containing moiety also has the capacity to directly interfere with oxidative phosphorylation. That this effect was driven by elevated State 4/non-phosphorylating respiration is consistent with a prior published report showing increased oligomycin-insensitive (non-phosphorylating) respiration in intact cells exposed to other TPP-containing linker moieties (Trnka et al., 2015). Notably, in this prior study the uncoupling-like response occurred with alkyl-TPP linker molecules containing lengthy alkyl chains (e.g. decyl-TPP) but not shorter alkyl chains, such as propyl-TPP. The hydroxyl group present at the end of the propyl chain of 3-hydroxypropyl-TPP is likely to be a significant additional structural feature in conferring any direct uncoupling-like activity of this short alkyl-chained TPP-containing molecule, as an acid-dissociable group is a crucial property allowing for a chemical uncoupler to mediate proton translocation (Terada, 1990).

Aside from a direct disruptive effect, it is also possible that 3-hydroxypropyl-TPP could work in conjunction with the free imidazole-oleic acid to potentiate disruptive activity. In agreement with this, there is evidence that lipophilic cations, including TPP-derivatives, can potentiate the protonophoric uncoupling activity of exogenous long chain fatty acids and have been proposed to do so by pairing with the anionic form of the fatty acid to form an ion-pair complex to facilitate movement across the inner mitochondrial membrane from the matrix (Schönfeld, 1992; Severin et al., 2010; Trendeleva et al., 2012). Regardless of the exact mechanism underlying the dysfunction, the data obtained here using isolated rat liver mitochondria indicate that the TPP-containing moiety of TPP-IOA can impact mitochondrial bioenergetic function at sufficiently high concentrations by stimulating non-phosphorylating respiration. In general, these data highlight the importance of including an experimental control of the TPP-moiety alone when studying small molecules targeted to mitochondria via TPP-

conjugation, particularly in the experimental context of bioenergetics as it is becoming increasingly evident that such molecules can impact energetic processes of mitochondria.

4.3 Effects of TPP-IOA on cultured cells:

In live cells, perturbed oxidative phosphorylation is associated with a more fragmented mitochondrial morphology. In this study, untreated SH-SY5Y cells contained mitochondrial networks with extensive branching, whereas cells treated with FCCP (positive control for fragmentation) featured more individual networks (i.e. network fragmentation) with less extensive branching. These findings are consistent with a recent study showing decreased network fiber lengths and networked area in response to uncoupling (CCCP), using a similar method for automated image processing (Leonard et al., 2015). Changes to the mitochondrial network in response to TPP-IOA observed here were generally similar to those elicited by FCCP, though the response was less pronounced. This observation, in addition to the elevated rates of basal respiration and decreased mitochondrial membrane potential, indicate that TPP-IOA's effects on mitochondria are consistent with uncoupling. Although the development of the processing/analysis macro was not a focal point of the current study, the experimental data obtained from it does serve as proof that it can be a useful quantitative diagnostic tool for identifying and describing mitochondrial network morphology changes.

Decreased mitochondrial membrane potential, fragmentation of mitochondria, and decreased levels of mitochondrial content makers were all observed within 3h of 1 μM TPP-IOA introduction. Together, these changes suggest the induction of uncoupling-induced mitophagy (e.g. Ashrafi & Schwartz, 2013) by TPP-IOA. This could have important physiological implications for TPP-IOA's anti-apoptotic activity, which revolves around the prevention of cytochrome *c* release into the cytosol. Although not measured in the current study, a decrease in mitochondrial content via mitophagy results in less cytochrome *c* within the cell (Saita et al.,

2013). With less total cytochrome *c* available for release, activation of Caspase-activating cascades and other downstream apoptotic cell death activities might be limited. Indeed, others have shown that enhanced activation of mitophagy suppresses cytochrome *c* release into the cytosol and inhibits apoptosis (Mariño et al., 2014; Xia et al., 2014; Choe et al., 2015). The decreased H_2O_2-induced Caspase-3 activity and total cell death elicited by TPP-IOA in glucose-cultured SH-SY5Y cells (discussed further below) are consistent with such a mechanism of cell death protection. It is also possible for this mechanism to have at least partly been involved in the protection by TPP-IOA (at 2.5 μM and 5 μM) from radiation-induced death in cultured fibroblasts previously observed (Atkinson et al., 2011). Notably, this possibility cannot be ruled out from the data provided in that study, as none of the measures provided could serve as mitochondrial content markers. It is therefore possible that, in addition to direct physical inhibition of cytochrome *c*'s pro-apoptotic peroxidase activity, TPP-IOA's anti-apoptotic mechanism of action could involve mitophagy induction secondary to the disruption of oxidative phosphorylation.

Proliferative cells, including those in culture that are cancerous or transformed, often feature increased rates of glycolysis relative to oxidative phosphorylation (e.g. Lunt & Vander Heiden, 2011). As a consequence of meeting a greater proportion of ATP demand via glycolysis, such cells may be particularly tolerant of perturbations affecting oxidative phosphorylation. Since initial results indicated that TPP-IOA offered protection against cell death but also interfered with oxidative phosphorylation, it was important to study cells growing under conditions that increased reliance on oxidative phosphorylation. This was achieved by altering the carbohydrate source, either glucose or galactose, provided in the culture medium. SH-SY5Y cells cultured in a galactose medium had higher rates of oxygen consumption [**Fig. 3.11**], as expected (Swerdlow et al., 2013; Gusdon et al., 2012), indicating a greater reliance on oxidative phosphorylation (e.g. Marroquin et al., 2007; MacVicar & Lane, 2014). SH-SY5Y cells in

galactose-based culture media were generally more sensitive to H_2O_2 than the same cells in a glucose-based medium; similar amounts of cell death and Caspase-3 activation were observed at 200 μM and 300 μM H_2O_2, respectively, in glucose and galactose media. This observation may be explained by increased reliance on oxidative phosphorylation in galactose media, but it may also relate to lowered intracellular oxidant defense resulting from decreased flux through the pentose phosphate pathway in the absence of glucose (eg. Le Goffe et al., 1999; Wu & Wei, 2012).

In any event, protection from H_2O_2-induced SH-SY5Y cell death by TPP-IOA observed in glucose media was not observed in galactose media. The discrepancy indicates that the metabolic context determines the anti-apoptotic effect of TPP-IOA. This may relate to differences in sensitivity to perturbed mitochondrial ATP output. If TPP-IOA sufficiently decreased mitochondrial ATP output, this should have a direct effect on cellular ATP levels in galactose-grown cells that are heavily reliant on oxidative phosphorylation. Notably, the mode of cell death under general lethal conditions can shift from apoptosis (which is ATP-dependent) to necrosis (ATP-independent) if there is insufficient cellular ATP. The lack of total cell death prevention (as assessed by Trypan blue exclusion counts that do not discriminate between apoptotic and necrotic cell death) combined with the minor, yet statistically insignificant, drop in the apoptotic activity marker Caspase-3 activity is consistent with such a shift in the presence of TPP-IOA. However, with this in mind, it is also important to note that over the concentration range tested, TPP-IOA did not exacerbate the amount of cell death caused by H_2O_2 in the galactose medium. This might be predicted to occur in these cells if TPP-IOA caused cellular ATP levels to decline to a catastrophic degree.

Considering that knowledge of cellular ATP levels is required in the above explanations for the discrepancy for TPP-IOA's protective effect, strengthening evidence for these interpretations could be provided with future measurements of cellular ATP levels following

TPP-IOA addition to cells. Additionally, these interpretations could be further supplemented with measurements of glucose utilization and/or lactate production to detect changes in glycolytic metabolism.

As discussed earlier, induction of mitophagy, the result of which is less cytochrome *c* and other pro-apoptotic mitochondrial proteins available for release under apoptotic conditions, could at least partly underlie TPP-IOA's anti-apoptotic mechanism in cells. Notably, mitochondrial content markers were measured in the glucose-grown cells but not the galactose-grown cells in response to TPP-IOA. Therefore, it is unknown whether the same decline in apparent mitochondrial content had occurred in galactose-grown SH-SY5Y cells. Importantly, there is evidence that sensitivity to mitophagy induction is influenced by cellular dependency on oxidative phosphorylation. For example, cytosolic mitophagy machinery translocated to mitochondria in response to mitochondrial depolarization in HeLa cells when cultured in a glucose medium, but not when in a galactose-medium (Van Laar et al., 2011). Likewise, in human telomerase immortalized retinal pigment epithelial cells, uncoupling-induced mitophagy occurred when cultured in a glucose medium but was suppressed in a galactose medium (MacVicar & Lane 2014). It is thus conceivable that TPP-IOA may not have elicited the same mitophagy-like response in the galactose medium, where cells are more reliant on oxidative phosphorylation and perhaps resultantly less inclined to initiate a mitophagy response to acute energetic stress. With this in mind, the fact that TPP-IOA failed to protect against oxidant-induced cell death in the galactose medium lends support to the notion that TPP-IOA's anti-apoptotic mechanism could involve a stimulation of mitophagy.

Future work using various autophagy/mitophagy assays (e.g. measuring co-localization of mitochondria with mitophagy machinery; Klionsky et al., 2016) could provide definitive evidence for whether TPP-IOA is a stimulator of mitophagy. Furthermore, testing whether the prevention of cell death by TPP-IOA persists in the presence of mitophagy/lysosomal inhibitors

could provide valuable proof for whether mitophagy is a part of TPP-IOA's anti-apoptotic mechanism of action in cells. Together, such findings would be yield a more complete understanding of TPP-IOA's biological effects that are relevant to the molecular mechanism(s) through which it exerts its anti-apoptotic effect in cells. In a more general sense, the identification of mitophagy as part of TPP-IOA's protective mechanism could have widespread implications for other mitochondrial-based therapeutics, as the functional implications of the previously identified disruptions to mitochondrial bioenergetics by TPP-cation based small molecules (e.g. Reily et al., 2013) are neither known nor been subject to experimental investigation. Induction of mitophagy owing to their interaction with mitochondrial energetics may be a fundamental effect of TPP-cation based small molecules that could at least partly contribute to their protective action in cells. Investigating this could be a worthwhile future goal.

4.4 Potential therapeutic applications for TPP-IOA –an energetics perspective:

From a variety of *in vitro* measures at multiple levels of biological organization, this thesis revealed altered mitochondrial energetics in response to the anti-apoptotic molecule TPP-IOA, and that ultimately TPP-IOA could only prevent oxidant-induced cell death of cells with propensity to use glycolytic metabolism rather than those reliant on oxidative phosphorylation. These findings imply that, in principle, relative reliance on mitochondrial energetics is an important cellular property that influences TPP-IOA's anti-apoptotic efficacy in cells. These results offer a more nuanced understanding of TPP-IOA's anti-apoptotic mechanism of protection in cells.

A prediction from the current work is that TPP-IOA is likely to be effective in preventing *in vivo* apoptotic cell death in pathologies where, in addition to dying via the mitochondrial pathway of apoptosis, the major cell types affected are generally glycolytic/fermentative or generally less reliant on oxidative phosphorylation. Importantly, the existing data for TPP-IOA's

in vivo anti-apoptotic/therapeutic utility comes from an experimental model of pathological cell loss (radiation exposure) in which the predominantly affected cell types are highly proliferative (Macià I Garau et al., 2011) and poised for glycolytic energy metabolism (Vander Heiden et al., 2009). Thus, these previous findings do not contradict the principle outcome of the current study, and additionally support a testable prediction of the current work.

Importantly, based on the current findings, TPP-IOA would be predicted to be ineffective in directly preventing loss of highly aerobic cells (e.g. neurons, cardiomyocytes) occurring through the mitochondrial pathway of apoptosis in pathological scenarios. This prediction, however, does not necessarily entirely rule out TPP-IOA's utility as a therapeutic agent in potential pathologies of highly aerobic tissues affecting quiescent cell types that feature both a low regenerative capacity and highly aerobic energy metabolism, which are generally of large biomedical interest. A reason for this relates to possible heterogeneity of cell types and their potential differing metabolic properties within a highly aerobic tissue of interest. If there is an abundance of highly glycolytic cell types that contribute to the overall tissue pathology via death through the mitochondrial apoptotic pathway, then TPP-IOA's ability to prevent such cell death could potentially prevent degeneration of the whole tissue.

For example, the brain possesses a large abundance of neurons, which have high aerobic activity, but also features a higher abundance of astrocytes, which are less aerobically-active and more highly glycolytic (Belanger et al., 2011). Importantly, astrocytes serve multi-faceted functions in the brain, which consequently ensures proper neuronal activity (e.g. Clarke & Barres, 2013). Astrocyte apoptosis via the mitochondrial pathway contributes to brain pathology in acute neurodegenerative contexts and there is evidence that it can precede the degeneration of neurons (e.g. Liu et al., 1999; Takuma et al., 2004; Sofroniew & Vinters, 2010). Therefore, in principle, TPP-IOA could potentially afford neuroprotection in various acute brain pathologies by effectively suppressing apoptotic cell death of this glycolytic cell type. Aside from this brain-

specific cell type, a more general example of a cell type suitable for protection by TPP-IOA is the endothelial cell. These cells are necessary for proper blood vessel functioning, which in turn is required for proper functioning of effector tissues (Sumpio et al., 2002). They are generally a highly glycolytic cell type whose apoptotic cell death is associated with acute pathologies of many highly aerobic tissues, including ischemia/reperfusion-like injuries (e.g. Verdegem et al., 2014; Goveia et al., 2014; Polet & Feron et al., 2013). Inhibiting apoptosis of this cell type could improve survival of downstream aerobic cell types. In general, combining knowledge of cell type-specific metabolic properties with cell-type specific involvement in pathologies of interest will be essential in informing decisions to pursue potential future therapeutic applications for TPP-IOA.

4.5 Overall Conclusions:

Here, investigations carried out at multiple levels of biological organization revealed important insights into the mitochondria-targeted anti-apoptotic molecule TPP-IOA's interactions with components of mitochondrial and cellular energetics. The data indicated that TPP-IOA can interfere with energetic processes of both its target protein and organelle, and notably, in the latter was virtually unable to appreciably inhibit pro-apoptotic oxidase activity without concomitantly interfering with oxidative phosphorylation. Additionally, TPP-IOA's protective efficacy from oxidant-induced cell death was only detectable in cultured cells with a propensity to use glycolytic metabolism rather than oxidative phosphorylation, indicating that relative cellular dependence on oxidative phosphorylation is a critical factor in allowing the anti-apoptotic effect to be realized. Altogether, these data indicate that TPP-IOA's interactions with mitochondrial energetics is likely an important factor influencing the small molecules anti-apoptotic utility. Importantly, this information, together with knowledge of cell-type specific metabolic properties, can serve as a basis for rationally predicting the suitability of TPP-IOA in

potential future therapeutic applications. With this in mind, potential future therapeutic applications with TPP-IOA may be restricted to disease contexts in which either aerobic metabolism is reduced or highly glycolytic/less aerobic cell types are major contributors tissue degeneration or the general pathology.

Appendix I - Data:

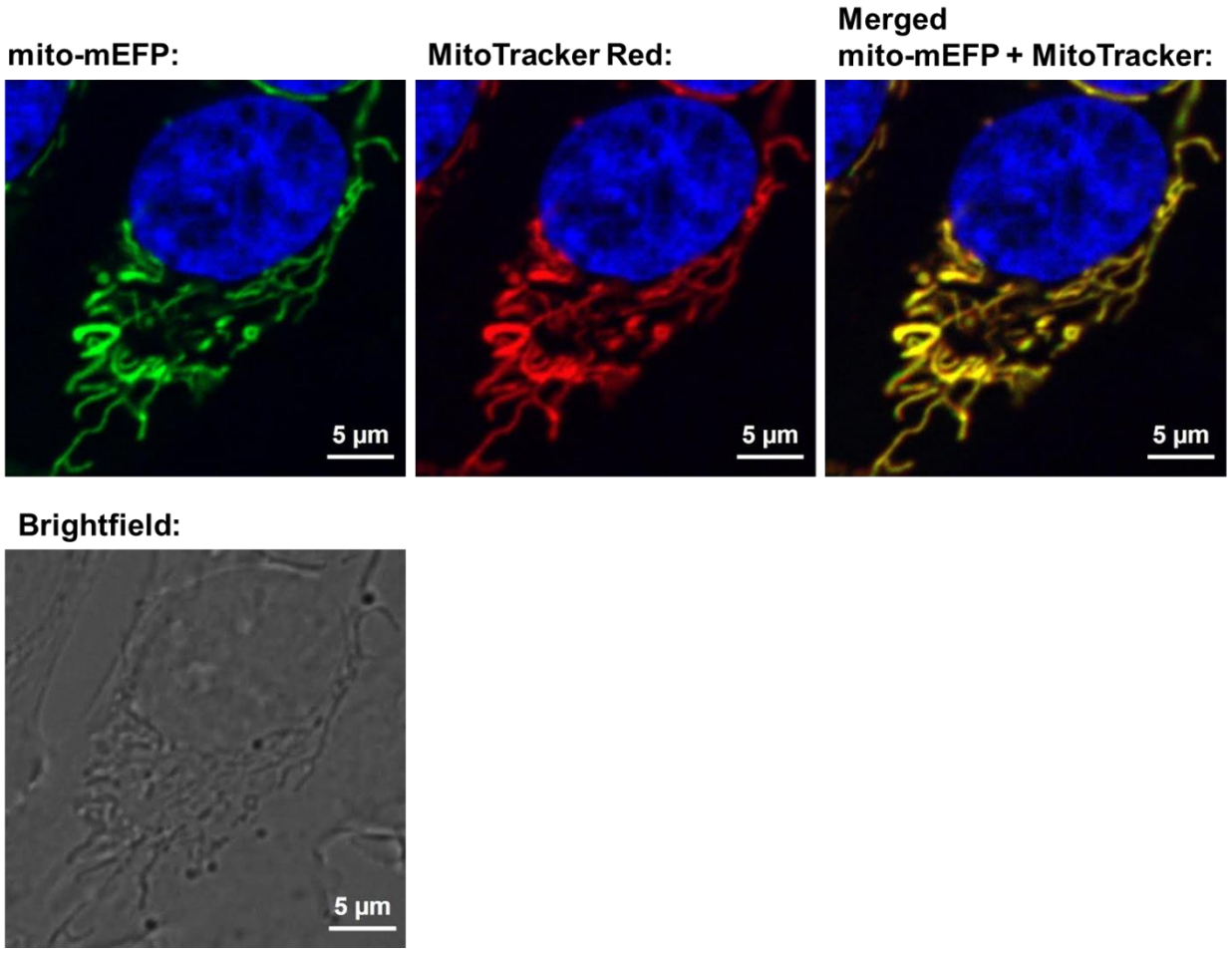

Figure AI.5.1: mEFP signal co-localizes with MitoTracker Red CMXRos dye signal in SH-SY5Y cells stably expressing a gene for mitochondria-targeted mEFP, confirming mitochondrial localization of the mEFP.
SH-SY5Y-mito-mEFP cells were pre-stained with MitoTracker Red CMXRos (simultaneously with Hoechst 33342 fluorescent dye for nuclear labelling; blue) for 30 minutes prior to imaging with a Zeiss Axio Observer.Z1 inverted epifluorescence microscope equipped with ApoTome.2 optical sectioning, a 63x oil objective, and Hamamatsu camera. Images are maximum intensity projections of a z-stack series consisting of 25 slices, 0.25 µm apart. The image shown is of a single cell.

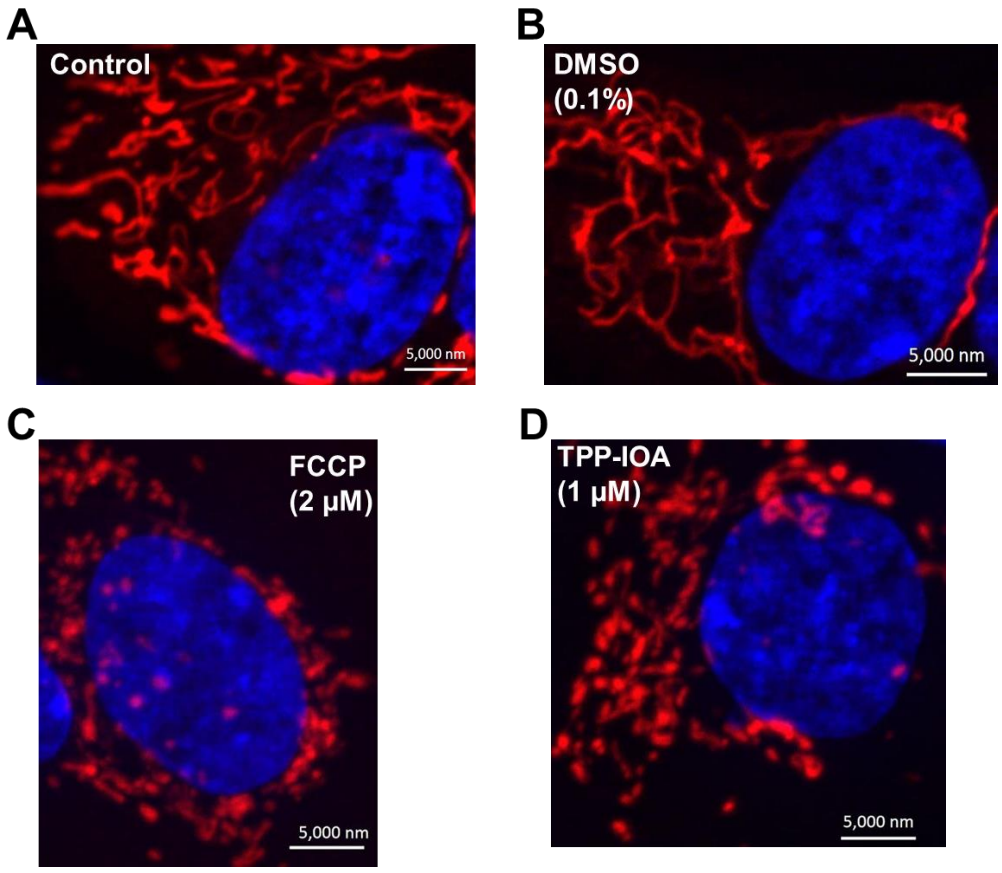

Figure AI.5.2: TPP-IOA alters mitochondrial network morphology in SH-SY5Y human neuroblastoma cells stained with MitoTracker Red CMXRos dye.
A - D) SH-SY5Y neuroblastoma cells were pre-stained with 50 nM MitoTracker Red CMXRos (red signal)and Hoechst 33342 fluorescent dye (blue signal; nuclear labeling) and then imaged after 90 min exposure to 0.1% DMSO (**B**), 2 µM FCCP (**C**), 1 µM TPP-IOA (**D**), or media change without chemical treatment (**A**). Images are representative of >25 cells from two independent experiments for each treatment. All images were acquired using a Zeiss Axio Observer.Z1 inverted epifluorescence microscope equipped with ApoTome.2 optical sectioning, a 63x oil objective, and Hamamatsu camera, and are maximum intensity projections of z-stack series (≥ 25 slices, 0.25 – 0.30 µm apart).

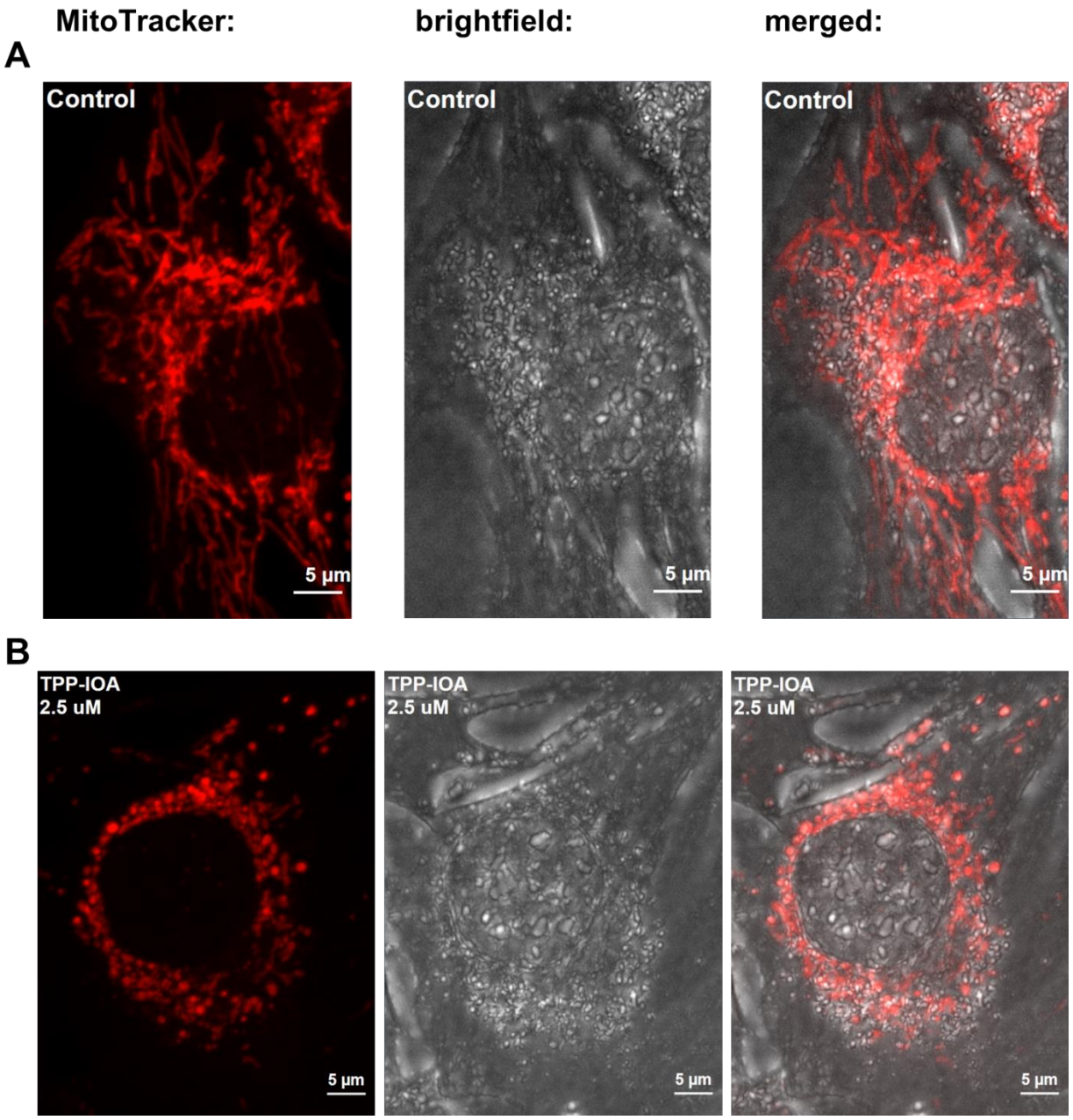

Figure AI.5.3: TPP-IOA alters mitochondrial network morphology in C2C12 murine myoblasts.

A, B) C2C12 mouse myoblasts were pre-stained with 50 nM MitoTracker Red CMXRos and imaged at 60 min exposure to 2.5 µM TPP-IOA (**B**) or 0.1% DMSO (**A**). Images are representative of >25 cells from two independent experiments for each treatment.

All images were acquired using a Zeiss Axio Observer.Z1 inverted epifluorescence microscope equipped with ApoTome.2 optical sectioning, a 63x oil objective, and Hamamatsu camera, and are maximum intensity projections of z-stack series (≥ 25 slices, 0.25 – 0.30 µm apart).

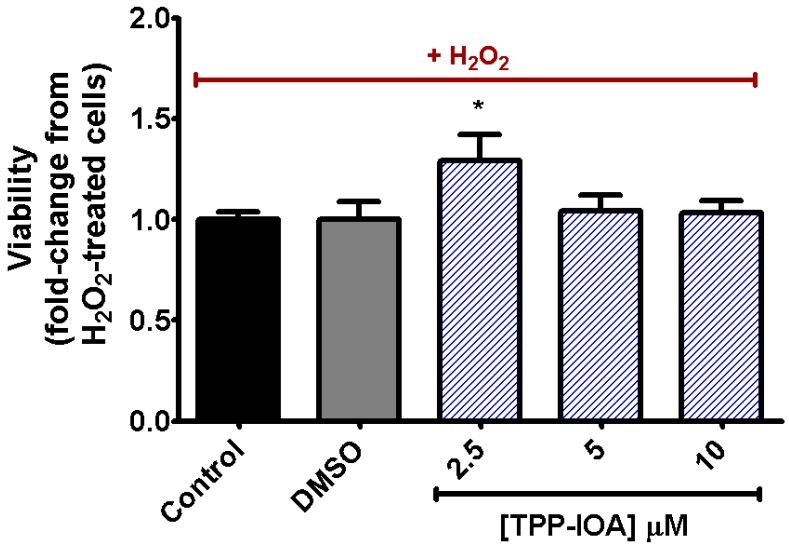

Figure AI.5.4: TP-IOA does not prevent H_2O_2-induced cell death of SH-SY5Y human neuroblastoma cells at 5 µM and above in a glucose culture medium.
TPP-IOA was added to culture medium simultaneously with 300 µM H_2O_2. Cells were harvested 24 hours later for cell viability counts with the Trypan blue dye exclusion assay.
Bars represent means + SEM from 3 – 5 total replicates from 2-3 independent experiments. * = p-value < 0.05 (one-way ANOVA with Tukey's HSD post-hoc test). ***Note:*** Here, the counts of viable cells were standardized to the 300 µM H_2O_2 treatment group (black bar). In other experiments (ten total replicates from five independent experiments), 300 µM H_2O_2 elicited 45.6 ± 1.9 % cell loss in other experiments (see Fig. 3.11).

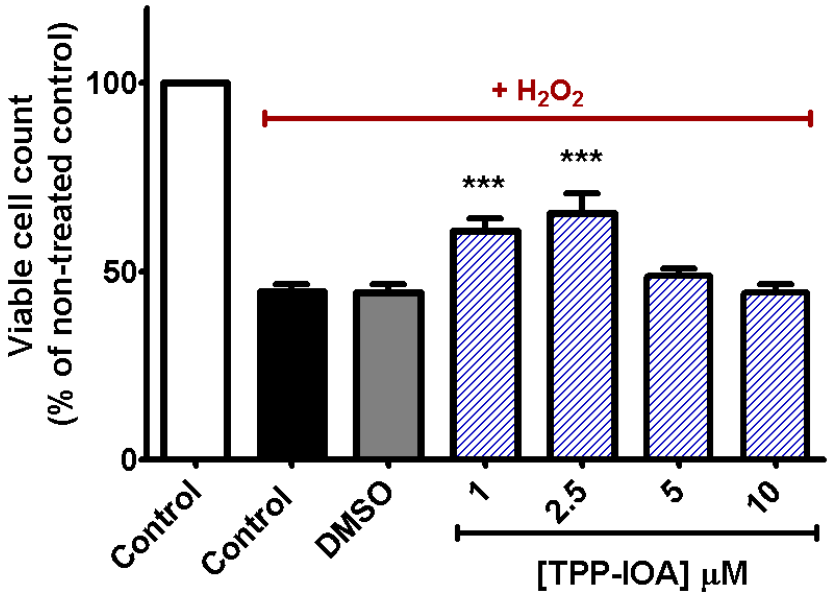

Figure AI.5.5: TP-IOA prevents H_2O_2-induced cell death of C2C12 myoblasts between 1 µM and 2.5 µM but not above 5 µM in a glucose culture medium.
TPP-IOA was added to culture medium simultaneously with 250 µM H_2O_2. Cells were harvested 24 hours later for cell viability counts with the Trypan blue dye exclusion assay.
Bars represent means + SEM from 4 – 6 total replicates from 2 -3 independent experiments. *** = p-value < 0.001 (one-way ANOVA with Tukey's HSD post-hoc test).

Appendix II – Methodology - Mitochondrial Network Analysis (MiNA V1.0.0):

Created by Andrew Valente | April 26, 2016

The morphology of mitochondrial networks has received much attention in recent years. Efforts to remove subjectivity in understanding their structure and relation to biological processes have been made by many individuals and groups (Ahmad et al., 2013; Koopman, Visch, Smeitink, & Willems, 2006; Rafelski, 2013). Working off of the contributions of such efforts, we have here developed a plugin with the goal of making consistent, accurate measurements of morphological characteristics of mitochondrial networks using a single fluorescent image. MiNA runs in the open source program ImageJ, making easy and objective analysis available to researchers without the need for specific operating platforms or expensive software. MiNA uses existing plugins and additional processing to provide a rapid method for determining quantitative values that can be used as proxies in mitochondrial morphology related research.

Analysis is based on prior works that make an effort to quantitatively bin features based on their attributes or more objectively classify features (Ahmad et al., 2013; Koopman et al., 2006; Nikolaisen et al., 2014; Rafelski, 2013). There have been various methods of classifying the features. The methods used here most strongly follow the categories presented by Leonard et al., which uses a system of puncta, rods, networks, and large round features as the potential categories for classification (Leonard et al., 2015). In an effort to reduce the complexity of the analysis the process is simplified here to contain only 2 types of features, individuals and networks.

Individuals are those which would fit the categories of puncta and rods. These features consist of a point or rod and do not demonstrate any sort of branching. Networks are features containing at least one branching point. An individual consists of only nodes and connecting pixels, while a network also contains branch points. This is demonstrated in **Figure AII.6.1**.

Figure AII.6.1: Demonstration of individual and network morphologies.

AII.1 - Image Preprocessing Algorithm:

AII.1.1 - Deconvolution using Estimated Blurring:

The blurring in an image is minimally produced by the point spread function of the optical system. Blurring is added to an image by convolution, mathematically represented in one dimension as $\int f(x)g(x-\tau)d\tau$. To remove this effect the opposite must be done, which is a deconvolution. Here, the function convolved with the real unblurred image is the point spread function. We estimate the PSF using the Diffraction PSF 3D plugin and the excitation wavelength of the dye used. The NA is set to ½ the NA of the objective (this was found to give good results through testing). NA or numerical aperture is a measure of the range of angles that the optics can accept light from. This is used as a guess for how blurred the image is and used for deconvolution using the DeconvolutionJ plugin. The plugin used employs an iterative Wiener filtering method to deconvoluted the image. A Wiener filter is not a typical kernel convolution, but a statistical estimate of how the signal appears without the addition of noise from the instrument and environment. This filter is iterated until the mean squared error between random processes and signal are minimized. The deconvoluted image's pixel dimensions are recalibrated

afterwards. This is to ensure the physical size of the image is not removed by the processing. The effects of this estimated deconvolution method are shown in **Figure AII.6.2**.

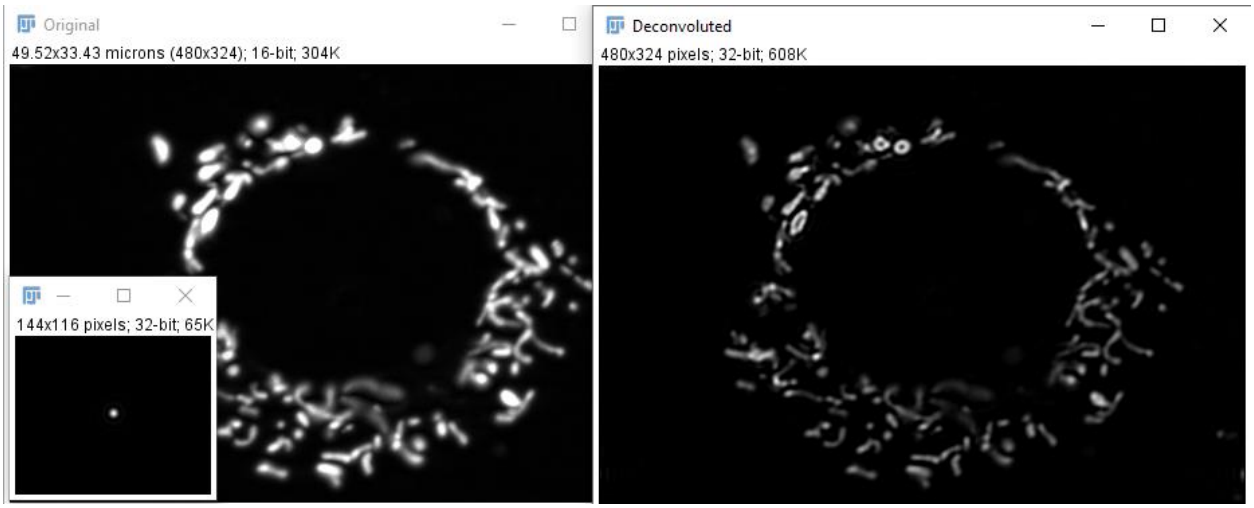

Figure AII.6.2: Effects of deconvolution to image. Blurring kernel shown in bottom left.

AII.1.2 - Contrast Limited Adaptive Histogram Equalization:

The images produced by deconvolution are often dimmed. They may also demonstrate regions of greater brightness than others. To improve the contrast between all features and the background CLAHE is used. The process aims to equalize the histogram about the image without exaggerating features too aggressively. CLAHE is demonstrated on the previously deconvoluted image and shown in **Figure AII.6.3**.

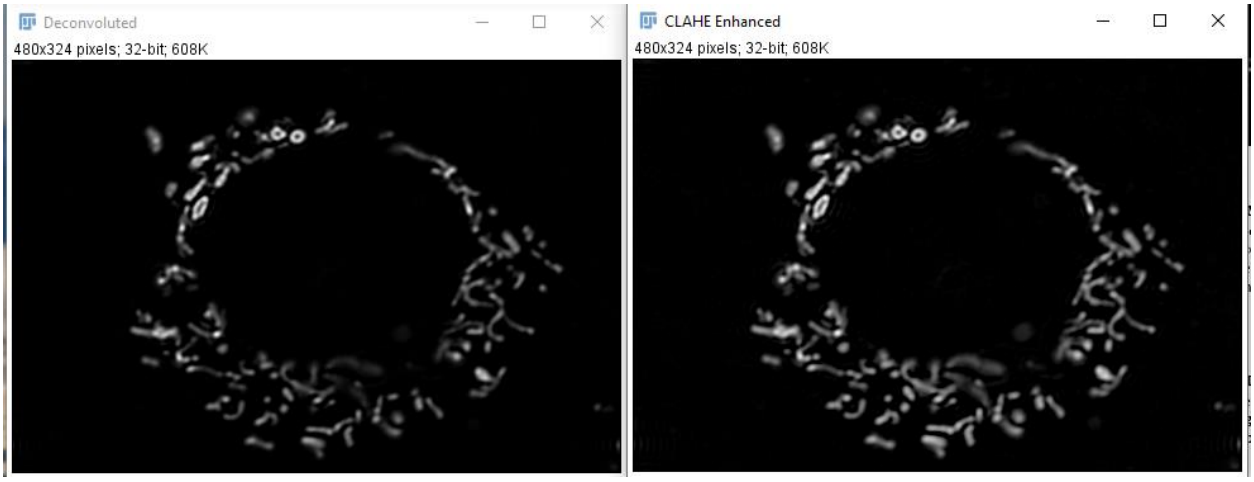

Figure AII.6.3: Effects of CLAHE on image.

AII.1.3 – Removal of Spurious Contrast by Median Filtering:

Using a 2-pixel radius, a median filter is applied to the image. This filter replaces the central pixel of the image with the median of the surrounding pixels in a 2-pixel radius. This aids in ensuring spurious details such as salt and pepper noise are removed and not counted as individuals by the program. This filtering method's effect is demonstrated in **Figure AII.6.4**.

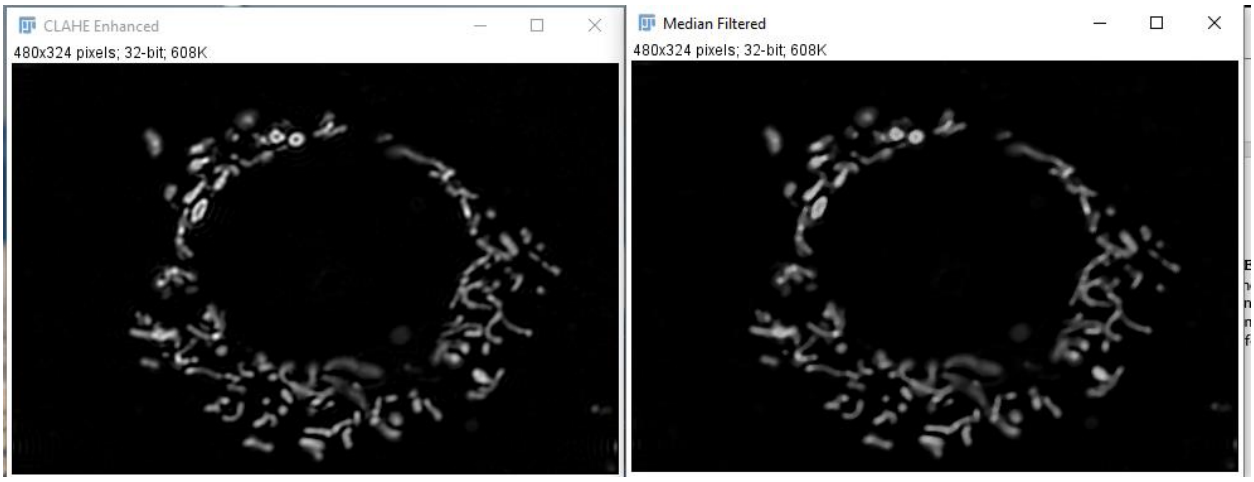

Figure AII.6.4: Median filtered image to reduce noise and spurious points.

AII.2 – Image Analysis Algorithm:

Now, the goal becomes to extract the number of features, classify them as individual or networked and make measurements as to how long individual features are. This is done by converting the image into a skeleton, which is only one pixel wide. To do this requires a number of steps outlined here.

AII.2.1 - Thresholding and Conversion to Binary:

The image is first step is to produce a threshold image using ImageJ's default algorithm. The default pics the threshold value by first removing outliers from the histogram, then iteratively smoothing the histogram with a 4 element averaging window until only 2 peaks exist. The midrange between these is the threshold value. Pixels with values greater than this are set to

a maximum, and those below it to a minimum. This is then converted to a binary image. This makes mitochondrial signal 1 and everywhere else 0. The result is shown in **Figure AII.6.5**.

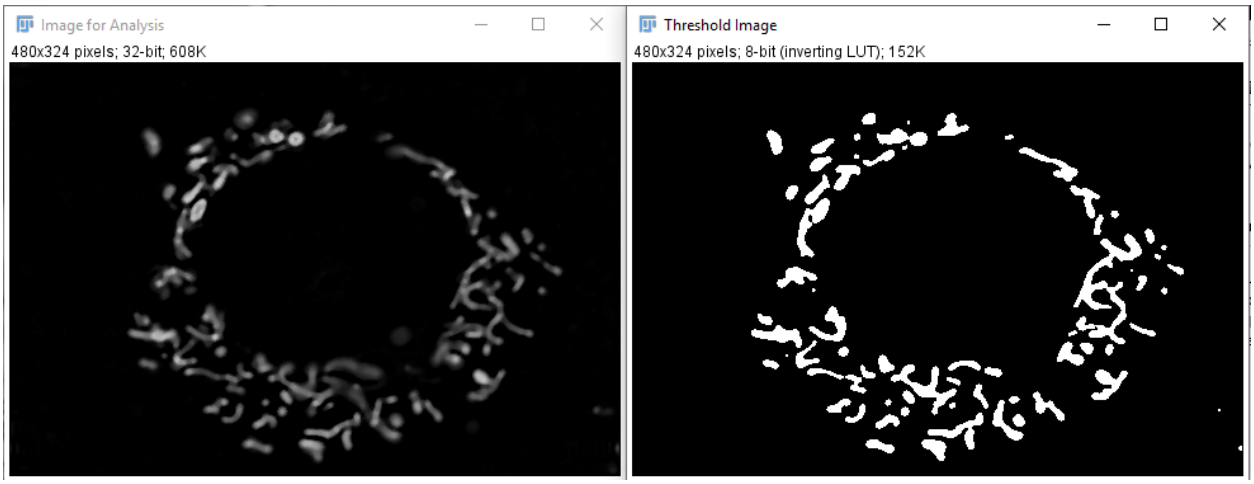

Figure AII.6.5: Binary Image produced by thresholding with default algorithm.

AII.2.2 - Skeletonizing the Binary Image:

A skeleton is then produced of the binary image using the Skeletonize 3D plugin. This iteratively removes external pixels until everything is represented by lines 1 pixel in width. The skeleton is shown overlaying the original image in **Figure AII.6.6**.

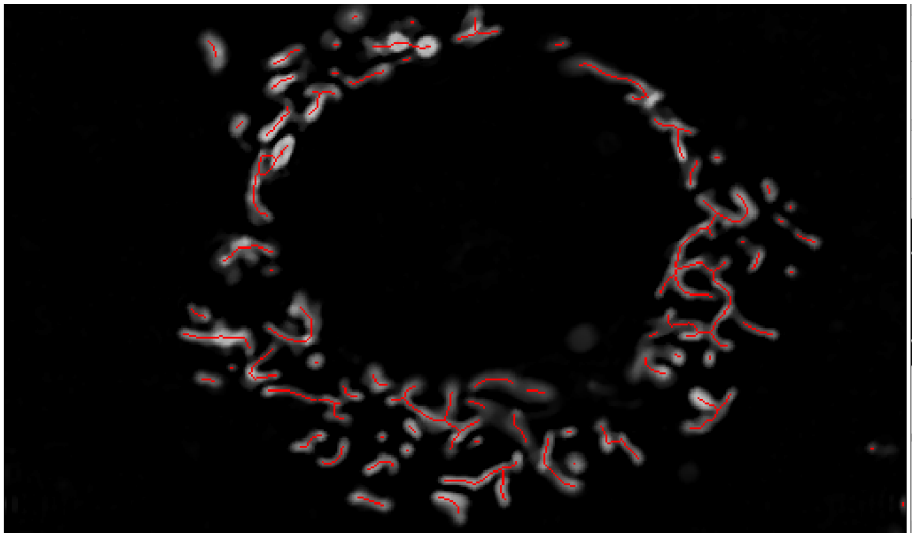

Figure AII.6.6: Skeleton overlayed on top of the binary image.

AII.3 - Limitations:

Currently there are some limitations to the software. It can only handle two-dimensional information effectively. The three-dimensional skeletons typically fail due to poor resolution in the Z plane causing discontinuities. This may be corrected using interpolation, but has not been implemented here. It is also important to note that the skeletons produced are not perfect. They are an approximation and errors do occur. It is important to look at the overlaid skeleton and determine whether or not the fit is deemed accurate enough for analysis purposes.

AII.4 – Literature Cited:

Ahmad, T., Aggarwal, K., Pattnaik, B., Mukherjee, S., Sethi, T., Tiwari, B. K., … Agrawal, A. (2013). Computational classification of mitochondrial shapes reflects stress and redox state. Cell Death Dis, 4(1), e461. http://doi.org/10.1038/cddis.2012.213

Koopman, W. J. H., Visch, H.-J., Smeitink, J. A. M., & Willems, P. H. G. M. (2006). Simultaneous quantitative measurement and automated analysis of mitochondrial morphology, mass, potential, and motility in living human skin fibroblasts. Cytometry Part A, 69A(1), 1–12. http://doi.org/10.1002/cyto.a.20198

Leonard, A. P., Cameron, R. B., Speiser, J. L., Wolf, B. J., Peterson, Y. K., Schnellmann, R. G., … Rohrer, B. (2015). Quantitative analysis of mitochondrial morphology and membrane potential in living cells using high-content imaging, machine learning, and morphological binning. Biochimica et Biophysica Acta (BBA) - Molecular Cell Research, 1853(2), 348–360. http://doi.org/10.1016/j.bbamcr.2014.11.002

Nikolaisen, J., Nilsson, L. I. H., Pettersen, I. K. N., Willems, P. H. G. M., Lorens, J. B., Koopman, W. J. H., & Tronstad, K. J. (2014). Automated quantification and integrative analysis of 2D and 3D mitochondrial shape and network properties. PLoS ONE, 9(7), 1–16. http://doi.org/10.1371/journal.pone.0101365

Rafelski, S. M. (2013). Mitochondrial network morphology: building an integrative, geometrical view. BMC Biology, 11(1), 71. http://doi.org/10.1186/1741-7007-11-71

Literature Cited:

Aguer C, Gambarotta D, Mailloux RJ, Moffat C, Dent R, et al. Galactose enhances oxidative metabolism and reveals mitochondrial dysfunction in human primary muscle cells. PLoS One. 2011;6(12):e28536. PubMed PMID: 22194845; PubMed Central PMCID: PMC3240634.

Andreux PA, Mouchiroud L, Wang X, Jovaisaite V, Mottis A, et al. A method to identify and validate mitochondrial modulators using mammalian cells and the worm *C. elegans*. Sci Rep. 2014 Jun 13;4:5285. PubMed PMID: 24923838; PubMed Central PMCID: PMC4055904.

Andreyev AYu, Bondareva TO, Dedukhova VI, Mokhova EN, Skulachev VP, et al. The ATP/ADP-antiporter is involved in the uncoupling effect of fatty acids on mitochondria. Eur J Biochem. 1989 Jul 1;182(3):585-92. PubMed PMID: 2546761.

Antonenko YN, Avetisyan AV, Bakeeva LE, Chernyak BV, Chertkov VA, et al. Mitochondria-targeted plastoquinone derivatives as tools to interrupt execution of the aging program 1 Cationic plastoquinone derivatives: synthesis and in vitro studies. Biochemistry (Mosc). 2008 Dec;73(12):1273-87. PubMed PMID: 19120014.

Ashrafi G, Schwarz TL. The pathways of mitophagy for quality control and clearance of mitochondria. Cell Death Differ. 2013 Jan;20(1):31-42. PubMed PMID: 22743996; PubMed Central PMCID: PMC3524633.

Asin-Cayuela J, Manas AR, James AM, Smith RA, Murphy MP. Fine-tuning the hydrophobicity of a mitochondria-targeted antioxidant. FEBS Lett. 2004 Jul 30;571(1-3):9-16. PubMed PMID: 15280009.

Atkinson J, Kapralov AA, Yanamala N, Tyurina YY, Amoscato AA, Pearce L, Peterson J, Huang Z, Jiang J, Samhan-Arias AK, Maeda A, Feng W, Wasserloos K, Belikova NA, Tyurin VA, Wang H, Fletcher J, Wang Y, Vlasova II, Klein-Seetharaman J, Stoyanovsky DA, Bayîr H, Pitt BR, Epperly MW, Greenberger JS, Kagan VE. A mitochondria-targeted inhibitor of cytochrome c peroxidase mitigates radiation-induced death. Nat Commun. 2011 Oct 11; 2:497. PubMed PMID: 21988913.

Babbar M, Sheikh MS. Metabolic Stress and Disorders Related to Alterations in Mitochondrial Fission or Fusion. Mol Cell Pharmacol. 2013;5(3):109-133. PubMed PMID: 24533171; NIHMSID: NIHMS553422; PubMed Central PMCID: PMC3921894.

Babul J, Stellwagen E. The existence of heme-protein coordinate-covalent bonds in denaturing solvents. Biopolymers. 1971 Nov;10(11):2359-61. PubMed PMID: 5118661.

Bakeeva LE, Grinius LL, Jasaitis AA, Kuliene VV, Levitsky DO, et al. Conversion of biomembrane-produced energy into electric form II Intact mitochondria. Biochim Biophys Acta. 1970 Aug 4;216(1):13-21. PubMed PMID: 4250571.

Barrientos, A., Fontanesi, F., & Díaz, F. (2009). Evaluation of the Mitochondrial Respiratory Chain and Oxidative Phosphorylation System using Polarography and Spectrophotometric Enzyme Assays. Current Protocols in Human Genetics / Editorial Board, Jonathan L. Haines ... [et Al.], CHAPTER, Unit19.3. http://doi.org/10.1002/0471142905.hg1903s63

Barsoum MJ, Yuan H, Gerencser AA, Liot G, Kushnareva Y, et al. Nitric oxide-induced mitochondrial fission is regulated by dynamin-related GTPases in neurons. EMBO J. 2006 Aug 23;25(16):3900-11. PubMed PMID: 16874299; PubMed Central PMCID: PMC1553198.

Bayir H, Fadeel B, Palladino MJ, Witasp E, Kurnikov IV, Tyurina YY, Tyurin VA, Amoscato AA, Jiang J, Kochanek PM, DeKosky ST, Greenberger JS, Shvedova AA, Kagan VE. Apoptotic interactions of cytochrome c: redox flirting with anionic phospholipids within

and outside of mitochondria. Biochim Biophys Acta. 2006 May-Jun; 1757 (5-6) :648-59. PubMed PMID: 16740248.

Bélanger M, Allaman I, Magistretti PJ. Brain energy metabolism: focus on astrocyte-neuron metabolic cooperation. Cell Metab. 2011 Dec 7;14(6):724-38. PubMed PMID: 22152301.

Belikova NA, Vladimirov YA, Osipov AN, Kapralov AA, Tyurin VA, et al. Peroxidase activity and structural transitions of cytochrome c bound to cardiolipin-containing membranes. Biochemistry. 2006 Apr 18;45(15):4998-5009. PubMed PMID: 16605268; NIHMSID: NIHMS60967; PubMed Central PMCID: PMC2527545.

Belikova NA, Tyurina YY, Borisenko G, Tyurin V, Samhan Arias AK, et al. Heterolytic reduction of fatty acid hydroperoxides by cytochrome c/cardiolipin complexes: antioxidant function in mitochondria. J Am Chem Soc. 2009 Aug 19;131(32):11288-9. PubMed PMID: 19627079.

Benard G, Bellance N, James D, Parrone P, Fernandez H, et al. Mitochondrial bioenergetics and structural network organization. J Cell Sci. 2007 Mar 1;120(Pt 5):838-48. PubMed PMID: 17298981.

Birk AV, Liu S, Soong Y, Mills W, Singh P, et al. The mitochondrial-targeted compound SS-31 re-energizes ischemic mitochondria by interacting with cardiolipin. J Am Soc Nephrol. 2013 Jul;24(8):1250-61. PubMed PMID: 23813215; PubMed Central PMCID: PMC3736700.

Brand, M. D., & Nicholls, D. G. (2011). Assessing mitochondrial dysfunction in cells. Biochemical Journal, 435(Pt 2), 297–312. http://doi.org/10.1042/BJ20110162

Broughton BR, Reutens DC, Sobey CG. Apoptotic mechanisms after cerebral ischemia. Stroke. 2009 May; 40 (5):331-9. PubMed PMID: 19182083.

Brown MF, Gratton TP, Stuart JA. Metabolic rate does not scale with body mass in cultured mammalian cells. Am J Physiol Regul Integr Comp Physiol. 2007 Jun;292(6):R2115-21. PubMed PMID: 17234960.

Chance B, Williams GR. Respiratory enzymes in oxidative phosphorylation I Kinetics of oxygen utilization. J Biol Chem. 1955 Nov;217(1):383-93. PubMed PMID: 13271402.

Choe SC, Hamacher-Brady A, Brady NR. Autophagy capacity and sub-mitochondrial heterogeneity shape Bnip3-induced mitophagy regulation of apoptosis. Cell Commun Signal. 2015 Aug 8;13:37. PubMed PMID: 26253153; PubMed Central PMCID: PMC4528699.

Clarke LE, Barres BA. Emerging roles of astrocytes in neural circuit development. Nat Rev Neurosci. 2013 May;14(5):311-21. PubMed PMID: 23595014; NIHMSID: NIHMS688679; PubMed Central PMCID: PMC4431630.

Cohen GM. Caspases: the executioners of apoptosis. Biochem J. 1997 Aug 15;326 (Pt 1):1-16. PubMed PMID: 9337844; PubMed Central PMCID: PMC1218630.

Crimi M, Esposti MD. Apoptosis-induced changes in mitochondrial lipids. Biochim Biophys Acta. 2011 Apr; 1813 (4) :551-7. PubMed PMID: 20888373.

De Duve C, Wattiaux R. Functions of lysosomes. Annu Rev Physiol. 1966;28:435-92. PubMed PMID: 5322983.

De Vos KJ, Allan VJ, Grierson AJ, Sheetz MP. Mitochondrial function and actin regulate dynamin-related protein 1-dependent mitochondrial fission. Curr Biol. 2005 Apr 12;15(7):678-83. PubMed PMID: 15823542.

DeBerardinis RJ, Mancuso A, Daikhin E, Nissim I, Yudkoff M, et al. Beyond aerobic glycolysis: transformed cells can engage in glutamine metabolism that exceeds the requirement for protein and nucleotide synthesis. Proc Natl Acad Sci U S A. 2007 Dec 4;104(49):19345-50. PubMed PMID: 18032601; PubMed Central PMCID: PMC2148292.

Detmer SA, Chan DC. Functions and dysfunctions of mitochondrial dynamics. Nat Rev Mol Cell Biol. 2007 Nov;8(11):870-9. PubMed PMID: 17928812.

Di Paola M, Lorusso M. Interaction of free fatty acids with mitochondria: coupling, uncoupling and permeability transition. Biochim Biophys Acta. 2006 Sep-Oct;1757(9-10):1330-7. PubMed PMID: 16697347.

Ding WX, Yin XM. Mitophagy: mechanisms, pathophysiological roles, and analysis. Biol Chem. 2012 Jul;393(7):547-64. PubMed PMID: 22944659; NIHMSID: NIHMS441631; PubMed Central PMCID: PMC3630798.

Divakaruni AS, Brand MD. The regulation and physiology of mitochondrial proton leak. Physiology (Bethesda). 2011 Jun;26(3):192-205. PubMed PMID: 21670165.

Dolman NJ, Chambers KM, Mandavilli B, Batchelor RH, Janes MS. Tools and techniques to measure mitophagy using fluorescence microscopy. Autophagy. 2013 Nov 1;9(11):1653-62. PubMed PMID: 24121704.

Dott W, Mistry P, Wright J, Cain K, Herbert KE. Modulation of mitochondrial bioenergetics in a skeletal muscle cell line model of mitochondrial toxicity. Redox Biol. 2014;2:224-33. PubMed PMID: 24494197; PubMed Central PMCID: PMC3909783.

Du C, Fang M, Li Y, Li L, Wang X. Smac, a mitochondrial protein that promotes cytochrome c-dependent caspase activation by eliminating IAP inhibition. Cell. 2000 Jul 7;102(1):33-42. PubMed PMID: 10929711.

Duque-Parra JE. Note on the origin and history of the term "apoptosis". Anat Rec B New Anat. 2005 Mar;283(1):2-4. PubMed PMID: 15761829.

Dykens JA, Jamieson J, Marroquin L, Nadanaciva S, Billis PA, et al. Biguanide-induced mitochondrial dysfunction yields increased lactate production and cytotoxicity of aerobically-poised HepG2 cells and human hepatocytes in vitro. Toxicol Appl Pharmacol. 2008 Dec 1;233(2):203-10. PubMed PMID: 18817800.

Earnshaw WC, Martins LM, Kaufmann SH. Mammalian caspases: structure, activation, substrates, and functions during apoptosis. Annu Rev Biochem. 1999;68:383-424. PubMed PMID: 10872455.

Elmore S. Apoptosis: a review of programmed cell death. Toxicol Pathol. 2007 Jun;35(4):495-516. PubMed PMID: 17562483; NIHMSID: NIHMS33547; PubMed Central PMCID: PMC2117903.

Engstová H, Zácková M, Růzicka M, Meinhardt A, Hanus J, et al. Natural and azido fatty acids inhibit phosphate transport and activate fatty acid anion uniport mediated by the mitochondrial phosphate carrier. J Biol Chem. 2001 Feb 16;276(7):4683-91. PubMed PMID: 11085992.

Erlanson-Albertsson C. The role of uncoupling proteins in the regulation of metabolism. Acta Physiol Scand. 2003 Aug;178(4):405-12. PubMed PMID: 12864746.

Fink BD, Herlein JA, Yorek MA, Fenner AM, Kerns RJ, et al. Bioenergetic effects of mitochondrial-targeted coenzyme Q analogs in endothelial cells. J Pharmacol Exp Ther. 2012 Sep;342(3):709-19. PubMed PMID: 22661629; PubMed Central PMCID: PMC3422527.

Frey TG, Mannella CA. The internal structure of mitochondria. Trends Biochem Sci. 2000 Jul;25(7):319-24. PubMed PMID: 10871882.

Fuentes-Prior P, Salvesen GS. The protein structures that shape caspase activity, specificity, activation and inhibition. Biochem J. 2004 Dec 1;384(Pt 2):201-32. PubMed PMID: 15450003; PubMed Central PMCID: PMC1134104.

Galloway CA, Lee H, Yoon Y. Mitochondrial morphology-emerging role in bioenergetics. Free Radic Biol Med. 2012 Dec 15;53(12):2218-28. PubMed PMID: 23032099; NIHMSID: NIHMS411611; PubMed Central PMCID: PMC3594133.

Garcia Fernandez M, Troiano L, Moretti L, Nasi M, Pinti M, Salvioli S, Dobrucki J, Cossarizza A. Early changes in intramitochondrial cardiolipin distribution during apoptosis. Cell Growth Differ. 2002 Sep; 13 (9) :449-55. PubMed PMID: 12354754.

Garrido C, Galluzzi L, Brunet M, Puig PE, Didelot C, Kroemer G. Mechanisms of cytochrome c release from mitochondria. Cell Death Differ. 2006 Sep; 13 (9) :1423-33. PubMed PMID: 16676004.

Ghavami S, Shojaei S, Yeganeh B, Ande SR, Jangamreddy JR, et al. Autophagy and apoptosis dysfunction in neurodegenerative disorders. Prog Neurobiol. 2014 Jan;112:24-49. PubMed PMID: 24211851.

Gnaiger E (2014) Mitochondrial pathways and respiratory control. An introduction to OXPHOS analysis. 4th ed. Mitochondr Physiol Network 19.12. OROBOROS MiPNet Publications, Innsbruck:80 pp

Gonzalvez F, Gottlieb E. Cardiolipin: setting the beat of apoptosis. Apoptosis. 2007 May;12(5):877-85. PubMed PMID: 17294083.

Goveia J, Stapor P, Carmeliet P. Principles of targeting endothelial cell metabolism to treat angiogenesis and endothelial cell dysfunction in disease. EMBO Mol Med. 2014 Jul 25;6(9):1105-20. PubMed PMID: 25063693; PubMed Central PMCID: PMC4197858.

Guex N, Peitsch MC. SWISS-MODEL and the Swiss-PdbViewer: an environment for comparative protein modeling. Electrophoresis. 1997 Dec;18(15):2714-23. PubMed PMID: 9504803.

Gusdon AM, Zhu J, Van Houten B, Chu CT. ATP13A2 regulates mitochondrial bioenergetics through macroautophagy. Neurobiol Dis. 2012 Mar;45(3):962-72. PubMed PMID: 22198378; NIHMSID: NIHMS344927; PubMed Central PMCID: PMC3291101.

Häcker G. The morphology of apoptosis. Cell Tissue Res. 2000 Jul;301(1):5-17. PubMed PMID: 10928277.

Hafner RP, Brown GC, Brand MD. Analysis of the control of respiration rate, phosphorylation rate, proton leak rate and protonmotive force in isolated mitochondria using the 'top-down' approach of metabolic control theory. Eur J Biochem. 1990 Mar 10;188(2):313-9. PubMed PMID: 2156698.

Haraldsdóttir HS, Thiele I, Fleming RM. Quantitative assignment of reaction directionality in a multicompartmental human metabolic reconstruction. Biophys J. 2012 Apr 18;102(8):1703-11. PubMed PMID: 22768925; PubMed Central PMCID: PMC3328694.

Hardie DG. AMP-activated protein kinase: an energy sensor that regulates all aspects of cell function. Genes Dev. 2011 Sep 15;25(18):1895-908. PubMed PMID: 21937710; PubMed Central PMCID: PMC3185962.

Hengartner MO. The biochemistry of apoptosis. Nature. 2000 Oct 12;407(6805):770-6. PubMed PMID: 11048727.

Holden HM, Thoden JB, Timson DJ, Reece RJ. Galactokinase: structure, function and role in type II galactosemia. Cell Mol Life Sci. 2004 Oct;61(19-20):2471-84. PubMed PMID: 15526155.

Honda HM, Korge P, Weiss JN. Mitochondria and ischemia/reperfusion injury. Ann N Y Acad Sci. 2005 Jun;1047:248-58. PubMed PMID: 16093501.

Hüttemann M, Pecina P, Rainbolt M, Sanderson TH, Kagan VE, Samavati L, Doan JW, Lee I. The multiple functions of cytochrome c and their regulation in life and death decisions of the mammalian cell: From respiration to apoptosis. Mitochondrion. 2011 May; 11 (3) :369-81. PubMed PMID: 21296189; PubMed Central PMCID: PMC3075374.

Iannetti EF, Willems PH, Pellegrini M, Beyrath J, Smeitink JA, et al. Toward high-content screening of mitochondrial morphology and membrane potential in living cells. Int J Biochem Cell Biol. 2015 Jun;63:66-70. PubMed PMID: 25668473.

Ishihara N, Fujita Y, Oka T, Mihara K. Regulation of mitochondrial morphology through proteolytic cleavage of OPA1. EMBO J. 2006 Jul 12;25(13):2966-77. PubMed PMID: 16778770; PubMed Central PMCID: PMC1500981.

Jiang J, Bakan A, Kapralov AA, Silva KI, Huang Z, et al. Designing inhibitors of cytochrome

c/cardiolipin peroxidase complexes: mitochondria-targeted imidazole-substituted fatty acids. Free Radic Biol Med. 2014 Jun;71:221-30. PubMed PMID: 24631490; NIHMSID: NIHMS577005; PubMed Central PMCID: PMC4216591.

Jiang X, Wang X. Cytochrome C-mediated apoptosis. Annu Rev Biochem. 2004; 73:87-106. PubMed PMID: 15189137.

Jourdain A, Martinou JC. Mitochondrial outer-membrane permeabilization and remodelling in apoptosis. Int J Biochem Cell Biol. 2009 Oct; 41 (10) :1884-9. PubMed PMID: 19439192.

Kagan VE, Bayir A, Bayir H, Stoyanovsky D, Borisenko GG, Tyurina YY, Wipf P, Atkinson J, Greenberger JS, Chapkin RS, Belikova NA. Mitochondria-targeted disruptors and inhibitors of cytochrome c/cardiolipin peroxidase complexes: a new strategy in anti-apoptotic drug discovery. Mol Nutr Food Res. 2009 Jan; 53 (1) :104-14. PubMed PMID: 18979502; PubMed Central PMCID: PMC2659540.

Kalogeris T, Baines CP, Krenz M, Korthuis RJ. Cell biology of ischemia/reperfusion injury. Int Rev Cell Mol Biol. 2012;298:229-317. PubMed PMID: 22878108; NIHMSID: NIHMS545698; PubMed Central PMCID: PMC3904795.

Kamo N, Muratsugu M, Hongoh R, Kobatake Y. Membrane potential of mitochondria measured with an electrode sensitive to tetraphenyl phosphonium and relationship between proton electrochemical potential and phosphorylation potential in steady state. J Membr Biol. 1979 Aug;49(2):105-21. PubMed PMID: 490631.

Kanduc D, Mittelman A, Serpico R, Sinigaglia E, Sinha AA, et al. Cell death: apoptosis versus necrosis (review). Int J Oncol. 2002 Jul;21(1):165-70. PubMed PMID: 12063564.

Kawai K, Shiojiri H, Watanabe R, Nozawa Y. Chlorination-induced enhancement of biological activities in imidazole antimycotics A possible explanation to the molecular mechanism for their antimycotic activities. Res Commun Chem Pathol Pharmacol. 1983 May;40(2):255-65. PubMed PMID: 6878866.

Kelso GF, Porteous CM, Coulter CV, Hughes G, Porteous WK, et al. Selective targeting of a redox-active ubiquinone to mitochondria within cells: antioxidant and antiapoptotic properties. J Biol Chem. 2001 Feb 16;276(7):4588-96. PubMed PMID: 11092892.

Kerr JF, Wyllie AH, Currie AR. Apoptosis: a basic biological phenomenon with wide-ranging implications in tissue kinetics. Br J Cancer. 1972 Aug;26(4):239-57. PubMed PMID: 4561027; PubMed Central PMCID: PMC2008650.

Klionsky DJ, Abdelmohsen K, Abe A, Abedin MJ, Abeliovich H, et al. Guidelines for the use and interpretation of assays for monitoring autophagy (3rd edition). Autophagy. 2016;12(1):1-222. PubMed PMID: 26799652; PubMed Central PMCID: PMC4835977.

Korytowski W, Basova LV, Pilat A, Kernstock RM, Girotti AW. Permeabilization of the mitochondrial outer membrane by Bax/truncated Bid (tBid) proteins as sensitized by cardiolipin hydroperoxide translocation: mechanistic implications for the intrinsic pathway of oxidative apoptosis. J Biol Chem. 2011 Jul 29;286(30):26334-43. PubMed PMID: 21642428; PubMed Central PMCID: PMC3143596.

Kovacevic Z, McGivan JD. Mitochondrial metabolism of glutamine and glutamate and its physiological significance. Physiol Rev. 1983 Apr;63(2):547-605. PubMed PMID: 6132422.

Krebs JJ, Hauser H, Carafoli E. Asymmetric distribution of phospholipids in the inner membrane of beef heart mitochondria. J Biol Chem. 1979 Jun 25;254(12):5308-16. PubMed PMID: 447651.

Kroemer G, Galluzzi L, Brenner C. Mitochondrial membrane permeabilization in cell death. Physiol Rev. 2007 Jan; 87 (1) :99-163. PubMed PMID: 17237344

Larsen S, Nielsen J, Hansen CN, Nielsen LB, Wibrand F, et al. Biomarkers of mitochondrial

content in skeletal muscle of healthy young human subjects. J Physiol. 2012 Jul 15;590(14):3349-60. PubMed PMID: 22586215; PubMed Central PMCID: PMC3459047.

Le Goffe C, Vallette G, Jarry A, Bou-Hanna C, Laboisse CL. The in vitro manipulation of carbohydrate metabolism: a new strategy for deciphering the cellular defence mechanisms against nitric oxide attack. Biochem J. 1999 Dec 15;344 Pt 3:643-8. PubMed PMID: 10585850; PubMed Central PMCID: PMC1220685.

Legros F, Lombès A, Frachon P, Rojo M. Mitochondrial fusion in human cells is efficient, requires the inner membrane potential, and is mediated by mitofusins. Mol Biol Cell. 2002 Dec;13(12):4343-54. PubMed PMID: 12475957; PubMed Central PMCID: PMC138638.

Lemasters JJ. Selective mitochondrial autophagy, or mitophagy, as a targeted defense against oxidative stress, mitochondrial dysfunction, and aging. Rejuvenation Res. 2005 Spring;8(1):3-5. PubMed PMID: 15798367.

Leonard AP, Cameron RB, Speiser JL, Wolf BJ, Peterson YK, et al. Quantitative analysis of mitochondrial morphology and membrane potential in living cells using high-content imaging, machine learning, and morphological binning. Biochim Biophys Acta. 2015 Feb;1853(2):348-60. PubMed PMID: 25447550; NIHMSID: NIHMS642479; PubMed Central PMCID: PMC4289477.

Levine B, Klionsky DJ. Development by self-digestion: molecular mechanisms and biological functions of autophagy. Dev Cell. 2004 Apr;6(4):463-77. PubMed PMID: 15068787.

Li LY, Luo X, Wang X. Endonuclease G is an apoptotic DNase when released from mitochondria. Nature. 2001 Jul 5;412(6842):95-9. PubMed PMID: 11452314.

Li P, Nijhawan D, Budihardjo I, Srinivasula SM, Ahmad M, Alnemri ES, Wang X. Cytochrome c and dATP-dependent formation of Apaf-1/caspase-9 complex initiates an apoptotic protease cascade. Cell. 1997 Nov 14; 91 (4) :479-89. PubMed PMID: 9390557.

Liberman EA, Topaly VP, Tsofina LM, Jasaitis AA, Skulachev VP. Mechanism of coupling of oxidative phosphorylation and the membrane potential of mitochondria. Nature. 1969 Jun 14;222(5198):1076-8. PubMed PMID: 5787094.

Lide, D.R. 1994. Handbook of chemistry and physics, 74th ed. CRC Press, Boca Raton, LA.

Liesa M, Shirihai OS. Mitochondrial dynamics in the regulation of nutrient utilization and energy expenditure. Cell Metab. 2013 Apr 2;17(4):491-506. PubMed PMID: 23562075.

Liot G, Bossy B, Lubitz S, Kushnareva Y, Sejbuk N, et al. Complex II inhibition by 3-NP causes mitochondrial fragmentation and neuronal cell death via an NMDA- and ROS-dependent pathway. Cell Death Differ. 2009 Jun;16(6):899-909. PubMed PMID: 19300456; NIHMSID: NIHMS112860; PubMed Central PMCID: PMC2757037.

Liu D, Smith CL, Barone FC, Ellison JA, Lysko PG, et al. Astrocytic demise precedes delayed neuronal death in focal ischemic rat brain. Brain Res Mol Brain Res. 1999 May 7;68(1-2):29-41. PubMed PMID: 10320781.

Liu X, Hajnóczky G. Altered fusion dynamics underlie unique morphological changes in mitochondria during hypoxia-reoxygenation stress. Cell Death Differ. 2011 Oct;18(10):1561-72. PubMed PMID: 21372848; NIHMSID: NIHMS321840; PubMed Central PMCID: PMC3172112.

Lopez-Neblina F, Toledo AH, Toledo-Pereyra LH. Molecular biology of apoptosis in ischemia and reperfusion. J Invest Surg. 2005 Nov-Dec;18(6):335-50. PubMed PMID: 16319055.

Lunt SY, Vander Heiden MG. Aerobic glycolysis: meeting the metabolic requirements of cell proliferation. Annu Rev Cell Dev Biol. 2011;27:441-64. PubMed PMID: 21985671.

Macià I Garau M, Lucas Calduch A, López EC. Radiobiology of the acute radiation syndrome. Rep Pract Oncol Radiother. 2011 Jul 6;16(4):123-30. PubMed PMID: 24376969; PubMed Central PMCID: PMC3863296.

MacVicar TD, Lane JD. Impaired OMA1-dependent cleavage of OPA1 and reduced DRP1 fission activity combine to prevent mitophagy in cells that are dependent on oxidative phosphorylation. J Cell Sci. 2014 May 15;127(Pt 10):2313-25. PubMed PMID: 24634514; PubMed Central PMCID: PMC4021475.

Manczak M, Mao P, Calkins MJ, Cornea A, Reddy AP, et al. Mitochondria-targeted antioxidants protect against amyloid-beta toxicity in Alzheimer's disease neurons. J Alzheimers Dis. 2010;20 Suppl 2:S609-31. PubMed PMID: 20463406; NIHMSID: NIHMS281205; PubMed Central PMCID: PMC3072711.

Mariño G, Niso-Santano M, Baehrecke EH, Kroemer G. Self-consumption: the interplay of autophagy and apoptosis. Nat Rev Mol Cell Biol. 2014 Feb;15(2):81-94. PubMed PMID: 24401948; NIHMSID: NIHMS560579; PubMed Central PMCID: PMC3970201.

Marroquin LD, Hynes J, Dykens JA, Jamieson JD, Will Y. Circumventing the Crabtree effect: replacing media glucose with galactose increases susceptibility of HepG2 cells to mitochondrial toxicants. Toxicol Sci. 2007 Jun;97(2):539-47. PubMed PMID: 17361016.

McIlwain DR, Berger T, Mak TW. Caspase functions in cell death and disease. Cold Spring Harb Perspect Biol. 2013 Apr 1;5(4):a008656. PubMed PMID: 23545416; PubMed Central PMCID: PMC3683896.

McLelland GL, Soubannier V, Chen CX, McBride HM, Fon EA. Parkin and PINK1 function in a vesicular trafficking pathway regulating mitochondrial quality control. EMBO J. 2014 Feb 18;33(4):282-95. PubMed PMID: 24446486; PubMed Central PMCID: PMC3989637.

Meister A. Metabolism of glutamine. Physiol Rev. 1956 Jan;36(1):103-27. PubMed PMID: 13297549.

Mirkin N, Jaconcic J, Stojanoff V, Moreno A. High resolution X-ray crystallographic structure of bovine heart cytochrome c and its application to the design of an electron transfer biosensor. Proteins. 2008 Jan 1;70(1):83-92. PubMed PMID: 17634981.

Mitchell P. Coupling of phosphorylation to electron and hydrogen transfer by a chemi-osmotic type of mechanism. Nature. 1961 Jul 8;191:144-8. PubMed PMID: 13771349.

Mitra K, Wunder C, Roysam B, Lin G, Lippincott-Schwartz J. A hyperfused mitochondrial state achieved at G1-S regulates cyclin E buildup and entry into S phase. Proc Natl Acad Sci U S A. 2009 Jul 21;106(29):11960-5. PubMed PMID: 19617534; PubMed Central PMCID: PMC2710990.

Mizushima N. Autophagy: process and function. Genes Dev. 2007 Nov 15;21(22):2861-73. PubMed PMID: 18006683.

Moore G R, Pettigrew G W. Cytochromes c: Evolutionary, Structural, and Physicochemical Aspects. New York: Springer; 1990

Muller PY, Milton MN. The determination and interpretation of the therapeutic index in drug development. Nat Rev Drug Discov. 2012 Oct;11(10):751-61. PubMed PMID: 22935759.

Mulukutla BC, Khan S, Lange A, Hu WS. Glucose metabolism in mammalian cell culture: new insights for tweaking vintage pathways. Trends Biotechnol. 2010 Sep;28(9):476-84. PubMed PMID: 20691487.

Murphy MP. Selective targeting of bioactive compounds to mitochondria. Trends Biotechnol. 1997 Aug;15(8):326-30. PubMed PMID: 9263481.

Murphy MP. Targeting lipophilic cations to mitochondria. Biochim Biophys Acta. 2008 Jul-Aug;1777(7-8):1028-31. PubMed PMID: 18439417.

Murphy MP, Smith RA. Targeting antioxidants to mitochondria by conjugation to lipophilic cations. Annu Rev Pharmacol Toxicol. 2007; 47:629-56. PubMed PMID: 17014364.

Nadanaciva S, Will Y. Current concepts in drug-induced mitochondrial toxicity. Curr Protoc Toxicol. 2009 May;Chapter 2:Unit 2.15. PubMed PMID: 20941696.

Narendra D, Tanaka A, Suen DF, Youle RJ. Parkin is recruited selectively to impaired mitochondria and promotes their autophagy. J Cell Biol. 2008 Dec 1;183(5):795-803. PubMed PMID: 19029340; PubMed Central PMCID: PMC2592826.

Narendra D, Kane LA, Hauser DN, Fearnley IM, Youle RJ. p62/SQSTM1 is required for Parkin-induced mitochondrial clustering but not mitophagy; VDAC1 is dispensable for both. Autophagy. 2010 Nov;6(8):1090-106. PubMed PMID: 20890124; PubMed Central PMCID: PMC3359490.

Nakagawa Y. Initiation of apoptotic signal by the peroxidation of cardiolipin of mitochondria. Ann N Y Acad Sci. 2004 Apr;1011:177-84. PubMed PMID: 15126295.

Neermann J, Wagner R. Comparative analysis of glucose and glutamine metabolism in transformed mammalian cell lines, insect and primary liver cells. J Cell Physiol. 1996 Jan;166(1):152-69. PubMed PMID: 8557765.

Nicholls DG. Fluorescence measurement of mitochondrial membrane potential changes in cultured cells. Methods Mol Biol. 2012;810:119-33. PubMed PMID: 22057564.

Nobes CD, Brown GC, Olive PN, Brand MD. Non-ohmic proton conductance of the mitochondrial inner membrane in hepatocytes. J Biol Chem. 1990 Aug 5;265(22):12903-9. PubMed PMID: 2376579.

Noji H, Yasuda R, Yoshida M, Kinosita K Jr. Direct observation of the rotation of F1-ATPase. Nature. 1997 Mar 20;386(6622):299-302. PubMed PMID: 9069291.

Ott M, Robertson JD, Gogvadze V, Zhivotovsky B, Orrenius S. Cytochrome c release from mitochondria proceeds by a two-step process. Proc Natl Acad Sci U S A. 2002 Feb 5;99(3):1259-63. PubMed PMID: 11818574; PubMed Central PMCID: PMC122177.

Papa S, Martino PL, Capitanio G, Gaballo A, De Rasmo D, et al. The oxidative phosphorylation system in mammalian mitochondria. Adv Exp Med Biol. 2012;942:3-37. PubMed PMID: 22399416.

Patriarca A, Eliseo T, Sinibaldi F, Piro MC, Melis R, et al. ATP acts as a regulatory effector in modulating structural transitions of cytochrome c: implications for apoptotic activity. Biochemistry. 2009 Apr 21;48(15):3279-87. PubMed PMID: 19231839.

Perry SW, Norman JP, Barbieri J, Brown EB, Gelbard HA. Mitochondrial membrane potential probes and the proton gradient: a practical usage guide. Biotechniques. 2011 Feb;50(2):98-115. PubMed PMID: 21486251; NIHMSID: NIHMS296965; PubMed Central PMCID: PMC3115691.

Petrosillo G, Ruggiero FM, Paradies G. Role of reactive oxygen species and cardiolipin in the release of cytochrome c from mitochondria. FASEB J. 2003 Dec;17(15):2202-8. PubMed PMID: 14656982.

Petrosillo G, Casanova G, Matera M, Ruggiero FM, Paradies G. Interaction of peroxidized cardiolipin with rat-heart mitochondrial membranes: induction of permeability transition and cytochrome c release. FEBS Lett. 2006 Nov 27;580(27):6311-6. PubMed PMID: 17083938.

Picard M, Csukly K, Robillard ME, Godin R, Ascah A, et al. Resistance to $Ca2^{+}$-induced opening of the permeability transition pore differs in mitochondria from glycolytic and oxidative muscles. Am J Physiol Regul Integr Comp Physiol. 2008 Aug;295(2):R659-68. PubMed PMID: 18495829.

Planchon TA, Gao L, Milkie DE, Davidson MW, Galbraith JA, et al. Rapid three-dimensional isotropic imaging of living cells using Bessel beam plane illumination. Nat Methods. 2011 May;8(5):417-23. PubMed PMID: 21378978; NIHMSID: NIHMS269412; PubMed Central PMCID: PMC3626440.

Polet F, Feron O. Endothelial cell metabolism and tumour angiogenesis: glucose and glutamine as essential fuels and lactate as the driving force. J Intern Med. 2013 Feb;273(2):156-65. PubMed PMID: 23216817.

Porter AG, Jänicke RU. Emerging roles of caspase-3 in apoptosis. Cell Death Differ. 1999 Feb;6(2):99-104. PubMed PMID: 10200555.

Rana P, Nadanaciva S, Will Y. Mitochondrial membrane potential measurement of H9c2 cells grown in high-glucose and galactose-containing media does not provide additional predictivity towards mitochondrial assessment. Toxicol In Vitro. 2011 Mar;25(2):580-7. PubMed PMID: 21126567.

Reily C, Mitchell T, Chacko BK, Benavides G, Murphy MP, et al. Mitochondrially targeted compounds and their impact on cellular bioenergetics. Redox Biol. 2013;1(1):86-93. PubMed PMID: 23667828; NIHMSID: NIHMS458706; PubMed Central PMCID: PMC3647698.

Reitzer LJ, Wice BM, Kennell D. Evidence that glutamine, not sugar, is the major energy source for cultured HeLa cells. J Biol Chem. 1979 Apr 25;254(8):2669-76. PubMed PMID: 429309.

Renehan AG, Booth C, Potten CS. What is apoptosis, and why is it important?. BMJ. 2001 Jun 23;322(7301):1536-8. PubMed PMID: 11420279; PubMed Central PMCID: PMC1120576.

Robb EL, Maddalena LA, Dunlop VA, Foster T, Stuart JA. Absence of metabolic rate allometry in an ex vivo model of mammalian skeletal muscle. Comp Biochem Physiol A Mol Integr Physiol. 2012 Jul;162(3):157-62. PubMed PMID: 22708124.

Robinson BH, Petrova-Benedict R, Buncic JR, Wallace DC. Nonviability of cells with oxidative defects in galactose medium: a screening test for affected patient fibroblasts. Biochem Med Metab Biol. 1992 Oct;48(2):122-6. PubMed PMID: 1329873.

Rock KL, Kono H. The inflammatory response to cell death. Annu Rev Pathol. 2008;3:99-126. PubMed PMID: 18039143; NIHMSID: NIHMS141099; PubMed Central PMCID: PMC3094097.

Roelofs BA, Ge SX, Studlack PE, Polster BM. Low micromolar concentrations of the superoxide probe MitoSOX uncouple neural mitochondria and inhibit complex IV. Free Radic Biol Med. 2015 Sep;86:250-8. PubMed PMID: 26057935; NIHMSID: NIHMS698275; PubMed Central PMCID: PMC4554824.

Rolfe DF, Brown GC. Cellular energy utilization and molecular origin of standard metabolic rate in mammals. Physiol Rev. 1997 Jul;77(3):731-58. PubMed PMID: 9234964.

Ross MF, Kelso GF, Blaikie FH, James AM, Cochemé HM, Filipovska A, Da Ros T, Hurd TR, Smith RA, Murphy MP. Lipophilic triphenylphosphonium cations as tools in mitochondrial bioenergetics and free radical biology. Biochemistry (Mosc). 2005 Feb; 70 (2):222-30. PubMed PMID: 15807662.

Rossignol R, Gilkerson R, Aggeler R, Yamagata K, Remington SJ, et al. Energy substrate modulates mitochondrial structure and oxidative capacity in cancer cells. Cancer Res. 2004 Feb 1;64(3):985-93. PubMed PMID: 14871829.

Roth KA, D'Sa C. Apoptosis and brain development. Ment Retard Dev Disabil Res Rev. 2001;7(4):261-6. PubMed PMID: 11754520.

Saita S, Shirane M, Nakayama KI. Selective escape of proteins from the mitochondria during ;mitophagy. Nat Commun. 2013;4:1410. PubMed PMID: 23361001.

Samartsev VN, Smirnov AV, Zeldi IP, Markova OV, Mokhova EN, et al. Involvement of aspartate/glutamate antiporter in fatty acid-induced uncoupling of liver mitochondria. Biochim Biophys Acta. 1997 Apr 11;1319(2-3):251-7. PubMed PMID: 9131047.

Sauvanet C, Duvezin-Caubet S, di Rago JP, Rojo M. Energetic requirements and bioenergetic modulation of mitochondrial morphology and dynamics. Semin Cell Dev Biol. 2010 Aug;21(6):558-65. PubMed PMID: 20025987.

Scaduto RC Jr, Grotyohann LW. Measurement of mitochondrial membrane potential using

fluorescent rhodamine derivatives. Biophys J. 1999 Jan;76(1 Pt 1):469-77. PubMed PMID: 9876159; PubMed Central PMCID: PMC1302536.
Schejter A, Aviram I. The reaction of cytochrome c with imidazole. Biochemistry. 1969 Jan;8(1):149-53. PubMed PMID: 5777317.
Schönfeld P, Schild L, Kunz W. Long-chain fatty acids act as protonophoric uncouplers of oxidative phosphorylation in rat liver mitochondria. Biochim Biophys Acta. 1989 Dec 7;977(3):266-72. PubMed PMID: 2556180.
Schönfeld P. Anion permeation limits the uncoupling activity of fatty acids in mitochondria. FEBS Lett. 1992 Jun 1;303(2-3):190-2. PubMed PMID: 1607018
Scorrano L, Ashiya M, Buttle K, Weiler S, Oakes SA, et al. A distinct pathway remodels mitochondrial cristae and mobilizes cytochrome c during apoptosis. Dev Cell. 2002 Jan;2(1):55-67. PubMed PMID: 11782314.
Sere PA. Citrate synthase. Methods in Enzymology. 1969:3–5.
Severin FF, Severina II, Antonenko YN, Rokitskaya TI, Cherepanov DA, et al. Penetrating cation/fatty acid anion pair as a mitochondria-targeted protonophore. Proc Natl Acad Sci U S A. 2010 Jan 12;107(2):663-8. PubMed PMID: 20080732; PubMed Central PMCID: PMC2818959.
Sinibaldi F, Mei G, Polticelli F, Piro MC, Howes BD, et al. ATP specifically drives refolding of non-native conformations of cytochrome c. Protein Sci. 2005 Apr;14(4):1049-58. PubMed PMID: 15741329; PubMed Central PMCID: PMC2253445.
Singh M, Sharma H, Singh N. Hydrogen peroxide induces apoptosis in HeLa cells through mitochondrial pathway. Mitochondrion. 2007 Dec;7(6):367-73. PubMed PMID: 17855174.
Smith RA, Murphy MP. Animal and human studies with the mitochondria-targeted antioxidant MitoQ. Ann N Y Acad Sci. 2010 Jul;1201:96-103. PubMed PMID: 20649545.
Sofroniew MV, Vinters HV. Astrocytes: biology and pathology. Acta Neuropathol. 2010 Jan;119(1):7-35. PubMed PMID: 20012068; PubMed Central PMCID: PMC2799634.
Stewart JM, Blakely JA, Johnson MD. The interaction of ferrocytochrome c with long-chain fatty acids and their CoA and carnitine esters. Biochem Cell Biol. 2000;78(6):675-81. PubMed PMID: 11206578.
Stuart JA, Bourque BM, de Souza-Pinto NC, Bohr VA. No evidence of mitochondrial respiratory dysfunction in OGG1-null mice deficient in removal of 8-oxodeoxyguanine from mitochondrial DNA. Free Radic Biol Med. 2005 Mar 15;38(6):737-45. PubMed PMID: 15721984.
Suen DF, Norris KL, Youle RJ. Mitochondrial dynamics and apoptosis. Genes Dev. 2008 Jun 15;22(12):1577-90. PubMed PMID: 18559474; PubMed Central PMCID: PMC2732420.
Sumpio BE, Riley JT, Dardik A. Cells in focus: endothelial cell. Int J Biochem Cell Biol. 2002 Dec;34(12):1508-12. PubMed PMID: 12379270.
Sun Y, Vashisht AA, Tchieu J, Wohlschlegel JA, Dreier L. Voltage-dependent anion channels (VDACs) recruit Parkin to defective mitochondria to promote mitochondrial autophagy. J Biol Chem. 2012 Nov 23;287(48):40652-60. PubMed PMID: 23060438; PubMed Central PMCID: PMC3504778.
Susin SA, Lorenzo HK, Zamzami N, Marzo I, Snow BE, et al. Molecular characterization of mitochondrial apoptosis-inducing factor. Nature. 1999 Feb 4;397(6718):441-6. PubMed PMID: 9989411.
Swerdlow RH, E L, Aires D, Lu J. Glycolysis-respiration relationships in a neuroblastoma cell line. Biochim Biophys Acta. 2013 Apr;1830(4):2891-8. PubMed PMID: 23313167; NIHMSID: NIHMS434597; PubMed Central PMCID: PMC3594384.
Takuma K, Baba A, Matsuda T. Astrocyte apoptosis: implications for neuroprotection. Prog Neurobiol. 2004 Feb;72(2):111-27. PubMed PMID: 15063528.

Talanian RV, Quinlan C, Trautz S, Hackett MC, Mankovich JA, et al. Substrate specificities of caspase family proteases. J Biol Chem. 1997 Apr 11;272(15):9677-82. PubMed PMID: 9092497.

Terada H. Uncouplers of oxidative phosphorylation. Environ Health Perspect. 1990 Jul;87:213-8. PubMed PMID: 2176586; PubMed Central PMCID: PMC1567840.

Thornberry NA, Rano TA, Peterson EP, Rasper DM, Timkey T, et al. A combinatorial approach defines specificities of members of the caspase family and granzyme B Functionalrelationships established for key mediators of apoptosis. J Biol Chem. 1997 Jul 18;272(29):17907-11. PubMed PMID: 9218414.

Toyama EQ, Herzig S, Courchet J, Lewis TL Jr, Losón OC, et al. Metabolism AMP-activated protein kinase mediates mitochondrial fission in response to energy stress. Science. 2016 Jan 15;351(6270):275-81. PubMed PMID: 26816379; NIHMSID: NIHMS778814; PubMed Central PMCID: PMC4852862.

Trendeleva TA, Rogov AG, Cherepanov DA, Sukhanova EI, Il'yasova TM, et al. Interaction of tetraphenylphosphonium and dodecyltriphenylphosphonium with lipid membranes and mitochondria. Biochemistry (Mosc). 2012 Sep;77(9):1021-8. PubMed PMID: 23157262.

Trnka, J., Elkalaf, M., & Anděl, M. (2015). Lipophilic Triphenylphosphonium Cations Inhibit Mitochondrial Electron Transport Chain and Induce Mitochondrial Proton Leak. PLoS ONE, 10(4), e0121837. http://doi.org/10.1371/journal.pone.0121837

Twig G, Elorza A, Molina AJ, Mohamed H, Wikstrom JD, et al. Fission and selective fusion govern mitochondrial segregation and elimination by autophagy. EMBO J. 2008 Jan 23;27(2):433-46. PubMed PMID: 18200046; PubMed Central PMCID: PMC2234339.

Van Laar VS, Arnold B, Cassady SJ, Chu CT, Burton EA, et al. Bioenergetics of neurons inhibit the translocation response of Parkin following rapid mitochondrial depolarization. Hum Mol Genet. 2011 Mar 1;20(5):927-40. PubMed PMID: 21147754; PubMed Central PMCID: PMC3033183.

Vander Heiden MG, Cantley LC, Thompson CB. Understanding the Warburg effect: the metabolic requirements of cell proliferation. Science. 2009 May 22;324(5930):1029-33. PubMed PMID: 19460998; NIHMSID: NIHMS165713; PubMed Central PMCID: PMC2849637.

Verdegem D, Moens S, Stapor P, Carmeliet P. Endothelial cell metabolism: parallels and divergences with cancer cell metabolism. Cancer Metab. 2014;2:19. PubMed PMID: 25250177; PubMed Central PMCID: PMC4171726.

Verhagen AM, Ekert PG, Pakusch M, Silke J, Connolly LM, et al. Identification of DIABLO, a mammalian protein that promotes apoptosis by binding to and antagonizing IAP proteins. Cell. 2000 Jul 7;102(1):43-53. PubMed PMID: 10929712.

Wainio WW. The mammalian respiratory chain. 1970. Academic Press, New York.

Wang C, Youle RJ. The role of mitochondria in apoptosis. Annu Rev Genet. 2009; 43:95-118. PubMed PMID: 19659442.

Wang X. The expanding role of mitochondria in apoptosis. Genes Dev. 2001 Nov 15; 15 (22) :2922-33. PubMed PMID: 11711427.

Wieckowski MR, Wojtczak L. Involvement of the dicarboxylate carrier in the protonophoric action of long-chain fatty acids in mitochondria. Biochem Biophys Res Commun. 1997 Mar 17;232(2):414-7. PubMed PMID: 9125192.

Wojtczak L. Effect of long-chain fatty acids and acyl-CoA on mitochondrial permeability, transport, and energy-coupling processes. J Bioenerg Biomembr. 1976 Dec;8(6):293-311. PubMed PMID: 137237.

Wojtczak L, Schönfeld P. Effect of fatty acids on energy coupling processes in mitochondria. Biochim Biophys Acta. 1993 Nov 2;1183(1):41-57. PubMed PMID: 8399375.

Wojtczak L, Zaluska H. The inhibition of translocation of adenine nucleotides through

mitochondrial membranes by oleate. Biochem Biophys Res Commun. 1967 Jul 10;28(1):76-81. PubMed PMID: 4227821.

Wu SB, Wei YH. AMPK-mediated increase of glycolysis as an adaptive response to oxidative stress in human cells: implication of the cell survival in mitochondrial diseases. Biochim Biophys Acta. 2012 Feb;1822(2):233-47. PubMed PMID: 22001850.

Xia M, Gonzalez P, Li C, Meng G, Jiang A, et al. Mitophagy enhances oncolytic measles virus replication by mitigating DDX58/RIG-I-like receptor signaling. J Virol. 2014 May;88(9):5152-64. PubMed PMID: 24574393; PubMed Central PMCID: PMC3993837.

Yanamala N, Kapralov AA, Djukic M, Peterson J, Mao G, et al. Structural re-arrangement and peroxidase activation of cytochrome c by anionic analogues of vitamin E, tocopherol succinate and tocopherol phosphate. J Biol Chem. 2014 Nov 21;289(47):32488-98. PubMed PMID: 25278024; PubMed Central PMCID: PMC4239604.

Yang QH, Church-Hajduk R, Ren J, Newton ML, Du C. Omi/HtrA2 catalytic cleavage of inhibitor of apoptosis (IAP) irreversibly inactivates IAPs and facilitates caspase activity in apoptosis. Genes Dev. 2003 Jun 15;17(12):1487-96. PubMed PMID: 12815069; PubMed Central PMCID: PMC196079.

Yin H, Zhu M. Free radical oxidation of cardiolipin: chemical mechanisms, detection and implication in apoptosis, mitochondrial dysfunction and human diseases. Free Radic Res. 2012 Aug;46(8):959-74. PubMed PMID: 22468920.

Youle RJ, van der Bliek AM. Mitochondrial fission, fusion, and stress. Science. 2012 Aug 31;337(6098):1062-5. PubMed PMID: 22936770; NIHMSID: NIHMS757703; PubMed Central PMCID: PMC4762028.

Zácková M, Krämer R, Jezek P. Interaction of mitochondrial phosphate carrier with fatty acids and hydrophobic phosphate analogs. Int J Biochem Cell Biol. 2000 May;32(5):499-508. PubMed PMID: 10736565.

Zheng J. Energy metabolism of cancer: Glycolysis versus oxidative phosphorylation (Review). Oncol Lett. 2012 Dec;4(6):1151-1157. PubMed PMID: 23226794; PubMed Central PMCID: PMC3506713.

Zhou M, Diwu Z, Panchuk-Voloshina N, Haugland RP. A stable nonfluorescent derivative of resorufin for the fluorometric determination of trace hydrogen peroxide: applications in detecting the activity of phagocyte NADPH oxidase and other oxidases. Anal Biochem. 1997 Nov 15;253(2):162-8. PubMed PMID: 9367498.

Zielke HR, Ozand PT, Tildon JT, Sevdalian DA, Cornblath M. Growth of human diploid fibroblasts in the absence of glucose utilization. Proc Natl Acad Sci U S A. 1976 Nov;73(11):4110-4. PubMed PMID: 1069299; PubMed Central PMCID: PMC431346.

Zou H, Li Y, Liu X, Wang X. An APAF-1cytochrome c multimeric complex is a functional apoptosome that activates procaspase-9. J Biol Chem. 1999 Apr 23; 274 (17): 11549-56. PubMed PMID:10206961